

MSci Project Report

Noise effects on Landau-Zener transitions of Bose-Einstein condensates

Matthias Kraft

June 18, 2012

Imperial College London
Ruprecht-Karls Universität Heidelberg

Supervisor: PD Dr. Sandro Wimberger

Quantum transport phenomena of Bose-Einstein condensates (BEC) ‘loaded’ into spatially periodic optical lattices are an active area of current research. For a sinusoidal lattice, the band structure of the energy spectrum is given by the eigenvalues of the Mathieu equation. If a small static force is applied to a BEC in such a lattice (corresponds to a tilted lattice and is called Wannier-Stark system), tunnelling of the BEC between the energy bands of the Mathieu spectrum occurs. A fruitful approach to describe these tunnelling processes within a two band approximation is given by the Landau-Zener model. Earlier research has shown that introducing noise into the Wannier-Stark system via a second ‘noisy’ optical lattice can provide a tool to ‘engineer’ the tunnelling processes. We therefore extend the simple Landau-Zener model to incorporate a second ‘noisy’ optical lattice. Results obtained for the extended Landau-Zener model are compared to simulations of the full system and successes and failures of the model are discussed. The possibility to control the tunnelling processes by means of a second deterministically oscillating (in space) optical lattice is outlined.

Quantentransporteffekte von Bose-Einstein Kondensaten (BEK) in optische Gittern bilden einen aufstrebenden Zweig der heutigen Forschung. Im Falle eines sinusförmigen optischen Gitters ist die Bandstruktur des Energiespektrums durch die Eigenwerte der sogenannten Mathieu-Gleichung gegeben. Wird eine schwache, statische Kraft an ein BEK in einem solchen Gitter angelegt (äquivalent zu einem gekippten optischen Gitter, auch Wannier-Stark System genannt), kommt es zu Tunnelprozessen des BEKs zwischen den Energiebändern des Mathieu-Spektrums. Ein besonders erfolgreicher Ansatzpunkt zur Beschreibung dieser Tunnelprozesse ist, im Rahmen einer zwei-Band Näherung, durch das Landau-Zener Modell gegeben. In vorangegangenen Forschungsprojekten konnte gezeigt werden, dass diese Tunnelprozesse im Wannier-Stark System durch hinzufügen eines zweiten stochastischen, optischen Gitters gezielt beeinflusst werden können. Daher erweitern wir das normale Landau-Zener Modell, so dass es auch ein zweites stochastisches, optisches Gitter beschreiben kann. Ergebnisse für das erweiterte Landau-Zener Modell werden im Folgenden mit Ergebnissen für das vollständige System verglichen. Die Möglichkeit der gezielten Beeinflussung der Tunnelprozesse mit Hilfe eines zweiten, deterministischen und räumlich oszillierenden, optischen Gitters wird aufgezeigt.

Contents

1	Introduction	1
2	Background	5
2.1	Bose-Einstein condensates in optical lattices	5
2.2	Periodic lattices and the Wannier-Stark system (WSS)	7
2.2.1	The energy spectrum of the Mathieu equation	8
2.2.2	Mapping the WSS onto the Landau-Zener (LZ) model	12
2.3	The Landau-Zener model	15
2.3.1	Transition probabilities and important time scales	15
2.3.2	Applicability limits of the Landau-Zener model	18
2.4	Harmonic Noise	19
3	Introducing noise into the system	23
3.1	Adding a second, stochastic optical lattice	23
3.2	The modified Landau-Zener model	24
4	Numerical investigation	27
4.1	Numerical methods	27
4.2	Numerical results	32
4.2.1	LZ transitions in the presence of harmonic noise	32
4.2.2	Main results: ‘Noisy’ WSS vs ‘noisy’ LZ approximation	33
4.2.3	The influence of harmonic noise versus a deterministic phase	38
5	Analytical investigation	41
5.1	Formal solution of the transition probabilities	41
5.1.1	Time evolution of states	41
5.1.2	Feynman’s disentanglement theorem	42
5.1.3	A perturbation series solution	44
5.2	Application of the solution to limiting cases	45
5.2.1	Small coupling limit	45
5.2.2	Small coupling and small damping limit	48
6	Conclusion	53
7	Appendix	I
7.1	Numerical algorithm to generate harmonic noise	I
7.2	Some more numerical results	V
7.3	Derivation of the perturbation series for the transition probabilities	VI

Preface

Nowadays, research in physics is almost exclusively done in groups of a few or even many individuals. As a result, it is often quite hard to tell what the exact contribution of each individual is. In this section, I will try to make clear what my share of the work presented in this thesis was, and also give a short outlook on what is going to follow.

Chapter one starts with a short motivation and non-technical introduction to the problem studied in this thesis. Also, the main observable in this thesis is introduced; namely the transition probabilities of Bose-Einstein condensates between the ground and first excited band of the so-called Mathieu energy spectrum.

Chapter two introduces the most important models and concepts that this thesis builds on. First, a brief and non-technical introduction to Bose-Einstein condensates in optical lattices is given. Then the so-called Wannier-Stark system is introduced and the energy spectrum of the Mathieu equation (a special case of the Wannier-Stark system) is discussed. The dynamics of a Bose-Einstein condensate in a Wannier-Stark system are explained via a semi-classical approach. It is further shown that the Wannier-Stark system can be locally approximated by a Landau-Zener model. Subsequently, the Landau-Zener model is explained. The chapter closes with the presentation of a special stochastic process called *harmonic noise*. Everything that is presented in chapter two has been discussed in the literature and my only contribution is to (hopefully) give a self-consistent introduction to the models mentioned.

Chapter three starts with an introduction of a modified Wannier-Stark system that has been subject to earlier research in my group in Heidelberg. In the second half of this chapter it is shown how this modified Wannier-Stark system can be mapped onto an effective Landau-Zener model and important properties of the model are discussed. The mapping onto the effective Landau-Zener model has been done jointly with my colleague Stephan Burkhardt; the discussion of its properties is my own work.

In chapter four, a numerical study of the transition probabilities of Bose-Einstein condensates in the Wannier-Stark system is given. Special emphasis is placed on a comparison between results obtained from simulations of the full system and simulations of the effective Landau-Zener model. This again, is joint work of Stephan Burkhardt and myself. Stephan wrote the code to simulate the full modified Wannier-Stark system and also provided the code to generate the harmonic noise. The code to simulate the effective Landau-Zener model has been written by myself. The analysis and interpretation of the results given in this chapter are my own work, although I am grateful for discussions with my supervisor.

Chapter five presents an analytic approach to calculate the transition probability in the effective Landau-Zener model. In the first part of this chapter a formal solution to the problem is derived and in the second part this solution is used to calculate two

limiting cases of the model. The derivation of the formal solution closely follows an approach given by Kayanuma [1], yet the derivation is presented in much more detail than it can be found in Kayanuma's original paper. In this sense my contribution is to extend Kayanuma's approach to the effective Landau-Zener model studied in this thesis and to give a (hopefully) clear presentation of his approach. The calculation of the two limiting cases has been done by myself.

Chapter six gives a summary of the main results obtained in this thesis and tries to identify to what extent the project aims have been fulfilled. The chapter closes with an outlook on possible future work.

1 Introduction

Since the first experimental realisation of a Bose-Einstein condensate (BEC) in the mid-nineties of the last century, physics with ultracold atoms has received ever growing attention from both experimentalists and theorists. Especially the field of BECs in optical lattices has experienced rapid growth *and* progress in the last decade. But what is hidden behind the field's fancy name and what is it good for?

Optical lattices are generated by two counter-propagating laser beams (of the same wavelength) that interfere to form a standing wave of laser light. As the name of the field suggests, it is possible to 'load' a BEC into such an optical lattice. In many ways BECs in optical lattices strongly resemble solid-state crystals, with the optical lattice producing a potential similar to the one generated by the lattice ions in a crystal and the atoms of the BEC taking the role of the electrons in the crystal. Consequently, it is not very surprising that many complex physical phenomena present in solid-state crystals, such as superconductivity, Bloch oscillations or Mott insulation, find direct counterparts for ultracold atoms in optical lattices. Yet the question remains, why bother going through the complex process of producing a BEC if the system shows the same effects as a 'normal' crystal does?

The answer is surprisingly simple. High precision always being one of the strengths of laser physics, it allows for almost perfect control of the system parameters by changing the geometry of the optical lattice, thus making it possible to simulate different types of crystals with the same system. Moreover, the high coherence of laser light ensures perfect periodicity of the lattice with no distortions over thousands of lattice sites, producing a 'cleaner' lattice than in any real crystal. A direct consequence of this is that phenomena such as Bloch oscillations are easily observed and studied with BECs in optical lattices, but very hard to detect in real crystals due to the many impurities. Furthermore, the BEC itself can be used to mimic different interaction strengths between the electrons in a real crystal by varying the density of the BEC.

It should be clear now that (BECs in) optical lattices provide an excellent tool to study solid-state phenomena in a controlled environment, but they are much more than that. Recent proposals suggest that by placing only two atoms into one lattice site the formation of molecules could be studied; having only one atom per lattice site allows to use the system as a high precision atomic clock [2]. Of course, there are also suggestions to use single, trapped atoms as 'qubits' which are crucial for the implementation of a quantum computer [2]. In this sense ultracold atoms in optical lattices can be used as a real quantum simulator in Feynman's spirit [3], in which a controllable and 'easily' realisable system is used to simulate the behaviour of a more complex physical system.

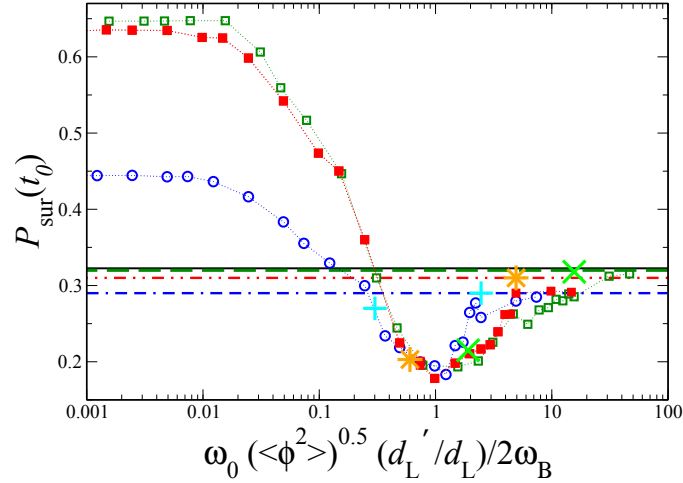


Figure 1.1: The survival probability of the BEC in the ground band at fixed time $t_0 = 6T_B$ versus the rescaled frequency ω_0 of the stochastic phase. Data from [6], courtesy of the corresponding authors ©APS. A detailed description can be found in section 3.1

In this thesis, a variation of the so-called Wannier-Stark system (WSS) will be studied. The standard WSS can be realised by trapping a BEC in a tilted optical lattice. The tilt can be implemented by the application of a static force [4] (see figure 2.1 and Eq.(2.3)). Solid-state physics teaches us that a periodic potential gives rise to a band structure in the energy spectrum, consisting of allowed and forbidden energy regions. The same holds true for a BEC in an optical lattice. Due to the applied static force, the atoms constituting the BEC ‘scan through’ the energy spectrum and undergo so-called Bloch oscillations. As the atoms ‘scan through’ the energy spectrum the band gap between the energy bands varies and at the point where the energy gap is minimal (known as avoided crossing) the atoms can tunnel into the upper energy band. For typical experimental parameters [5], the dynamics of the BEC close to such an avoided crossing can be well approximated by the so-called Landau-Zener (LZ) model, which accurately predicts the probability to tunnel into the upper band.

Earlier research in Heidelberg has shown that the tunnelling probability can be actively engineered by superimposing a second optical lattice, which fluctuates in time and space due to a stochastic phase, over the first one [6]. Figure 1.1 shows the survival probability of the BEC in the ground band versus the characteristic frequency of the stochastic phase, as obtained by numerical simulations of the modified WSS (red squares, green squares and blue circles are for different potential depths; the horizontal lines are of no importance here). The functional dependence of the survival probability on the frequency of the stochastic phase with its clear minima unambiguously demonstrates that it is possible to control the tunnelling probability of the BEC by altering the frequency of the phase. Due to the complexity of the system, an interpretation of the frequency dependence of the tunnelling probability has proven difficult. Consequently, one of the

major aims of this project is to gain a better understanding of the frequency dependence of the tunnelling probability, by reducing the complexity of the system without ‘throwing away’ too much of the physics contained in the full system. In this spirit, three questions that this thesis tries to answer have been formulated:

Is it possible to approximate the dynamics of the BEC close to an avoided crossing in the full modified WSS by an effective Landau-Zener model? If so, can the effective Landau-Zener model reproduce the functional dependence of the tunnelling probability on the frequency of the stochastic phase? And, is it possible to predict and explain the position of the minimum shown in figure 1.1?

Lastly, it should be mentioned that all calculations given in this thesis are done within the single particle approximation, i.e. the interactions between the atoms of the BEC are neglected. In the case of a sufficiently dilute BEC, this approximation is expected to give reasonable results [7]. Moreover, Stephan Burkhardt of our group has done numerical simulations [8], in which the interactions have been taken account of via a mean-field approach based on the Gross-Pitaevskii equation [9]. From those simulations he concluded that the tunnelling probability (and decay rate) of the BEC into higher bands is remarkably stable with respect to (moderate) interactions between the atoms (see figure 1.2). All three graphs in figure 1.2 are in very good agreement, indicating that interactions are of little importance for the decay rate (and hence tunnelling probability) in our system when noise is present. Therefore, the next chapter will start with an introduction of the single-particle and interaction free Schrödinger equation for the Wannier-Stark Hamiltonian.

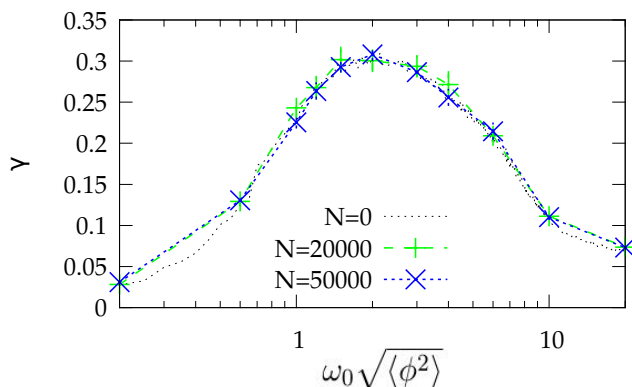


Figure 1.2: The decay rate of the BEC from the ground band into higher bands versus the rescaled frequency of the stochastic phase ϕ . The different graphs correspond to different interaction strengths between the atoms. $N=0$ means no interaction, higher N means stronger interaction. Data from [8], courtesy of the corresponding author.

2 Background

2.1 Bose-Einstein condensates in optical lattices

In 1924/25, following the work of Bose on the quantum statistics of photons [10] Einstein predicted a new state of matter [11], nowadays known as Bose-Einstein condensate (BEC). Einstein calculated that if the temperature of a bosonic gas drops below a critical temperature, a finite fraction of the bosons will occupy the energetic ground state of the system. Furthermore, this fraction increases with decreasing temperature. The bosons in the ground state constitute the so-called BEC. The critical temperature at which this phase transition occurs can be estimated as the temperature at which the deBroglie wavelength $\lambda_{dB} = (2\pi\hbar/Mk_B T)^{1/2}$ of the bosons becomes comparable to the mean distance between them. Hereafter \hbar is Planck's constant, k_B is Boltzmann's constant, M is the mass of the bosons and T is their temperature. Typically the critical temperature is of the order of $10^{-7} - 10^{-5} K$ (e.g. 1.7×10^{-7} for ^{87}Rb and 5×10^{-5} for ^1H) [12]. Such low temperatures can, for example, be realised via laser cooling followed by a stage of magnetic evaporative cooling. Even so, it is not an easy task and this is reflected in the fact that it took about 70 years until the first BECs have been realised in the laboratory [13–15]. Today, 17 years after their first observation, BECs are routinely created in laboratories around the world.

It is apparent that at temperatures as low as a few hundred nano Kelvin, any system can only be described within the framework of quantum mechanics and its behaviour should be governed by the corresponding Schrödinger equation. Treating the BEC as an ideal non-interacting gas allows to write its wavefunction as the product of all constituent single-particle wavefunctions. Hence, the BECs behaviour (in 1-D) is governed by the single particle Schrödinger equation,

$$i\hbar\partial_t\psi(x,t) = -\frac{\hbar^2}{2M}\partial_x^2\psi(x,t) + V(x,t)\psi(x,t) . \quad (2.1)$$

Naturally, in any real BEC the bosons interact and the above equation does not hold. Yet, if the BEC is sufficiently dilute those interactions can be taken account of via mean-field theories, leading to modified (non-linear) Schrödinger equations. The best known of those is the Gross-Pitaevskii equation [9]. Nevertheless, for the problem studied in this thesis interactions can be neglected, as has been mentioned in the introduction.

In the following we will study the behaviour of BECs when they are 'loaded' into an optical lattice and are subject to a static force (see figure 2.1. Optical lattices can be generated by two counter propagating laser beams with the same wavelength λ . The two laser beams will interfere and form a *standing* wave with a wavelength of $\frac{\lambda}{2}$. Such an

optical lattice can be used as a dipole trap for the BEC, provided that the laser frequency is sufficiently detuned from atomic resonances within the BEC [16]. If this condition is fulfilled the process of stimulated absorption and emission leads to a potential of the form,

$$V(x) = V \cos(2k_L x) , \quad (2.2)$$

where k_L is the wavenumber of the laser beams defined by $k_L = \frac{2\pi}{\lambda}$ and V is the potential depth. The potential depth is proportional to the square of the Rabi frequency (and hence laser intensity) and inversely proportional to the detuning from atomic resonance [16]. Strictly speaking this potential should not be conservative, because apart from stimulated absorption and emission, also spontaneous emission is taking place. However, if the detuning from atomic resonance is sufficiently large the spontaneous emission process can be neglected and the above potential provides an excellent approximation to the real one.

Furthermore it is possible to exert a static force on the atoms by accelerating the lattice. Experimentally this can be done by introducing a small difference in the frequency of the two laser beams. This will effectively add another term $-Fx$ to the Hamiltonian and the full Schrödinger equation of the system now reads,

$$i\hbar\partial_t\psi = \left(-\frac{\hbar^2}{2M}\partial_x^2 + V \cos(2k_L x) - Fx \right) \psi . \quad (2.3)$$

This system is commonly referred to as Wannier-Stark system (WSS) and can be imagined as a cosine potential tilted in space.

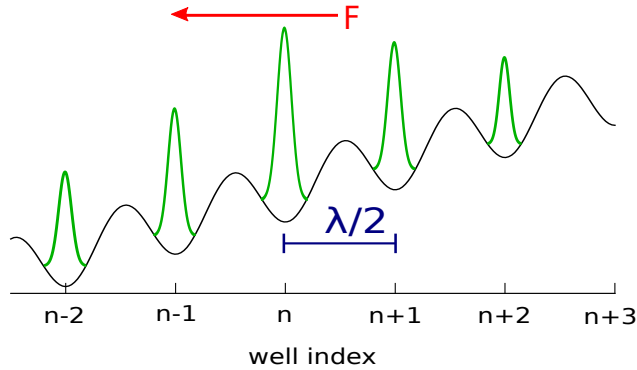


Figure 2.1: Schematic representation of a tilted optical lattice, the well separation is given by half the laser wavelength. The red arrow gives the direction of the force. The green gaussians in the wells represent the delocalised wavefunction of the BEC in the lattice (real space). In typical experiments the wavefunction extends over 50 . . . 100 lattice sites [5].

As an aside, an experiment relevant to the problem studied in this thesis has been realised with a BEC of ca. 5×10^4 rubidium-87 atoms and an optical lattice with a wavelength of 421nm, i.e. the laser beams had a wavelength of 842nm. The small frequency offset to accelerate the lattice has been introduced via acousto-optic modulators [5].

2.2 Periodic lattices and the Wannier-Stark system (WSS)

In this section, basic properties of the Hamiltonian of Eq. (2.3) introduced in the previous section will be reviewed. A new set of dimensionless units will be introduced and it will be shown how the application of a gauge transformation can be used to restore the translational invariance of the WS-Hamiltonian. The energy spectrum of this reduced Hamiltonian will be discussed and compared to the *free particle* case, i.e. the limit of a vanishing potential.

The starting point for further investigations is the time-dependent Schrödinger equation given in Eq.(2.3),

$$i\hbar\partial_t\psi = \left(-\frac{\hbar^2}{2M}\partial_x^2 + V\cos(2k_Lx) - Fx \right) \psi. \quad (2.4)$$

It is convenient to introduce a new set of dimensionless variables $E_{\text{rec}} = \frac{\hbar^2 k_L^2}{2M}$, $t' = t\frac{8E_{\text{rec}}}{\hbar}$ and $x' = 2xk_L$. E_{rec} is called the recoil energy and corresponds to the energy transferred in a *one photon exchange process* between photons of wavenumber k_L and an atom in the BEC. As k_L is also the wavenumber of the photons in the laser beam, E_{rec} sets the characteristic energy scale of the system (note, during an absorption followed by re-emission the energy exchanged is actually $4E_{\text{rec}}$ as the momentum transfer is $2\hbar k_L$).

The differential operators in terms of the new variables t' and x' read,

$$\partial_{t'} = \frac{\hbar}{8E_{\text{rec}}}\partial_t \quad \text{and} \quad \partial_{x'}^2 = \frac{1}{4k_L^2}\partial_x^2. \quad (2.5)$$

Re-expressing the above Schrödinger equation in terms of the new variables yields,

$$i8E_{\text{rec}}\partial_{t'}\psi = \left(-\frac{4\hbar^2 k_L^2}{2M}\partial_{x'}^2 + V\cos(x') - \frac{F x'}{2k_L} \right) \psi. \quad (2.6)$$

Division by $8E_{\text{rec}}$ brings the above equation into the concise form,

$$i\partial_{t'}\psi = \left(-\frac{1}{2}\partial_{x'}^2 + V_0\cos(x') - F_0x' \right) \psi, \quad (2.7)$$

with a rescaled potential depth V_0 and force F_0 :

$$V_0 = \frac{V}{8E_{\text{rec}}} \quad \text{and} \quad F_0 = \frac{F}{16E_{\text{rec}}k_L}. \quad (2.8)$$

For convenience the dashes in the above Schrödinger equation are dropped and, unless stated otherwise, the system of dimensionless units is used from now on. Typical experimental values of the potential V_0 and the force F_0 are, 0.0156...0.25 and 0.00597...0.0298, respectively [5, 17].

Table 2.1: Summary of the new unit system

	Energy	Momentum
1 photon exchange	$E_{\text{rec}} = \frac{\hbar^2 k_L^2}{2M}$	$p_{\text{rec}} = \hbar k_L$
2 photon exchanges	$4E_{\text{rec}} = 4 \frac{\hbar^2 k_L^2}{2M}$	$2p_{\text{rec}} = 2\hbar k_L$
	Old variable	New variable
Energy	E	$E' = \frac{E}{8E_{\text{rec}}}$
Time	t	$t' = t \frac{8E_{\text{rec}}}{\hbar}$
Space	x	$x' = 2xk_L$
Force	F	$F_0 = \frac{F}{16E_{\text{rec}}k_L}$
Potential	V	$V_0 = \frac{V}{8E_{\text{rec}}}$

2.2.1 The energy spectrum of the Mathieu equation

The determination of the energy spectrum of the Wannier-Stark Hamiltonian is by no means a trivial task and there has been a long discussion about it in the literature [18–21]. A more recent and comprehensive review on the matter can be found in [22]. To gain an understanding of the physics underlying the Wannier-Stark Hamiltonian we will therefore start by considering a limiting case of the full Hamiltonian, namely the situation in which the driving force $F_0 = 0$. We will then use an analogy to solid-state physics to develop some intuition for the system’s behaviour when the force is non-zero.

Formally one has to solve the time-independent Schrödinger equation (TISE) to find the energy spectrum of the underlying Hamiltonian. In the case of $F_0 = 0$ that means one needs to solve,

$$\hat{H}\psi = E\psi \quad , \text{ i.e., } \quad \left(-\frac{1}{2}\partial_x^2 + V_0 \cos(x) \right) \psi = E\psi . \quad (2.9)$$

However, some of the features of the resulting solutions can be immediately inferred from the translational invariance of the above Hamiltonian. It is known since the early days of solid-state physics [23] that a spatially periodic potential leads to energy bands of allowed and forbidden regions in the energy spectrum and that the most general solutions to an equation as the one above, are of the form:

$$\psi_{n,k}(x) = u_{n,k}(x)e^{ikx} , \quad (2.10)$$

where k represents the real valued wavenumber of the solution and runs over the first Brillouin zone, i.e. in real units $k \in [-k_L, k_L]$. Those solutions have an associated energy eigenvalue $E_n(k)$. This is commonly known as Bloch’s theorem (in 1-dimension) and $\psi_{n,k}$ is called Bloch wave/state. An important property of these solutions is that $u_{n,k}(x)$ is periodic with the spatial periodicity of the potential, i.e.

$$u_{n,k}(x) = u_{n,k}(x + n2\pi) \quad \text{with } n \in \mathbb{Z}_0 . \quad (2.11)$$

Moreover the energy eigenvalues $E_n(k)$ are periodic with the periodicity of the recipro-

cal lattice¹ [24]. The standard condition (in 1-dimension and the dimensionless units introduced above)

$$e^{iKR} = 1 \quad \Leftrightarrow \quad KR = 2\pi m \quad m \in \mathbb{Z}_0, \quad (2.12)$$

where R is the periodicity of the real lattice and K the periodicity of the reciprocal lattice [24], immediately leads to $K = 1l$ with l being an integer, as $R = 2\pi$. Hence for the energy eigenvalues the relation

$$E_n(k) = E_n(k + 1l) \quad \text{with } l \in \mathbb{Z}_0 \quad (2.13)$$

holds.

Still, to obtain the actual energy spectrum of the Hamiltonian in Eq. (2.9), the TISE has to be solved explicitly. This can be done by recasting it in the following form,

$$\partial_{\tilde{x}}^2 \tilde{\psi}(\tilde{x}) + (a - 2q \cos(2\tilde{x})) \tilde{\psi}(\tilde{x}) = 0, \quad (2.14)$$

where $\tilde{x} = \frac{x}{2}$, $a = \frac{E}{4}$, $\tilde{\psi}(\tilde{x}) = \psi(\frac{x}{2})$ and $q = \frac{V_0}{2}$. This equation is known as Mathieu's equation [25]. In the literature its solutions have also been discussed in the context of optical lattices [26]. Unfortunately, there are no simple closed form expressions for the functions (called Mathieu functions) solving the above equation, but they fulfil all conditions that would be expected from Bloch's theorem. As the actual form of the Mathieu functions is of little importance for the rest of this thesis we will merely give a graphical representation of the energy spectrum generated by their eigenvalues.

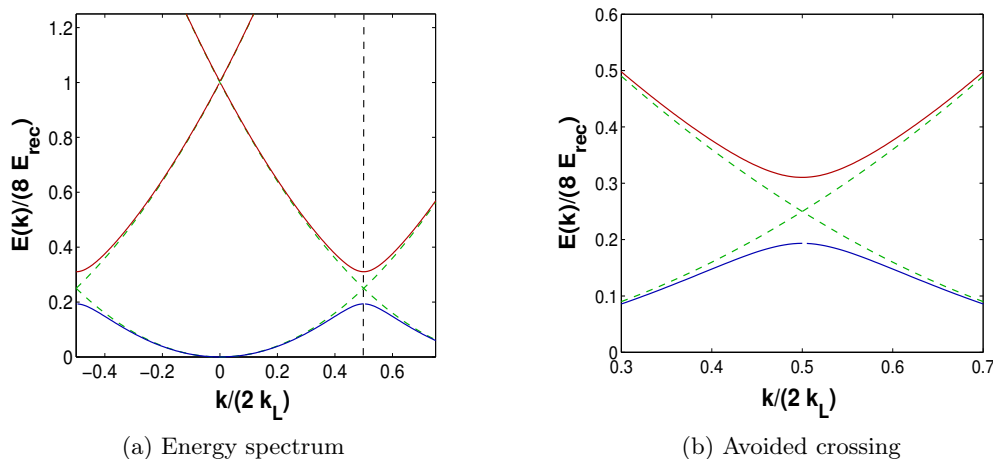


Figure 2.2: Energy spectrum generated by the WS-Hamiltonian of Eq. (2.7) in the case of $F_0 = 0$. The vertical dashed line marks the end of the 1st Brillouin zone

The figure on the left shows the energy spectrum in the reduced zone scheme [24]. The solid lines are the eigenenergies of the Mathieu equation and are commonly referred to

¹As a reminder the reciprocal lattice/space is the Fourier transform of the real lattice/space, in this thesis we may also refer to reciprocal space as momentum space.

as the *adiabatic states* of the system. The dashed lines show the eigenenergies for a free particle, usually referred to as *diabatic states*. At the edge of the 1st Brillouin zone the diabatic states of the system cross, whereas the adiabatic ones do not. Such points are called *avoided crossings* and they divide the energy spectrum in so-called *energy bands* with *band gaps* at avoided crossings. In this thesis the focus lies on the BECs dynamics close to avoided crossings.

The dynamics of the BEC when a static force is applied (i.e. of the full Wannier-Stark system) can be understood by applying a *semiclassical* approach and using the *adiabatic approximation*. If a non-interacting Bose-Einstein condensate is loaded into the optical lattice such that at $t = 0$, the condensate ‘sits’ at $k = 0$ in the centre of the 1st Brillouin zone, its time evolution can be calculated by using *wave packets* [27]. Due to Heisenberg’s uncertainty principle the trapped BEC cannot have a single momentum but rather has a distribution of momenta $g_n(k, t = 0)$, where n gives the energy band. This means that the full wavefunction at $t = 0$ must be a superposition of Bloch waves with momenta k according to some initial momentum distribution. If it is further assumed that the condensate occupies exclusively the lowest energy band, the wavefunction representing the BEC can be written as:

$$\Psi(x, t = 0) = \int_{-\frac{1}{2}}^{\frac{1}{2}} g_1(k, t = 0) \psi_{1,k}(x) dk , \quad (2.15)$$

where the integration runs over one Brillouin zone, the subscript ‘1’ indicates that the condensate occupies the ground band only and $\psi_{1,k}(x)$ is defined via Eq.(2.10). Strictly speaking, the treatment that follows is only valid in the *adiabatic limit*, i.e. the limit of vanishing force and hence infinitely slow passage through momentum space. In this limit it can be shown that if the wave packet is well localised in momentum space² (see figure 2.3) and interaction with higher energy bands can be neglected, the expectation value of the total momentum evolves according to *Ehrenfest’s theorem* [23, 27]:

$$\begin{aligned} \langle p(t) \rangle &\equiv k(t) = k(t = 0) + F_0 t \\ &= F_0 t , \end{aligned} \quad (2.16)$$

where $k(t = 0)$ is the initial position of the wave packet’s centre in momentum space, which is equal to zero as has been specified before.

Due to the periodic structure of the energy spectrum, the linear growth of $k(t)$ leads to oscillations of the wavepacket in momentum space. In the reduced zone scheme this means, that if the wavepacket leaves the first Brillouin zone at $k/(2k_L) = 0.5$ it reappears at the other zone edge $k/(2k_L) = -0.5$. The time period T_B with which this happens can be explicitly calculated from the periodicity of the energy spectrum $E_n(k) = E_n(k + 1l)$,

$$k(t + T_B) = k(t) + 1 \quad (2.17)$$

$$F_0(t + T_B) = F_0 t + 1 \quad \implies \quad T_B = \frac{1}{F_0} , \quad (2.18)$$

²Practically this means that the width of the wavefunction in momentum space should be much smaller than a single Brillouin zone; this in turn leads to a wavefunction in real space that extends over at least a few (in the experiments reported in [5] ca. 10...100) lattice sites.

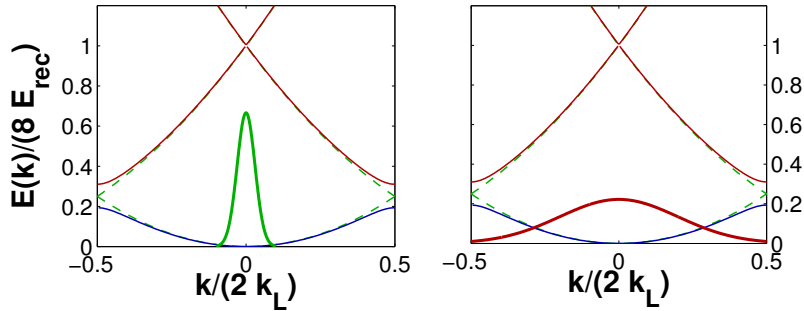


Figure 2.3: Schematic representation of the momentum distribution in the first Brillouin zone. The green gaussian curve on the left shows an initial momentum distribution that is well localised, whereas on the right (red gaussian) the distribution extends over the full Brillouin zone. The area under the two gaussians is the same.

where T_B is termed *Bloch period*. We can also define a corresponding angular frequency, called *Bloch frequency* $\omega_B = \frac{2\pi}{T_B} = 2\pi F_0$. Again the adiabatic approximation was implicitly used in the last paragraph. The oscillations of the wavepacket in momentum space lead to another interesting phenomena called *Bloch oscillations* [27].

Applying Ehrenfest's theorem is, of course, only possible under the two conditions stated above. Namely that the initial momentum distribution of the BEC is well localised in momentum space and that the influence of higher bands can be neglected. Why this is the case and what it means is best illustrated in a plot (see figure 2.3). The green gaussian in the left figure shows an initial momentum distribution that is well localised, in such a scenario the BEC can be imagined as a 'point' particle in momentum space. It is thus expected that its evolution in momentum space is governed by Eq. (2.16) until the second assumption breaks down. This second assumption is put to a serious test around an avoided crossing and one might expect from experience that if the band gap at the avoided crossing is small enough, a part of the BEC can tunnel into the upper band. After the avoided crossing the motion of the BEC should be governed by Eq. (2.16) again. In fact this is exactly what happens, as has been shown in experiments [5] (see figure 2.4).

However, if the momentum distribution is spread out over the Brillouin zone as shown by the red gaussian on the right of figure 2.3, the BEC clearly cannot be approximated as a 'point' particle. Moreover, the influence of higher bands is always given as the BEC is so spread out that a fraction of it is always close to an avoided crossing. Hence the dynamics of the BEC cannot be separated into the two classes, 'unperturbed evolution in momentum space' and 'tunnelling into higher bands'. This time scale separation is an absolutely crucial condition for the description of the tunnelling dynamics via the Landau-Zener model that will be introduced in the next section. In experiments and numerical simulations a gaussian momentum distribution of width $\delta p = (0.1 - 0.2)p_{\text{rec}}$ was sufficiently localised to ensure this separation, whereas a gaussian distribution of width $\delta p \approx 0.6p_{\text{rec}}$ leads to a breakdown of the assumptions [5].

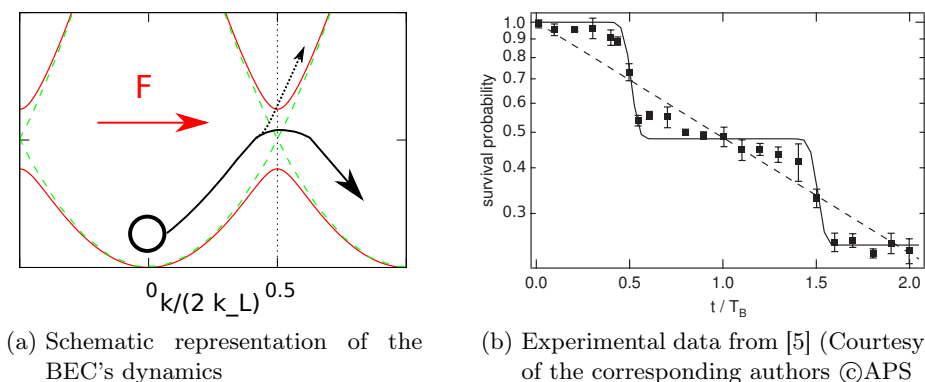


Figure 2.4: Schematic representation of the tunnelling process at an avoided crossing (left) and the time evolution of the survival probability in the ground band (right), i.e. no tunnelling takes place. The black squares are experimental data, the solid black line is obtained via numerical simulations of the full WSS and the dashed line is an exponential fit based on the Landau-Zener (LZ) model, see [5] for further details.

Figure 2.4a shows a schematic representation of the BEC's dynamics. The splitting in two arrows at an avoided crossing illustrates the fact that a part of the BEC can tunnel into the upper band. Figure 2.4b shows the probability for the BEC to remain in the ground band versus time. We observe that each time the BEC reaches an avoided crossing (at $t/T_B=0.5$ and 1.5) a part of the condensate tunnels into the upper energy band; the tunnelling probability can be calculated with the LZ model. The steplike structure of the data also reveals that between avoided crossings the probability to stay in the ground band remains constant, indicating that Eq.(2.16) holds. Moreover, the time between two avoided crossings equals one Bloch period, as predicted. In case of an initial momentum distribution that is not well localised in momentum space, the step structure in figure 2.4b is lost and the decay happens gradually [5].

2.2.2 Mapping the WSS onto the Landau-Zener (LZ) model

In this section, it is shown that the translational invariance of the Hamiltonian of Eq.(2.7) can be recovered by applying a gauge transformation. Then this 'new' Hamiltonian is rewritten in the momentum basis and its matrix representation is used to approximate the system's dynamics around an avoided crossing. This will lead to the Landau-Zener model [17].

Recall that the full Schrödinger equation of the system reads,

$$i\partial_t\psi = \left(-\frac{1}{2}\partial_x^2 + V_0 \cos(x) - F_0x \right) \psi . \quad (2.19)$$

Application of the gauge transformation $\psi = e^{iF_0xt}\tilde{\psi}$ leads to

$$\left(i\partial_t\tilde{\psi} - F_0x\tilde{\psi}\right) e^{iF_0xt} = -\frac{1}{2}\left(\partial_x^2\tilde{\psi} + 2iF_0t\partial_x\tilde{\psi} - F_0^2t^2\tilde{\psi}\right) e^{iF_0xt} \quad (2.20)$$

$$+ (V_0 \cos(x) - F_0x)\tilde{\psi}e^{iF_0xt} . \quad (2.21)$$

Cancellation of like terms on both sides and division by e^{iF_0xt} then gives,

$$i\partial_t\tilde{\psi} = \frac{1}{2}(-i\partial_x + F_0t)^2\tilde{\psi} + V_0\cos(x)\tilde{\psi} \quad (2.22)$$

$$= \frac{1}{2}(\hat{p} + F_0t)^2\tilde{\psi} + V_0\cos(x)\tilde{\psi} , \quad (2.23)$$

where $-i\partial_x$ has been identified as the momentum operator \hat{p} . So the Hamiltonian of our system is now given by,

$$\hat{H} = \frac{1}{2}(\hat{p} + F_0t)^2 + V_0\cos(x) . \quad (2.24)$$

Physically the above transformation corresponds to the change of the frame of reference from the lab system into the accelerated reference frame of the lattice.

For further analysis it is advantageous to rewrite the above Hamiltonian in its momentum basis. To do this, the momentum operator \hat{p} is expanded in terms of its eigenvalues and eigenstates and the identity $\int_x dx|x\rangle\langle x| = \mathbb{1}$ is inserted. This leads to,

$$\hat{H} = \int_p dp \frac{1}{2}(p + F_0t)^2 |p\rangle\langle p| + \int_x dx V_0 \cos(x) |x\rangle\langle x| , \quad (2.25)$$

where the integrations run over all possible momentum and position eigenstates, respectively. The first term of this equation is already in terms of the momentum eigenstates; let us proceed by also writing the second term in the momentum basis:

$$\begin{aligned} \int_x dx V_0 \cos(x) |x\rangle\langle x| &= \frac{V_0}{4\pi} \int_x \int_p \int_{p'} dx dp dp' (e^{ix} + e^{-ix}) e^{-ipx} |p\rangle\langle p'| e^{ip'x} \\ &= \frac{V_0}{4\pi} \int_p \int_{p'} dp dp' |p\rangle\langle p'| \int_x dx \left(e^{-ix(p-1-p')} + e^{-ix(1+p-p')} \right) e^{-ipx} e^{ip'x} \\ &= \frac{V_0}{2} \int_p \int_{p'} dp dp' |p\rangle\langle p'| (\delta(p-1-p') + \delta(1+p-p')) \\ &= \frac{V_0}{2} \int_p dp (|p\rangle\langle 1+p| + |p\rangle\langle 1-p|) \\ &= \frac{V_0}{2} \int_p dp (|p\rangle\langle 1+p| + |1+p\rangle\langle p|) . \end{aligned} \quad (2.26)$$

In the above calculation the definition of the delta-function $\int_x dx \frac{e^{ipx}}{2\pi} = \delta(p)$ and the fact that momentum and position eigenstates are related via $|x\rangle = \int_p dp \frac{e^{-ipx}}{\sqrt{2\pi}} |p\rangle$ ³ have been used. The Hamiltonian of Eq. (2.24) is now of the following form,

$$\hat{H} = \int_p dp \frac{1}{2} \left[(p + F_0t)^2 |p\rangle\langle p| + V_0 (|p\rangle\langle 1+p| + |1+p\rangle\langle p|) \right] . \quad (2.27)$$

³The missing ' \hbar ' is due to the dimensionless units used here.

2.3 The Landau-Zener model

The Landau-Zener (LZ) model is one of the archetypal models to study quantum transport phenomena in a variety of fields, ranging from solid-state physics to ultracold atoms in accelerated optical lattices or even electron transfer in chemical reactions. In fact, ultracold atoms in accelerated optical lattices provide an excellent experimental setup to test the theoretical predictions of the model [17]. The Landau-Zener theory itself has been developed independently by Landau, Zener, Stückelberg and Majorana in 1932 [28–31].

In this section basic results about the Landau-Zener model are reviewed and its applicability limits to the WSS are discussed.

2.3.1 Transition probabilities and important time scales

As has been pointed out in the previous section, the Hamiltonian of the Landau-Zener model is given by Eq.(2.32). Hence, the system is governed by the the time-dependent Schrödinger equation,

$$i\partial_t|\psi\rangle = \frac{1}{2} \begin{pmatrix} -F_0t & V_0 \\ V_0 & F_0t \end{pmatrix} |\psi\rangle, \quad (2.33)$$

from which it is evident that this is a two-state system. Henceforth, the ground state of the system is denoted by $|1\rangle$ and the first excited state by $|2\rangle$. The most important features of the Landau-Zener Hamiltonian are the linearity of the diagonal terms with respect to time and the constant off-diagonal coupling terms. Due to the explicit time dependence, the Hamiltonian does not possess proper energy eigenvalues and eigenvectors; however, it is possible to write down the *instantaneous* eigenvalues/-vectors by diagonalising it:

$$E_{1,2} = \mp \frac{1}{2} \sqrt{(F_0t)^2 + V_0^2} \quad (2.34)$$

with

$$|1\rangle_a = \begin{pmatrix} \frac{-Ft + \sqrt{(F_0t)^2 + V_0^2}}{V_0} \\ 1 \end{pmatrix} \quad \text{and} \quad |2\rangle_a = \begin{pmatrix} \frac{-Ft - \sqrt{(F_0t)^2 + V_0^2}}{V_0} \\ 1 \end{pmatrix}, \quad (2.35)$$

where the ‘1’ and ‘2’ correspond to the lower and higher energy level. The subscript ‘a’ indicates that this is the adiabatic basis of the system. The states for the diabatic basis $|1\rangle_d$ and $|2\rangle_d$ are trivially obtained from Eq.(2.32) with $V_0 = 0$, as $|1\rangle_d = \begin{pmatrix} 1 \\ 0 \end{pmatrix}$ and $|2\rangle_d = \begin{pmatrix} 0 \\ 1 \end{pmatrix}$. Evidently, the non-zero off-diagonal terms lead to a splitting of the energy levels at $t = 0$ and thus give rise to an avoided crossing with a band gap of $\Delta E = V_0$, at $t = 0$.

In close analogy to the discussion in section 2.2.1, one can intuitively understand the system’s dynamics by means of the adiabatic approximation. Assuming the system is initially prepared in its ground state at $t = -\infty$, the adiabatic approximation tells us

that for an infinitely slow evolution (vanishing F_0) the system will remain in its ground state.

On the other hand, if F_0 is finite, tunnelling between the bands is possible and there is a finite probability to find the system in its first excited state after the evolution. A large band gap at $t = 0$ (big V_0) will, however, suppress the tunnelling probability. Those considerations are reflected in the famous Landau-Zener formula for the survival probability in the ground state [28]:

$$P_{\text{sur}}(t = \infty) = 1 - e^{-\frac{\pi}{\gamma}}, \quad (2.36)$$

where the *adiabaticity parameter* $\gamma = \frac{2F_0}{V_0^2}$ has been introduced and the evolution started in $|1\rangle_{\text{d,a}}$ at $t = -\infty$. The same equation is valid if one starts out in the first excited band.

The problem can also be solved for arbitrary times in terms of the parabolic cylinder functions, however the formulas for the diabatic and adiabatic basis are not the same for a finite evolution times [32]. Vitanov analysed the transition probability in both, the adiabatic and diabatic basis [32, 33].

In the following, numerical results obtained by Vitanov are reproduced and shown in figures 2.5 and 2.6. To obtain the time evolution of the transition probabilities, Eq.(2.33) has been integrated numerically over the time interval as shown in the figures. Details on the numerical method are given in section 4.1.

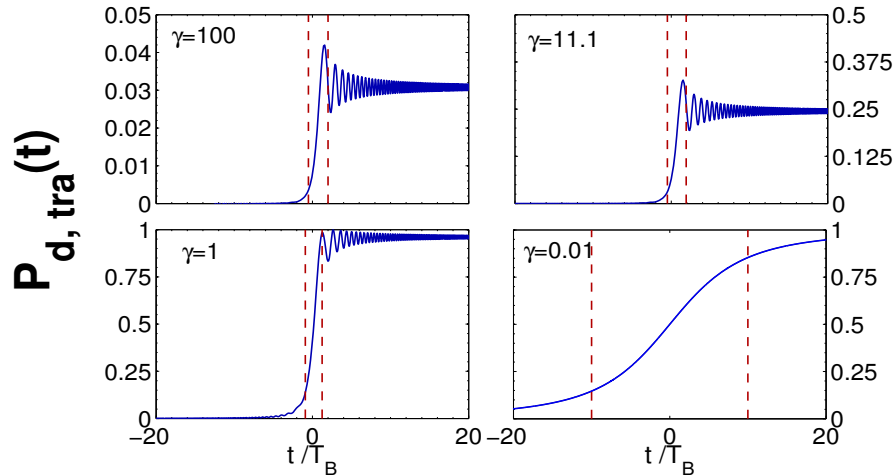


Figure 2.5: The figures show the time evolution of the transition probability (blue solid line) in the diabatic basis (‘remain in ground band’) for different values of the adiabaticity parameter γ . The red dashed lines show the regions where the transitions occur. The widths of those regions are given by the jump times. Their starting points are defined by the points where the tangents of $P_{\text{tra,d}}(t = 0)$ intersect with the x-axis; while its end points are defined by the points where the tangents of $P_{\text{tra,d}}(t = 0)$ reach the asymptotic value of the transition probabilities.

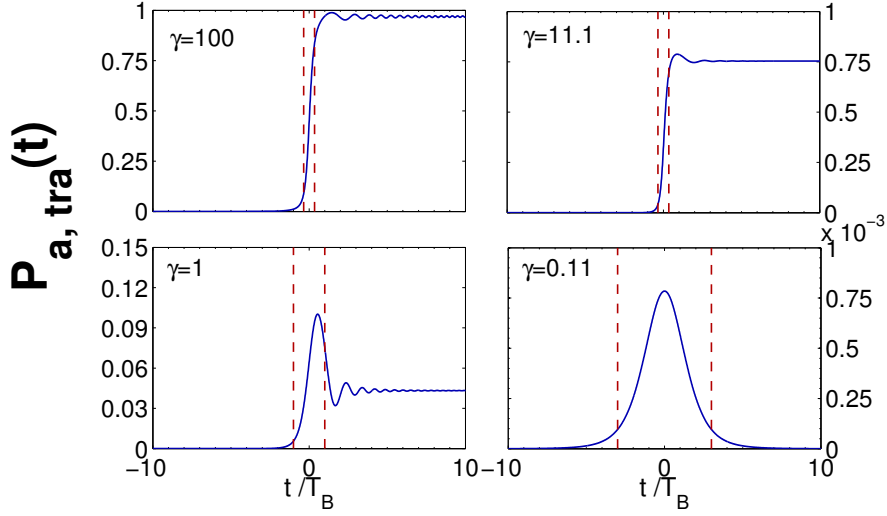


Figure 2.6: The figures show the time evolution of the transition probabilities (blue solid lines) in the adiabatic basis (‘tunnel to upper band’) for different values of the adiabaticity parameter γ . The red dashed lines show the regions where the transitions occur, they are centred around 0 and their widths correspond to the jump times.

Note that the oscillations around the asymptotic value of the transition probabilities in the diabatic basis (figure 2.6) are much less pronounced than in the diabatic basis (see figure 2.5). Yet, their asymptotic values agree in the sense that $P_{\text{tra,d}}(t = \infty) + P_{\text{tra,a}}(t = \infty) = 1$. It is obvious from the above figures that Landau-Zener transitions are not instantaneous processes but rather take place during a finite time interval around $t = 0$. Defining this transition time, hereafter called jump time, in a meaningful way is not an easy task, but Vitanov introduced a reasonable measure [33]. He defines the diabatic/adiabatic jump time via the asymptotic value of the transition probability and the derivative of the transition probability at $t = 0$ such that,

$$T_{\text{d/a}}^{\text{jump}} = \frac{P_{\text{d/a}}(\infty)}{P'_{\text{d/a}}(0)}. \quad (2.37)$$

Using the parabolic cylinder functions Vitanov derived analytical expressions for the jump times. The diabatic jump time can be approximated by $T_{\text{d}}^{\text{jump}} = \sqrt{2\pi}$ for $\gamma \gg 1$ and $T_{\text{d}}^{\text{jump}} = 2\gamma^{-1/2}$ for $\gamma \ll 1$, the adiabatic one can be estimated to be $T_{\text{a}}^{\text{jump}} = 2\gamma^{-1/2}$ for $\gamma \gg 1$ and $T_{\text{a}}^{\text{jump}} \propto \gamma^{-1/6} e^{\pi/(\gamma^6)}$ for $\gamma \ll 1$.

Furthermore, there exists a second important time scale associated with LZ transitions; namely the time after which the oscillations of the transition probabilities die out. This time is called the relaxation time $T_{\text{d/a}}^{\text{relax}}$ and Vitanov defines it as the time it takes

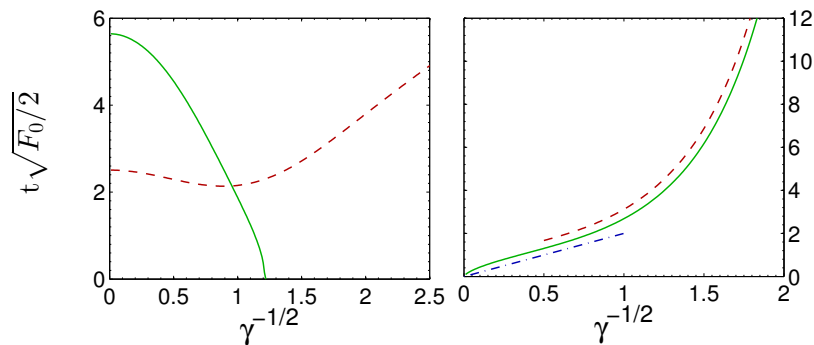


Figure 2.7: Jump and relaxation times for the diabatic and adiabatic basis. The left figure shows the jump time (red dashed line) and relaxation time (solid green line) in the diabatic basis. The figure on the right shows those times in the adiabatic basis, the blue dashed-dotted line represents the jump time for $\gamma \gg 1$ and the red dashed line shows the jump time for $\gamma \ll 1$. The solid green line gives the relaxation time in the adiabatic basis.

(starting from $t = 0$) for the oscillation amplitude to decay to $\epsilon P_{d/a}(\infty)$ where $\epsilon \ll 1$. Vitanov calculated the times to be

$$T_d^{\text{relax}} \approx \gamma^{-1/2} \sqrt{\frac{1}{\epsilon^2(e^{\pi/\gamma} - 1)} - 1} \quad \text{and} \quad T_a^{\text{relax}} \approx \gamma^{-1/2} \sqrt{\left(\frac{(e^{\pi/\gamma} - 1)\gamma^2}{4\epsilon^2}\right)^{1/3} - 1}. \quad (2.38)$$

It can be seen in figure 2.7 that the relaxation time in the diabatic basis quickly decays to zero for large $\gamma^{-1/2}$, whereas it increases exponentially in the adiabatic basis. Note that the plots are in units of Vitanov's rescaled time $t\sqrt{F_0}/2$, to convert to the usual time unit t/T_B Vitanov's time has to be multiplied by $\sqrt{2F_0}$.

2.3.2 Applicability limits of the Landau-Zener model

In reality the applicability of the LZ formula is limited as any practical experiment can only be observed over a finite time period. It is thus necessary to find out under which conditions the transition time can be safely assumed to be infinite. For a specific system this means one has to compare the time scales of the system, with the time scales (jump and relaxation time) of the LZ model.

In the case of the WSS the time scale is set by the Bloch period T_B , because every Bloch period the BEC arrives at an avoided crossing. Hence if the jump time in the LZ model exceeds one Bloch period we expect the LZ approximation to break down. Therefore one can introduce the condition

$$T_{\text{jump}} < T_{\text{Bloch}}, \quad (2.39)$$

as a first indicator of the applicability of the LZ model. Furthermore it was shown in the previous section that the transition probabilities exhibit oscillations around their

asymptotic value. To ensure convergence of the transition probabilities the relation $T_{\text{relax}} < T_{\text{Bloch}}$ should therefore hold as well. Fortunately, those conditions can be easily satisfied in experiments [5, 17].

In addition to the issues addressed above, there is another phenomena arising in the WSS that cannot be described separate by LZ transitions. It is, for example, possible that at an avoided crossing a fraction of the BEC tunnels into the first excited band, evolves in that band and then interferes at the next avoided crossing with the fraction that remained in the ground band. The two fractions gather a phase difference of $\phi = \int_0^{T^B} i(E_2(k(t)) - E_1(k(t)))dt$ and depending on the value of ϕ , can interfere constructively or destructively, albeit changing the transition probabilities [34]. However, if the depth of the optical lattice V_0 is shallow enough such that the energy spectrum turns into a continuum after the first two bands, the BEC will immediately tunnel from the second to the third band etc. and escape the potential. In this case there should not be any interference effects. This can be ensured by choosing the potential depth $V_0 \ll 1$, because band gaps between higher bands scale as V_0^n , where $n > 1$ [8].

There exists another phenomenon that can enhance the tunnelling probabilities called *resonantly enhanced tunnelling*. In essence resonantly enhanced tunnelling occurs when the energy difference between neighbouring lattice sites (remember figure 2.1) coincides with the average⁴ band gap of the untilted system [34]. Unfortunately, a proper discussion of this phenomenon and the so-called Wannier-Stark ladder states [22] goes beyond the scope of this thesis and will not be considered here. Hereafter, unless stated otherwise, it is assumed that the system is ‘off resonance’.

2.4 Harmonic Noise

The advent of the analysis of noise/stochastic processes in physical systems can be dated back to Einstein’s famous work on Brownian motion [35]. Since then, there has been a vast amount of work on the subject and stochastic processes are widely used throughout different fields of physics. Not only can many phenomena such as Brownian motion only be understood in terms of stochastic processes, but any experimentally realisable system is subject to stochastic fluctuations too. Hence a thorough understanding of the system requires in many cases the inclusion of stochastic processes in the analysis.

From an experimentalists point of view it seems natural to keep those stochastic fluctuations to a minimum to obtain reliable data. However, it has been shown that it is possible to use stochastic processes to *control* the system as well [36]. As mentioned in the introduction, this influenced earlier research in the group by Tayebirad and co-workers. In the following, the main features that characterise a stochastic process are introduced and the specific process used by Tayebirad *et. al.* is discussed.

Consider a stochastic variable $\xi(t)$, where t stands for time. The most important features of the variable $\xi(t)$ can be characterised by its first ($\langle \xi \rangle$) and second moments

⁴Here average is understood as the average over the first Brillouin zone

$\langle \xi^2 \rangle$), its autocorrelation ($R(h)$) and its power spectrum ($S(\omega)$). One defines those quantities as

$$\langle \xi \rangle = \lim_{T \rightarrow \infty} \frac{1}{T} \int_0^T \xi(t) dt \quad \text{and} \quad \langle \xi^2 \rangle = \lim_{T \rightarrow \infty} \frac{1}{T} \int_0^T \xi(t)^2 dt , \quad (2.40)$$

$$R(h) = \langle \xi(t)\xi(t+h) \rangle = \lim_{T \rightarrow \infty} \frac{1}{T} \int_0^T \xi(t)\xi(t+h) dt \quad \text{and} \quad S(\omega) = \frac{1}{2\pi} \int_{-\infty}^{\infty} e^{-i\omega h} R(h) dh . \quad (2.41)$$

Note that the above definitions assume that the stochastic process is *ergodic*, which means that the ensemble average over the static probability density distribution ($P(\xi)$) underlying $\xi(t)$ can be replaced by the time average over the stochastic variable $\xi(t)$ [37], i.e.

$$\langle \xi \rangle = \int_{\text{all } \xi} \xi P(\xi) d\xi = \lim_{T \rightarrow \infty} \frac{1}{T} \int_0^T \xi(t) dt . \quad (2.42)$$

This relation holds for functions of ξ as well (given that the process is ergodic).

In this thesis, emphasis will be placed on a stochastic process called *harmonic noise* (hereafter denoted by $\phi(t)$). Harmonic noise can be thought of as the amplitude of a *damped harmonic oscillator* driven by *gaussian white noise* and is defined via the two coupled stochastic differential equations (SDEs) [38],

$$\partial_t \phi = \mu \quad (2.43)$$

$$\partial_t \mu = -2\Gamma\mu - \omega_0^2 \phi + \sqrt{4\Gamma T} \xi(t) , \quad (2.44)$$

where Γ corresponds to a damping coefficient in units of frequency and ω_0 sets the characteristic frequency of the noise process and T determines the noise strength and is given in units of frequency squared. $\xi(t)$ represents gaussian white noise and has the following properties:

$$\langle \xi(t) \rangle = 0 , \quad \langle \xi(t)\xi(t+h) \rangle = \delta(h) , \quad S(\omega) = \frac{2\Gamma T}{\pi} . \quad (2.45)$$

From the above properties it is evident that gaussian white noise is very unphysical because its constant power spectrum implies an infinite amount of energy for finite T . Nevertheless, it is the standard noise model to construct other types of noise such as harmonic noise. In principle the two coupled SDEs can be solved by applying the formalism of stochastic calculus⁵. Alternatively harmonic noise can be generated by an numerical algorithm (see appendix section 7.1 and figure 2.8).

Harmonic noise has not been given much attention in the literature and might seem to be a peculiar choice, but the reason for this choice becomes apparent after investigating

⁵The interested reader is referred to [39].

its power spectrum. The static probability density distribution of the noise is known to be a bivariate gaussian [36, 38],

$$P(\phi, \mu) = \frac{e^{-\frac{\phi^2 \omega_0^2}{2T}}}{(2\pi T/\omega_0^2)} \frac{e^{-\frac{\mu^2}{2T}}}{(2\pi T)} . \quad (2.46)$$

Starting from this distribution the first and second moments of the variables ϕ and μ can be derived as [36, 38],

$$\langle \phi \rangle = 0 , \langle \mu \rangle = 0 , \langle \phi^2 \rangle = \frac{T}{\omega_0^2} \text{ and } \langle \mu^2 \rangle = T . \quad (2.47)$$

The autocorrelations and cross-correlation between ϕ and μ also follow,

$$\begin{aligned} \langle \phi(t)\phi(t+h) \rangle &= \langle \phi^2 \rangle e^{-\Gamma h} \left(\cos(\omega_1 h) + \frac{\Gamma}{\omega_1} \sin(\omega_1 h) \right) , \\ \langle \mu(t)\mu(t+h) \rangle &= \langle \mu^2 \rangle e^{-\Gamma h} \left(\cos(\omega_1 h) + \frac{\Gamma}{\omega_1} \sin(\omega_1 h) \right) , \\ \langle \mu(t)\phi(t+h) \rangle &= \frac{T}{\omega_1} e^{-\Gamma h} \sin(\omega_1 h) , \end{aligned} \quad (2.48)$$

with $\omega_1 = \sqrt{\omega_0^2 - 2\Gamma^2}$. Finally, the power spectrum with respect to ϕ is given by,

$$S_\phi(\omega) = \frac{2\Gamma T}{\pi (4\Gamma^2 \omega^2 + (\omega^2 - \omega_0^2)^2)} . \quad (2.49)$$

The definition of ω_1 indicates that the properties of the harmonic noise fall into three classes, one in which $\omega_0 < \sqrt{2}\Gamma$, one where $\omega_1 = 0$ and one where $\omega_0 > \sqrt{2}\Gamma$ [8, 38]. In the first regime the parameter ω_1 is imaginary and the autocorrelations and cross-correlation lose their oscillatory behaviour, as $\cos(iz)/(\sin(iz)) = \cosh(z)/(i \sinh(z))$ with $z \in \mathbb{R}$ and neither \cosh nor $i \sinh$ are periodic functions. The same holds true for the second regime as $\sin(0) = 0$ and $\cos(0) = 1$, with the difference that the cross-correlation function vanishes. Still, in the third regime ω_1 is real and the correlation functions retain their oscillatory behaviour. In the case of a harmonic oscillator those classes correspond to the overdamped, critically damped and underdamped cases. The implications of this on the power spectrum and specific noise realisation are best illustrated by plotting them in figure 2.8.

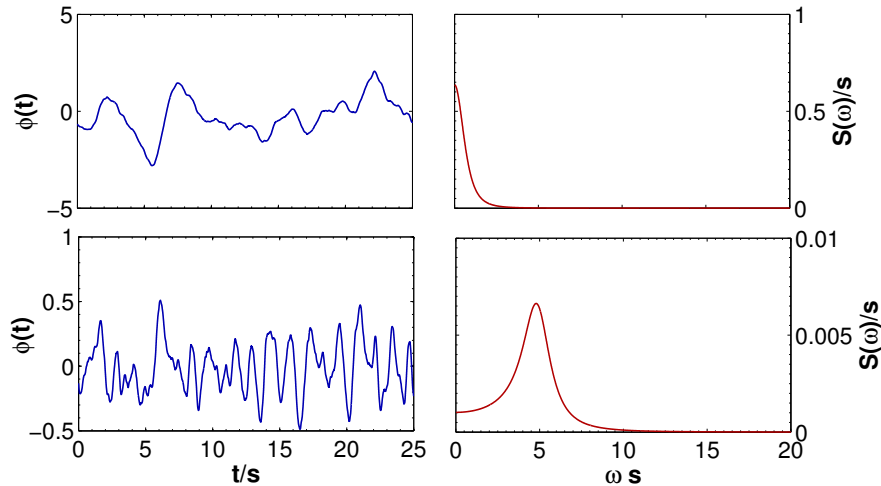


Figure 2.8: The figures at the top show typical harmonic noise amplitudes $\phi(t)$ (left) and power spectra $S(\omega)$ (right) for the overdamped ($\Gamma = 1.0/s$, $T = 1.0/s^2$, $\omega_0 = 1.0$) case. The figures at the bottom show the same quantities for the underdamped case ($\Gamma = 1.0/s$, $T = 1.0/s^2$, $\omega_0 = 5.0/s$). The ‘s’ stands for the SI-unit ‘second’. The critically damped case has been omitted as there exists no qualitative difference to the overdamped one.

It is apparent from figure 2.8 that the power spectra in the over- and underdamped case look very different and so do the noise amplitudes. In the overdamped case the noise amplitude fluctuates ‘quite’ slowly and the power spectrum decays exponentially. On the other hand in the underdamped case the noise amplitude fluctuates much more rapidly and the power spectrum shows a clear peak (at $\omega_1 = |\sqrt{-24}|$). The peak in the spectrum is a very general feature of the underdamped regime and always occurs at ω_1 with an approximate full width at half maximum of 2Γ for $\frac{\Gamma}{\omega_0} \ll 1$. Furthermore, it is exactly the peaked spectrum in the underdamped regime that makes harmonic noise worthwhile studying. In classical systems it has been shown [36] that the peaked spectrum at a characteristic frequency can lead to resonance phenomena. The thriving question for Tayebirad *et. al.* was if such resonance phenomena will also appear in the quantum mechanical system introduced in the next section.

As an aside, the evolution of the noise amplitude and the shape of the power spectrum in the overdamped case is very similar to another important class of noise processes, called *exponentially correlated noise*. This is also true for the critically damped regime. As the name suggests the autocorrelation function and the power spectrum of exponentially correlated decay exponentially.

3 Introducing noise into the system

In the previous chapter the Wannier-Stark system has been introduced and a procedure has been given that shows how one can map the BEC's dynamics around an avoided crossing onto a Landau-Zener model. All of the material presented has been studied in depth in the literature [17]. This chapter will be used to introduce the modified Wannier-Stark system (WSS) that will be analysed in this thesis. The Hamiltonian that governs the system studied in this thesis is given and an effective Landau-Zener (LZ) model is deduced from it.

3.1 Adding a second, stochastic optical lattice

Tayebirad *et. al.* modified the original Wannier-Stark system by adding a second cosinusoidal potential that has a different spatial periodicity than the first one and is influenced by a stochastic, time-dependent phase shift. The Hamiltonian of this new system is given by,

$$\hat{H}_{Tayebirad} = -\frac{1}{2}\partial_x^2 + V_0 \cos(x) + V_0 \cos(\alpha x + \phi(t)) - F_0 x , \quad (3.1)$$

where α is chosen such that the periodicities of the two potentials are incommensurable and $\phi(t)$ represents a stochastic phase shift, given by the harmonic noise variable introduced in the previous section. Hence, one obtains a potential that is intrinsically aperiodic (due to the incommensurability) and subject to stochastic fluctuations in time and space (due to the phase shift). Tayebirad *et. al.* analysed this system in the context of BECs in optical lattices. As an observable she chose the time evolution of the survival probability in the ground band as outlined in chapter 2 and analysed it for different noise parameters.

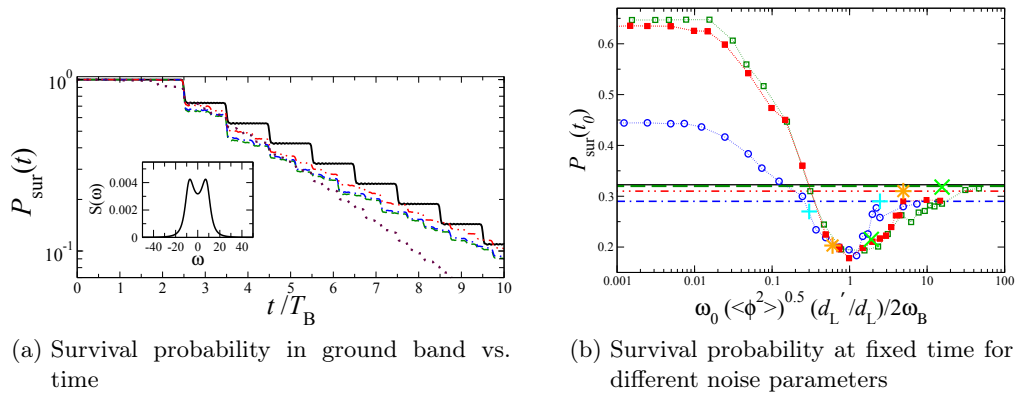


Figure 3.1: Fig.(a) shows the survival probability of the BEC in the ground band versus time. The black solid line is the curve for the noiseless system (Hamiltonian 2.7), the dashed/dotted coloured lines represent the ‘noisy’ system Eq.(3.1) for different noise parameters. Note that the step structure (see figure 2.4b) is destroyed by the noise process. Fig.(b) shows the survival probability in the ground band at fixed time $t_0 = 6T_B$ versus the rescaled noise frequency ω_0 . $\langle\phi^2\rangle$ is the variance of the noise process, ω_B the Bloch frequency and (d'_L/d_L) represents α of Eq.(3.1). The curved lines showing the minimum are numerical simulations of the full system for $F_0 = 0.029$, $\Gamma = 5/T_B$, $\langle\phi^2\rangle = 0.25$ and changing V_0 . $V_0 \approx 0.15625$ (green open squares), $V_0 \approx 0.15625 \times 0.99$ (red filled squares) and $V_0 \approx 0.15625 \times 0.85$ (blue open circles). The horizontal lines are calculations based on an effective model that will not be used in this thesis. The ‘+’, ‘ \times ’ and ‘*’ symbols are of no importance here. Data from [6], courtesy of the corresponding authors ©APS.

The most striking feature of figure 3.1b is the universal behaviour of the different curves in the sense that they all show a minimum at a rescaled angular noise frequency of unity. This demonstrates that the inclusion of a second ‘noisy’ potential can indeed be used to control the transition probabilities of a BEC by changing the noise parameters.

In order to gain a better understanding of the influence of the noise process, the question arose if the dynamics of the system in Eq.(3.1) can still be locally approximated by a LZ model and if it is possible to explain the minimum in the survival probability observed figure 3.1b. This question will be addressed in the rest of this thesis and represents, to the author’s best knowledge, a new contribution to the study of ‘noisy’ WSSs.

3.2 The modified Landau-Zener model

In the following, a modified LZ model for the Hamiltonian in Eq. (3.1) is presented. In the analysis to come the parameter α is set to one and hence the intrinsic aperiodicity of the potential stemming from α is removed. That this is possible without completely changing the systems dynamics is not *a priori* clear, but numerical simulations have

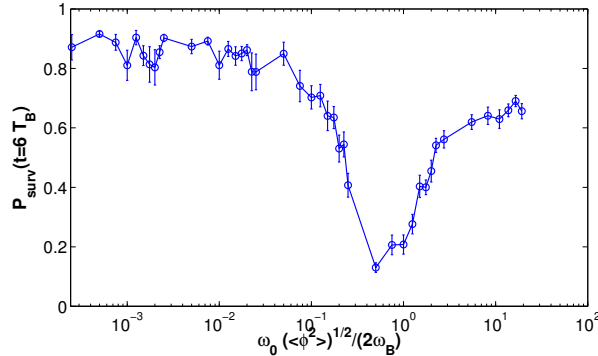


Figure 3.2: The figure shows the same quantities as figure 3.1b but with a ratio of $\frac{d_L}{d_L}$ equal to one. Otherwise the same parameters as for the green open squares in figure 3.1b have been used.

shown that the curves in figure 3.1b retain their shape (figure 3.2). Thus the important feature of the system is the noise term and not the incommensurability of the two lattices 3.2. The Hamiltonian of the system for $\alpha = 1$ simplifies to

$$\hat{H}_{Noise} = -\frac{1}{2}\partial_x^2 + V_0 (\cos(x) + \cos(x + \phi(t))) - F_0 x . \quad (3.2)$$

Moreover, the simplification, $\alpha = 1$, is crucial to be able to locally approximate the system by a two state model. If α deviates from unity the above Hamiltonian also couples momentum states p such that $\Delta p = p - p' \notin \mathbb{Z}_0^1$ and the matrix representation of the Hamiltonian loses its tridiagonal shape. Thus, at least a 3-by-3 or 4-by-4 matrix is needed to locally approximate the BEC's dynamics around an avoided crossing.

Assuming $\alpha = 1$ and following the procedure given in section 2.2.2, the BEC's dynamics around an avoided crossing can be approximated by a modified LZ model. The 2-by-2 Hamiltonian is then given by,

$$\hat{H}_{LZ,N} = \frac{1}{2} \begin{pmatrix} -F_0 t & V_0(1 + e^{i\phi(t)}) \\ V_0(1 + e^{-i\phi(t)}) & F_0 t \end{pmatrix} . \quad (3.3)$$

Note that the harmonic noise variable ϕ now appears as a complex phase factor, as one would expect from standard Fourier theory (recall that in section 2.2.2, we re-expressed the Hamiltonian in its momentum basis). It is important to recognise that the appearance of this phase means that the off-diagonal terms not only carry an explicit time dependence, but also are stochastic variables! This makes the definition of an eigenbasis of the Hamiltonian 3.3 even more difficult.

In analogy to section 2.2.2, the instantaneous eigenstates/-values have been obtained by diagonalising the 2-by-2 matrix given above;

$$E_{N;1,2} = \mp \frac{1}{2} \sqrt{(F_0 t)^2 + 2V_0^2(\cos(\phi(t)) + 1)} , \quad (3.4)$$

¹Compare to section 2.2.2

with

$$|1\rangle_{N;a} = \begin{pmatrix} \frac{-Ft + \sqrt{(F_0t)^2 + 2V_0^2(\cos(\phi(t)) + 1)}}{V_0(1 + e^{-i\phi(t)})} \\ 1 \end{pmatrix} \text{ and } |2\rangle_{N;a} = \begin{pmatrix} \frac{-Ft - \sqrt{(F_0t)^2 + 2V_0^2(\cos(\phi(t)) + 1)}}{V_0(1 + e^{-i\phi(t)})} \\ 1 \end{pmatrix}, \quad (3.5)$$

where the subscript N stands for the noisy system and all the others have their usual meaning. Hence, at $t = 0$ the gap between the two energy levels is $\Delta E = V_0\sqrt{2(\cos(\phi(0)) + 1)}$. Using the static probability distribution of Eq. (2.46) an effective band gap can be introduced such that

$$\Delta E_{eff} = V_0 \left[\langle \sqrt{2(\cos(\phi(0)) + 1)} \rangle \pm \text{Std} \left(\sqrt{2(\cos(\phi(0)) + 1)} \right) \right]. \quad (3.6)$$

Here $\langle f(\phi) \rangle$ denotes the average as introduced in Eq. (2.47) and ‘Std’ denotes the standard deviation defined as $\sqrt{\langle f(\phi)^2 \rangle - (\langle f(\phi) \rangle)^2}$. The actual value of this effective bandgap depends on the noise parameters T, Γ and ω_0 . Accordingly, an effective adiabaticity parameter can be defined as $\gamma_{eff} = \frac{2F_0}{\Delta E_{eff}^2}$.

Furthermore it is crucial to note that the instantaneous eigenstates and -values are now stochastic variables as well. This means that the adiabatic ‘basis’ does not exist anymore as it would assume different values for *each* noise realisation! This is one of the reasons why all of the numerical calculations in the next chapter of this thesis are carried out in the diabatic basis of the system, which obviously (it is the free particle basis) is the same as in the noiseless case.

There are two more things that should be mentioned in this chapter. First, almost all of the derivations in chapter 2 were based on the fact that the potential was periodic in space and one could thus use the Bloch ansatz to find the energy spectrum of the system. Of course, this is in principal not possible for an aperiodic potential. Setting α to one eases this problem. Unfortunately, the second potential still leads to aperiodicity due to the stochastic phase, but if the noise process is not too strong, its influence can be imagined as a small perturbation to the otherwise periodic potential. Secondly, after setting $\alpha = 1$, it is not clear why the second potential is still needed and why the stochastic phase is not applied to the first potential term. The reason is that for high ω_0 the phase term fluctuates on a much shorter time scale than the one of the system. In such a scenario it is allowed to average the potential over the noise distribution to obtain an effective potential [6]. The depth of this effective potential will be greatly reduced and the BEC thus be able to escape from the trap. One therefore needs two potentials, one that fluctuates due to the stochastic phase and another one as reference system that ensures that the BEC does not simply escape the trap.

4 Numerical investigation

This chapter deals with the numerical simulation of the ‘noisy’ Landau-Zener (LZ) model given in Eq.(3.3). The main focus lies on the computation of the diabatic transition probability and its dependence on the noise parameter ω_0 . In the first part of this chapter the numerical methods to obtain these transition probabilities are explained. In the second part, the main results of this thesis are presented. Numerical results for the diabatic transition probabilities, as obtained from the ‘noisy’ LZ model are given. Moreover, they are compared to those obtained from a simulation of the full ‘noisy’ Wannier-Stark system (WSS) (3.2). The chapter will end with an interpretation of the results and a brief comparison to an effective model, in which the harmonic noise variable ϕ is replaced by a deterministically oscillating phase [6].

4.1 Numerical methods

In principle, the calculation of the transition probability from the ground to the first excited band, or vice versa, is quite simple. All that is needed is to specify an initial state $|\psi(t = t_0)\rangle$ and evolve it according to the corresponding Schrödinger equation. The transition probability is then obtained by projecting the evolved state $|\psi(t)\rangle$ onto one of the energy eigenstates of the system. Depending on the basis chosen, those can be the diabatic energy eigenstates or the adiabatic instantaneous eigenstates. Numerically, the calculation is not too hard for the LZ model, but becomes quite involved when simulating the full system. The numerical simulation of the ‘noisy’ LZ model can be done as follows.

The Schrödinger equation corresponding to the ‘noisy’ LZ Hamiltonian (Eq.(3.3)) reads,

$$i\partial_t|\psi(t)\rangle = \frac{1}{2} \begin{pmatrix} -F_0t & V_0(1 + e^{i\phi(t)}) \\ V_0(1 + e^{-i\phi(t)}) & F_0t \end{pmatrix} |\psi(t)\rangle, \quad (4.1)$$

where $|\psi(t)\rangle = a_1(t)|1\rangle + a_2(t)|2\rangle$. Thus, the evolution of the two expansion coefficients $a_1(t)$ and $a_2(t)$ is governed by two coupled differential equations,

$$i\partial_t a_1(t) = -F_0t a_1(t) + V_0(1 + e^{i\phi(t)}) a_2(t) \quad (4.2)$$

$$i\partial_t a_2(t) = V_0(1 + e^{-i\phi(t)}) a_1(t) + F_0t a_2(t). \quad (4.3)$$

Those two equations can be integrated numerically by specifying an initial state, $a_1(t_0)$ and $a_2(t_0)$. The probability of being in the ground state (first excited state) at time t is then given by $|a_1(t)|^2$ ($|a_2(t)|^2$).

In this thesis, the numerical integration has been carried out using a Cash-Karp Runge-Kutta¹ algorithm, as presented in [40]. In essence, all Runge-Kutta schemes advance the solution to a differential equation from an initial point $a_1(t_0)$ to the next point $a_1(t_0 + \Delta t)$ by calculating the derivative of $a_1(t)$ at the initial point, one or more trial midpoints between t and $t + \Delta t$ and at the final point $t + \Delta t$. Then those derivatives are multiplied by the step size Δt and a weighted average of all the terms is taken. The final point $a_1(t_0 + \Delta t)$ is obtained by adding the weighted average and the initial function value $a_1(t_0)$ (a detailed explanation of Runge-Kutta methods is omitted here, as it can be found in any text book on numerical methods or in [40]). In the case presented here the derivatives for all times t are given by Eq.(4.2) and Eq.(4.3).

Evidently, the derivatives in Eq.(4.2) and Eq.(4.3) depend explicitly on the harmonic noise amplitude $\phi(t)$. Thus to calculate these derivatives for all times t , the time series of $\phi(t)$ needs to be known. The algorithm and the code to generate a sample time series for $\phi(t)$ have been supplied by Stephan Burkhardt [8]. A short derivation of the algorithm can be found in the appendix, section 7.1.

In summary, the transition probabilities in this thesis have been calculated as follows:

- The initial state $|\psi(t = t_0)\rangle$ has been chosen as the diabatic ground state of the system $|1\rangle_d$.
- The initial state has been advanced to $t = t_0 + \Delta t$ and further, using a Cash-Karp Runge-Kutta algorithm applied to the differential equations Eq.(4.2) and Eq.(4.3); $\phi(t)$ has been calculated using the algorithm of section 7.1.
- At each time step, the new state $|\psi(t)\rangle$ has been projected onto the ground state of the system $|1\rangle_d$ to obtain $a_{1,d}(t)$; the transition probability has been calculated via $P_{d,tra}(t) = 1 - |a_{1,d}(t)|^2$.
- The asymptotic value of the transition probability as given by the LZ formula has been estimated by an average over $P_{d,tra}(t)$ from a time t' to the final integration time t_{final} . The time t' has been chosen as $t' = t_{\text{final}} - (0.05 \dots 0.1)t_{\text{int}}$ with t_{int} given by the total integration time $t_{\text{final}} - t_{\text{initial}}$.

The same procedure has been used to calculate the transition probabilities for the standard LZ model in chapter 2. To obtain the adiabatic transition probability for the standard LZ model one just has to start out in the adiabatic ground state and project

¹The reader familiar with numerical simulations might wonder why, after choosing the Cash-Karp Runge Kutta algorithm, no adaptive step-size routine has been employed. The reason lies in the harmonic noise variable $\phi(t)$. Because the sample path of $\phi(t)$ depends on the step size Δt , changing the step size each step also changes the noise properties in each step. This makes it hard to compare results. Of course, this could be circumvented by defining the sample path of $\phi(t)$ on a very fine grid (step size δt) and requiring that the Cash-Karp algorithm takes only steps that are integer multiples of δt . Thus for each time step the same noise realisation could be used. However, this adaptive method does not lead to a faster algorithm, because generating $\phi(t)$ is the most time consuming operation in our algorithm and $\phi(t)$ would still have to be defined on a very fine grid with fixed step size δt .

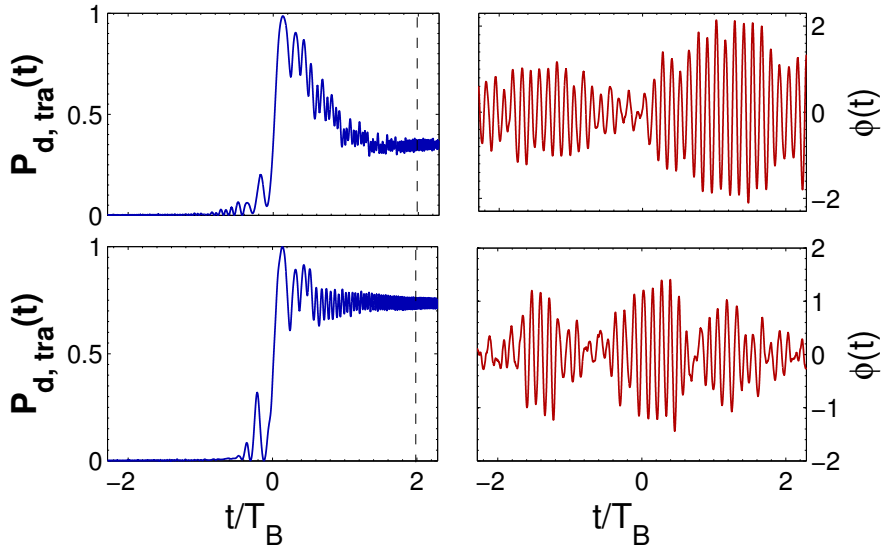


Figure 4.1: Diabatic transition probabilities (left figures) and their underlying noise processes (right figures) are shown for two sample realisations. The parameters were in both cases, $V_0 = 0.015625$, $F_0 = 0.00762$, $\Gamma = 0.00762$, $\omega_0/\omega_B = 8$ and $\langle \phi^2 \rangle = 0.5$. The time window to the right of the vertical line (left figures) is the one over which $P_{d,tra}(t)$ is averaged to estimate the asymptotic value of the transition probability.

onto the adiabatic basis after each time step (see Eq.(3.5)). Note that this cannot be easily done in the ‘noisy’ LZ model, as the instantaneous energy eigenstates are stochastic variables in this case (see section 3.2).

Figure 4.1 shows the diabatic transition probability for two different noise realisations (but same system parameters), as obtained with the procedure described above. It is noticeable that the transition probabilities show much stronger oscillations than in the noiseless case (see section 2.3). Additionally, the results for the two noise realisations are rather different, even though they were obtained for the same system parameters. To get statistically meaningful results it is thus necessary to take an average over different noise realisations. In the remainder of this thesis, emphasis will be placed on the asymptotic value of the diabatic transition probability. Due to the gaussian nature of the harmonic noise process, the average of the asymptotic value of the transition probability (denoted $P_{d,tra}$ from now on) can be estimated as,

$$P_{d,tra} = \frac{1}{N} \sum_{i=1}^N P_{d,tra}^{(i)}. \quad (4.4)$$

Here the sum runs over all noise realisations i . The standard deviation of this average can be estimated as [41]

$$\text{Std}(P_{d,tra}) = \frac{\sqrt{\sum_{i=1}^N (P_{d,tra}^{(i)} - P_{d,tra})^2}}{N}. \quad (4.5)$$

A few checks have been made to ensure numerical stability of the results. First, the normalisation of the state $|\psi(t)\rangle$ has been monitored throughout the simulation. The deviation of its magnitude from unity has been of the order 10^{-13} . Secondly, the results have been checked for various step sizes δt . Figure 4.2 (left) shows the time evolution of the transition probability for two step sizes $\Delta t = 0.0004$ and $\Delta t = 0.0002$ with the same underlying noise process. As there is no deviation between the two visible, a step size of $\Delta t = 0.0002$ is probably smaller than needed², yet all simulations that follow have been done with $\Delta t = 0.0002$. The results to come have all been checked on numerical convergence by these two criteria.

In addition to the above, the total integration time has been varied. In this case, it is actually not even expected to get the same results in the noiseless case, as the system might not have enough time to complete a full LZ transition. But this is then a physical property of the system and has nothing to do with numerics. However, even in the case where the system has enough time to evolve, the transition probability suddenly increases for high ω_0/ω_B . The point where this happens moves with increasing integration time and the phenomenon strongly resembles the increase of the transition probability, as observed in the full ‘noisy’ WSS (see figure 3.1b). A qualitative explanation of this effect will be given in the conclusion, as emphasis is placed on the initial decrease and the minimum of the transition probability ((see figure 3.1b again) in this chapter. Note that all simulations in section 4.2.2 would show this increase if the graphs were displayed for higher ω_0/ω_B .

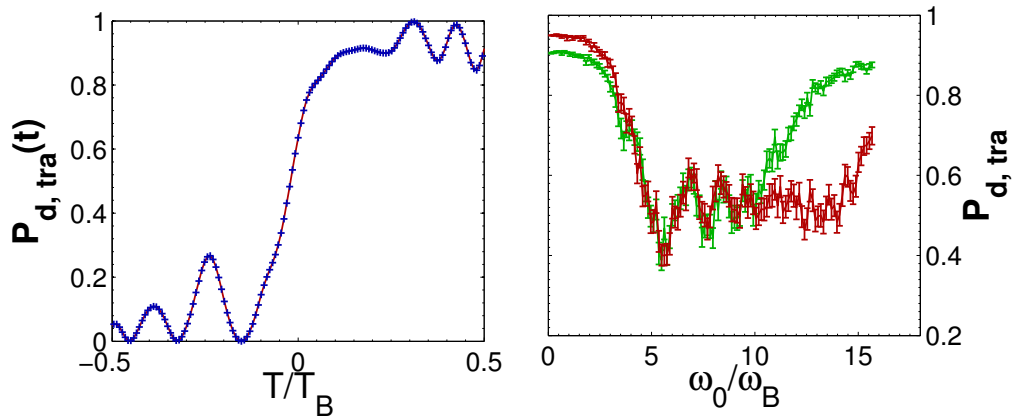


Figure 4.2: The left figure shows a typical time evolution of the transition probability with step sizes $\Delta t = 0.0002$ (red solid line) and $\Delta t = 0.0004$ (blue crosses). The figure on the right shows the asymptotic value of the transition probability versus the noise parameter ω_0/ω_B , with a total integration time of $1T_B$ (green line) and $1.5T_B$ (red line). The error bars give the standard deviation of the average transition probability as defined in Eq.(4.5).

²In fact the step size could have been increased by an order of magnitude and the results would still have been stable. Unfortunately, this was only realised quite late in the project, but computation time was not a big issue anyway.

In the next section, the transition probabilities obtained from the ‘noisy’ LZ model will be compared with those obtained from a numerical simulation of the full ‘noisy’ WSS system (Eq.(3.2)). The numerical simulation of the full system was not part of this thesis, but has been done by my colleague Stephan Burkhardt. Details on how this is done can be found in [8, 42]. Of course, to obtain comparable data, the transition probability in the full system has to be calculated after one Bloch period to make sure that only one LZ transition can have taken place (see figure 4.3). Likewise, the total integration time in the ‘noisy’ LZ model has to be set to one Bloch period.

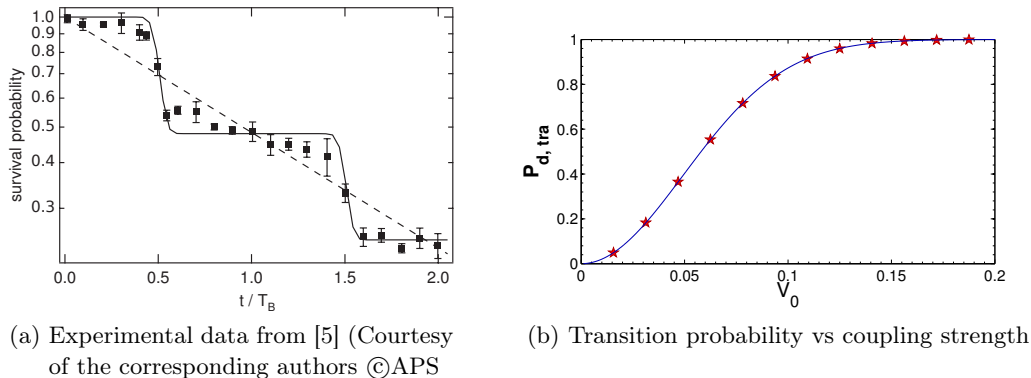


Figure 4.3: A description of figure 4.3a is given in section 2.2.1. Figure 4.3b shows the diabatic transition probability as obtained from numerical simulations of the noiseless WSS (red stars) after $t/T_B = 1$. The numerical data is compared to the LZ prediction (blue solid line). $F_0 = 0.00762$ in both cases. With respect to figure 4.3a, the transition probability shown in figure 4.3b is the one at time $t/T_B = 1$.

Figure 4.3a shows the familiar step structure of the transition probability versus time as it is obtained from numerical simulations of the WSS (noiseless) and observed in experiments. As discussed in section 2.2.1, each step is due to a Landau-Zener transition. Figure 4.3b shows the transition probability after one LZ transition versus the coupling strength V_0 and compares it to the prediction obtained from the LZ formula in Eq.(2.36). Note that in the noiseless case presented ($F_0 = 0.00762$) here the LZ prediction and the numerical simulation of the full WSS are in perfect agreement.

It needs to be clear that in the following, whenever reference is made to the transition probability in the full system, it is understood as the transition probability after *one* LZ transition, i.e. at $t/T_B = 1$. Likewise, if reference is made to the transition probability in the ‘noisy’ LZ model, it is understood as the asymptotic value of the transition probability, as defined in Eq.(4.4). In principle, those two probabilities should coincide if the ‘noisy’ LZ model perfectly captures all features of the full system during a single transition; of course this is not expected. The LZ model can, for example, only account for transitions close to an avoided crossing but not for all transitions across the whole Brillouin zone. This is not a problem in the noiseless case as transitions far away from the avoided crossing are rare (large energy gap between ground band and first excited

band). Yet, in the ‘noisy’ model such transitions may occur more frequently because the noise feeds additional energy into the system (see section 4.2.2).

4.2 Numerical results

The main results of this thesis are presented in this section. A numerical study of the diabatic transition probability for the ‘noisy’ LZ model (Eq.(3.3)) is given, and emphasis is placed on its dependence on the noise parameter ω_0 . The results of the ‘noisy’ LZ model are compared to numerical simulations of the full system and successes and failures of the LZ approximation are discussed. Furthermore, a numerical study is presented, in which the harmonic noise variable ϕ is replaced by a deterministically oscillating phase.

4.2.1 LZ transitions in the presence of harmonic noise

In figure 4.1, the time evolution of the transition probability for the ‘noisy’ LZ model (Eq.(3.3)) has been given. In the following, the asymptotic value of this transition probability is analysed in dependence on the harmonic noise variable ω_0 and the coupling strength V_0 . Unless stated otherwise, the system parameters are $F_0 = 0.00762$, $\Gamma = 0.00762$ and $\langle \phi^2 \rangle = 0.5$ from now on. For those parameters, $\phi(t)$ shows oscillatory behaviour with a peaked power spectrum if $\omega_0/\omega_B \gtrsim 0.32$ (see section 2.4).

Figure 4.4 shows the transition probability in the ‘noisy’ LZ model versus ω_0/ω_B for different coupling strengths V_0 . The numerical data is shown together with an estimation of the transition probability (P_{est}), as obtained from the standard LZ formula with an effective band gap ΔE_{eff} (as defined in Eq.(3.6)),

$$P_{\text{est}} = 1 - e^{-\frac{\pi \Delta E_{\text{eff}}^2}{2F_0}} = 1 - e^{-\frac{\pi}{\gamma_{\text{eff}}}} . \quad (4.6)$$

In the case of small V_0 , figure 4.4a, nothing spectacular can be seen and the transition probability just fluctuates around the estimated value obtained from the LZ formula. This does not come as a great surprise, because for small V_0 ($\gamma_{\text{eff}} \gg 1$) the behaviour of the system is dominated by the diagonal terms $\pm F_0 t$ and thus the influence of the noise is quite small.

Increasing the coupling strength such that $\gamma_{\text{eff}} \lesssim 1$ leads to an interplay between diagonal and off-diagonal terms and the noise strongly influences the transition probability (figure 4.4b and figure 4.4c). In this regime, the modified LZ formula (Eq.(4.6)) still gives a good estimate of the transition probability for very small ω_0/ω_B . Here, the noise fluctuates so slowly that $\phi(t)$ can be regarded as constant throughout the transition and thus averaging over ϕ at $t = 0$ to obtain an effective band gap works well. However, when the time scales of the system and the noise become comparable there is a strong decrease in the transition probability (region $\omega_0/\omega_B = 2 \dots 5$ in figures 4.4b and 4.4c). Increasing ω_0/ω_B even further leads to oscillations of the transition probability around its saturation value (region $\omega_0/\omega_B = 5 \dots 13$ in figures 4.4b and 4.4c). A discussion of this behaviour is deferred to the end of the next section.

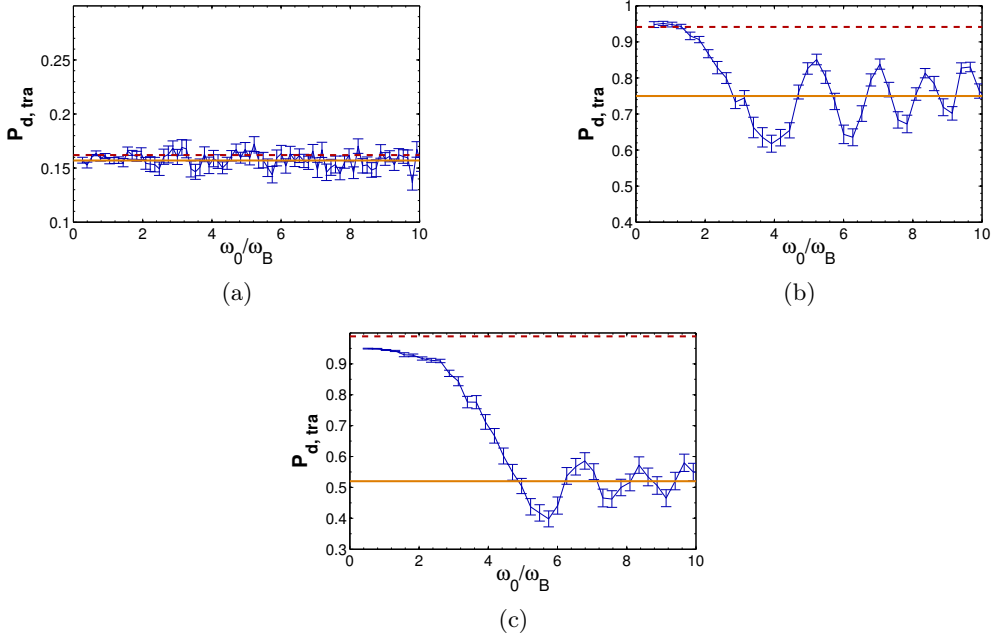


Figure 4.4: The diabatic transition probability in the ‘noisy’ LZ model is shown versus noise frequency ω_0/ω_B . The blue solid lines give the transition probability as obtained from numerical simulations. The error bars give the standard deviation of the transition probability, as defined in Eq.(4.5); the number of realisations is $N=100$. The red dashed lines give the transition probability as obtained from the LZ formula with an effective bandgap ΔE_{eff} (see Eq.(3.6)). The orange solid lines give the saturation value around which $P_{\text{d,tra}}$ oscillates. The parameters are $V_0 = 0.015625$ (a), $V_0 = 0.0625$ (b) and $V_0 = 0.125$ (c).

4.2.2 Main results: ‘Noisy’ WSS vs ‘noisy’ LZ approximation

In the following, the transition probabilities as obtained from the ‘noisy’ LZ model and the full ‘noisy’ WSS are compared. The system parameters are the same as in the previous section.

Figures 4.5 to 4.8 give a sequence of the diabatic transition probability versus ω_0/ω_B , for increasing coupling strength V_0 . A first look at the results already makes it clear that the agreement between the ‘noisy’ WSS and the ‘noisy’ LZ model is not as good as in the noiseless case (compare figure 4.3). Yet, a good qualitative agreement is still given and the graphs reveal the following discrepancies and accordances:

- The ‘noisy’ LZ model overestimates the diabatic transition probability; this is the worst for small V_0 (figures 4.5 and 4.6).
- The initial decrease in the diabatic transition probability can also be seen in the full system and is well described by the ‘noisy’ LZ approximation.
- The position (with respect to ω_0/ω_B) of the first minimum after the initial decrease is approximately the same for both models; furthermore it increases with increasing

V_0 .

- For $V_0 = 0.0625$ ($\gamma_{\text{eff}} = 1.116$) to $V_0 = 0.15625$ ($\gamma_{\text{eff}} = 0.178$) the transition probability oscillates around its saturation value in the regime $\omega_0/\omega_B \approx 5 \cdots 13$; period of oscillation and position of local maxima and minima are similar for the full system and the ‘noisy’ LZ model, but do not agree perfectly.
- The amplitude of those oscillations decreases with increasing V_0 and dies out for $V_0 \gtrsim 0.15625$ ($\gamma_{\text{eff}} \lesssim 0.178$) (in both models).
- For increasing V_0 the saturation value of the diabatic transition probability converges to $\approx 1/2$ (in both models).

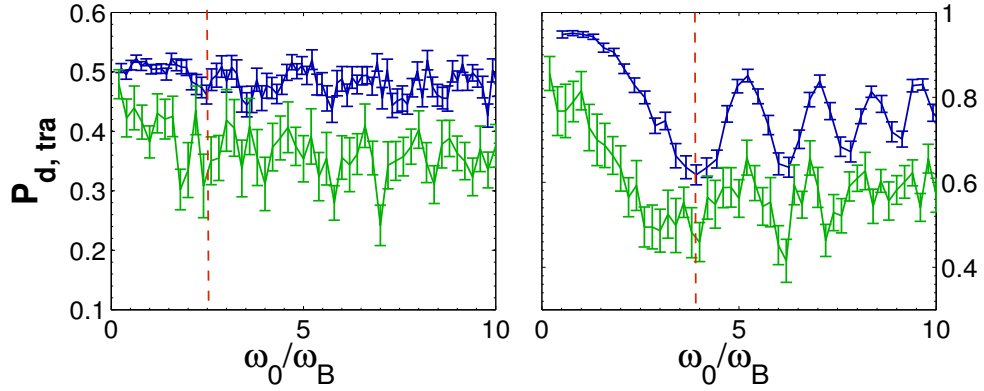


Figure 4.5: Diabatic transition probabilities versus ω_0/ω_B . The green solid lines show the numerical simulations for the full system. The blue solid lines show the numerical simulations for the ‘noisy’ LZ model. The error bars give the standard deviation of the transition probability as defined in Eq.(4.5), with the number of realisations being $N=20$ for the full system and $N=100$ for the ‘noisy’ LZ model. The vertical dashed red lines indicate the position of the first minimum. $V_0 = 0.03125$ (left) and $V_0 = 0.0625$ (right).

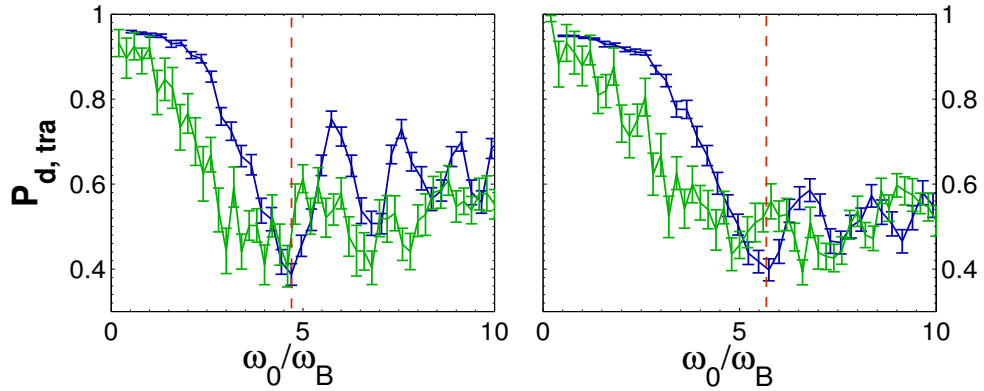


Figure 4.6: Description see figure 4.5. $V_0 = 0.09375$ (left) and $V_0 = 0.125$ (right).

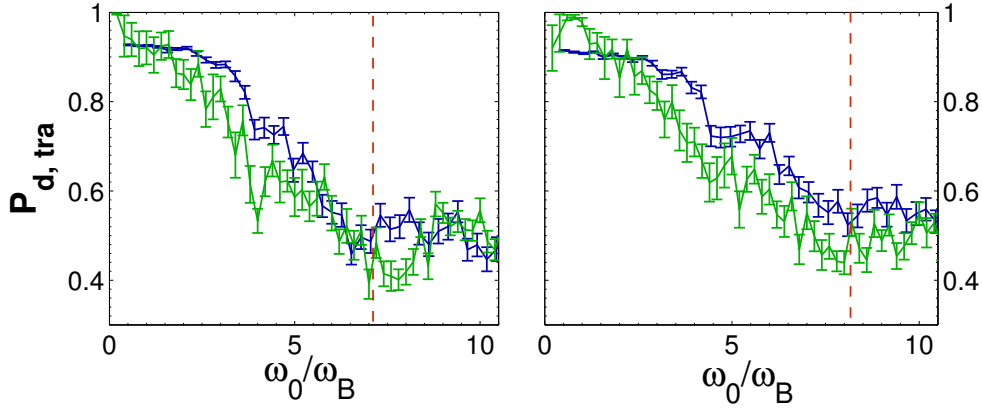


Figure 4.7: Description see figure 4.5. $V_0 = 0.15625$ (left) and $V_0 = 0.1875$ (right).

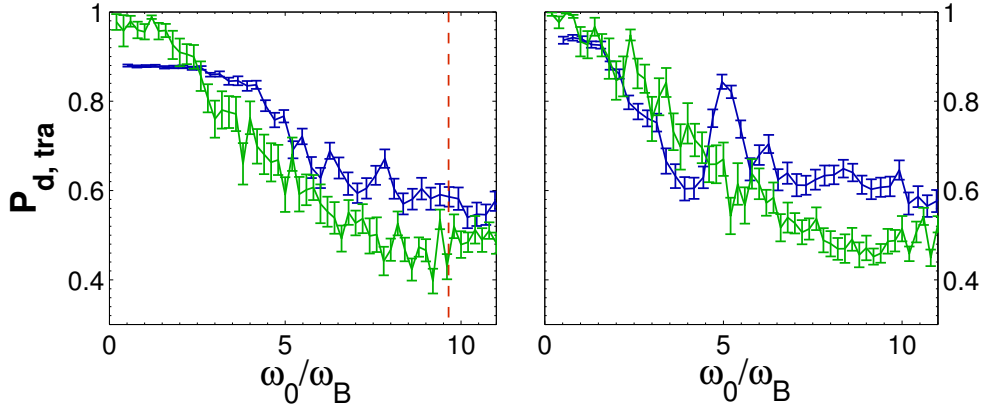


Figure 4.8: Description see figure 4.5. $V_0 = 0.21875$ (left) and $V_0 = 0.25$ (right). In the left figure, the first minimum cannot be determined unambiguously anymore, as the oscillations observed in figures 4.5 to 4.7 have completely vanished. Therefore, the point where $P_{d, tra}$ reaches its saturation value for the first time has been taken as the position of the ‘first minimum’. In the right figure, even this point cannot be determined unambiguously anymore.

On a side note, in section 2.3.2 two conditions were given that need to be fulfilled to be able to approximate the WSS around an avoided crossing with the LZ model. Namely, that jump and relaxation times in the LZ model are less than one Bloch period. Both conditions are fulfilled for the parameters chosen above, with $T_{d, \text{jump}} \approx 0.28 \dots 0.92 T_B$ (for $V_0 = 0.03125 \dots 0.25$) and $T_{d, \text{relax}} \approx 0.47 \dots 0$ (for $V_0 = 0.03125 \dots 0.25$). The jump and relaxation times have been obtained from the formulas given in section 2.3.1, with an effective adiabaticity parameter γ_{eff} . Admittedly, it has not been proven that the formulas for the jump and relaxation times of the noiseless model can be used in our ‘noisy’ model, so the above conditions should be considered anything but strict.

Figure 4.9 shows the position of the first minimum of the transition probability after

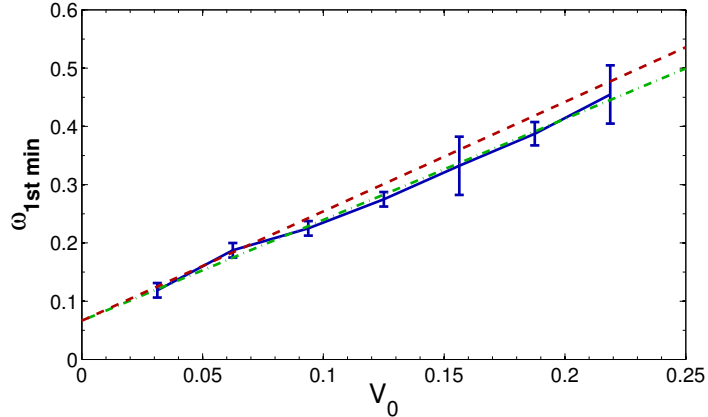


Figure 4.9: Here, the position of the first minimum of the transition probability, as obtained from the ‘noisy’ LZ model, is plotted versus V_0 . The blue solid line shows numerical data ($F_0 = 0.00762$). The green dashed-dotted line is a linear fit to the numerical data and the red dashed line shows the effective band gap ΔE_{eff} as a function of V_0 with a vertical offset of $+0.07$. Note that the axes are in terms of the dimensionless units V_0 and ω_0 . Energy and angular frequency can thus be compared directly.

the rapid initial decrease, as it can be seen in figures 4.5 to 4.8. The numerical data demonstrates that there exists a linear relationship between the position of the first minimum and the coupling strength V_0 . A linear fit to the data (green dashed-dotted line) determined the slope as 1.73 and the y-intercept as 0.07. The linear fit compares well to the formula for the effective band gap, which is

$$\Delta E_{\text{eff}} = (1.88 \pm 0.15)V_0, \quad (4.7)$$

as can be calculated from Eq.(3.6) and Eq.(2.46) with $\langle \phi^2 \rangle = 0.5$. Thus, figure 4.9 indicates that the position of the first minimum is approximately determined by the effective band gap $\Delta E_{\text{eff}} +$ a constant offset.

Ignoring the constant offset for now, this behaviour can be understood as follows. Recall that the diabatic transition probability corresponds to the probability to remain in the ground band, i.e. a minimum in the diabatic transition probability means a maximum in the tunnelling rate. Furthermore, one of the effects of harmonic noise is to feed an energy of $\omega_1 = \sqrt{\omega_0^2 - 2\Gamma^2} \approx \omega_0$ into the system (see peaked spectrum section 2.4). Hence, as soon as the characteristic frequency of the noise is large enough to overcome the effective band gap, tunnelling into the upper band is enhanced. The oscillations for even higher frequencies can then be understood as being on and off-resonance with the effective band gap. This mechanism can also explain why the ‘noisy’ LZ model overestimates the diabatic transition probability for small V_0 . For small V_0 , the band gap between the ground band and the first excited band is comparatively small over the whole Brillouin zone. Feeding only a small amount of energy into the system can thus lead to tunnelling into the upper band throughout the whole Brillouin zone. However, the

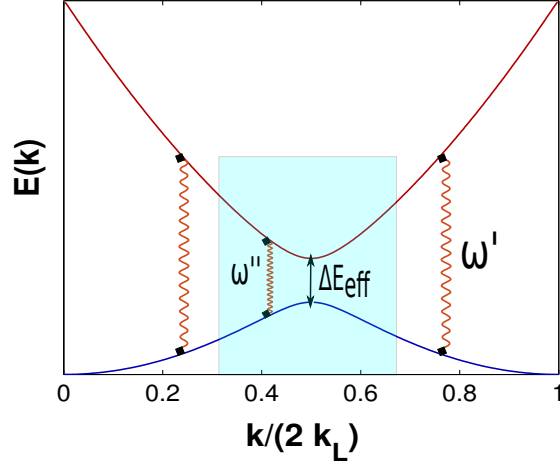


Figure 4.10: Schematic representation of the band structure of the full ‘noisy’ WSS around an avoided crossing. The orange wiggly lines indicate tunnelling from the ground to the first excited band (i.e. no diabatic transition). To trigger a transition, the characteristic frequency ω_0 needs to bridge the energy difference between the two bands, e.g. for the transition on the right ω_0 needs to be $\approx \omega'$. The blue shaded rectangle indicates the region in which the ‘noisy’ LZ model gives a good approximation to the full system. Transitions outside this region are not captured (well) by the ‘noisy’ LZ model.

‘noisy’ LZ model approximates the full system only around an avoided crossing. This means it cannot account for transitions far away from an avoided crossing and hence overestimates (underestimates) the diabatic transition probability (tunnelling rate). For higher V_0 tunnelling far from an avoided crossing is strongly suppressed and the ‘noisy’ LZ model gives good estimates of the transition probabilities in the full system (as can be seen in figures 4.7 and 4.8).

The interpretation given above is purely based on considerations about matching of energy scales and completely ignores many important features of the system, such as the driving force F_0 or the noise parameters $\langle \phi^2 \rangle$ and Γ . Consequently, it is not a great surprise that the slope of the fit to the numerical data does not agree completely with the formula for ΔE_{eff} . Additionally, the constant offset at $V_0 = 0$ cannot be explained by the above considerations and the following figures show that it is sensitive to the driving force F_0 .

Figure 4.11 shows the same quantities as figure 4.9 but for $F_0 = 0.00597$ (left) and $F_0 = 0.00995$ (right). Linear fits to the numerical data gave a slope of 1.87 (left) and 1.73 (right) and y-intercepts at 0.04 (left) and 0.06 (right). As previously, the position of the first minimum approximately scales with the effective band gap ($\Delta E_{\text{eff}} = (1.88 \pm 0.15)V_0$), thereby strengthening the above interpretation. However, the value of the y-intercept changed and seems to depend on F_0 ; an exact relation between F_0 and the value of the

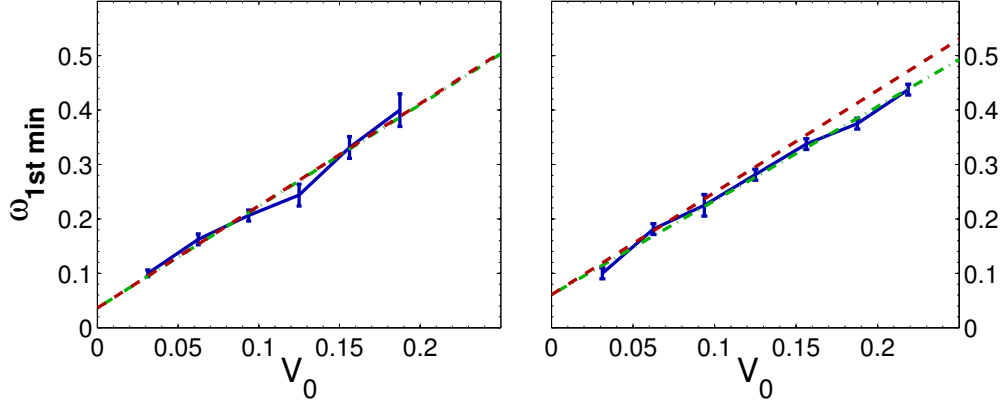


Figure 4.11: For a description see figure 4.9. The parameters are $F_0 = 0.00597$ (left figure) and $F_0 = 0.00995$ (right figure). The other two noise parameters Γ and $\langle\phi^2\rangle$ are the same as before.

y-intercept has not been found yet.

4.2.3 The influence of harmonic noise versus a deterministic phase

In the last section of this chapter the harmonic noise variable ϕ is approximated by a deterministically oscillating phase and the data in the previous section is compared to this toy model.

In the high frequency regime $\phi(t)$ shows oscillatory behaviour, therefore the following ansatz has been proposed by Tayebirad and co-workers [6],

$$\phi(t) = A \sin(\omega_0 t) , \quad (4.8)$$

with a corresponding power spectrum of $S_d(\omega) = \frac{A^2}{4\pi}[\delta(\omega - \omega_0) + \delta(\omega + \omega_0)]$. Now the amplitude A can be determined by requiring that the total energy fed into the system is the same for the deterministic phase and the harmonic noise, i.e. the integrated power spectrum must be the same. With the power spectrum for the harmonic noise given by Eq.(2.49) this condition reads,

$$\begin{aligned} \int_0^\infty d\omega \frac{A^2}{4\pi} [\delta(\omega - \omega_0) + \delta(\omega + \omega_0)] &= \int_0^\infty d\omega \frac{2\Gamma T}{\pi (4\Gamma^2\omega^2 + (\omega^2 - \omega_0^2)^2)} \\ \frac{A^2}{4\pi} &\approx \int_{\omega_0-\delta}^{\omega_0+\delta} d\omega \frac{T}{2\pi\Gamma\omega_0^2} \approx \frac{T}{2\pi\Gamma\omega_0^2} 2\Gamma \\ A^2 &\approx 4 \frac{T}{\omega_0^2} = 4\langle\phi^2\rangle \\ \implies A &\approx 2\sqrt{\langle\phi^2\rangle} . \end{aligned} \quad (4.9)$$

In the above derivation the fact has been used that the power spectrum has a sharp peak at $\omega \approx \omega_0$. The integral over the power spectrum has been approximated as the value of the spectrum at $\omega \approx \omega_0$ times the full width at half maximum (2Γ , see section 2.4).

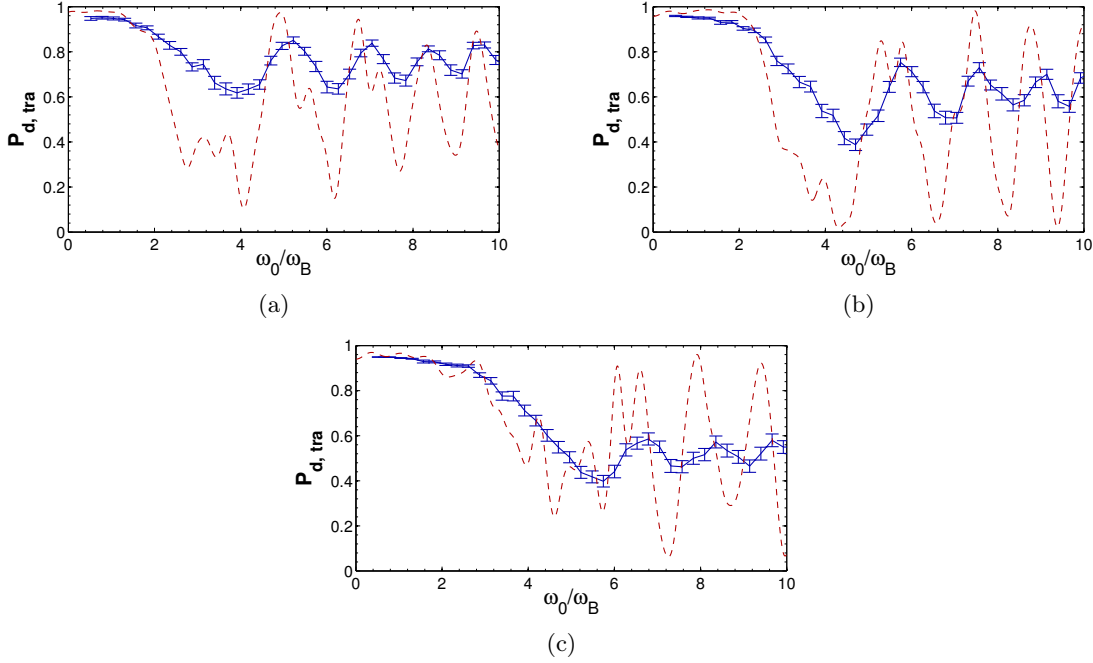


Figure 4.12: Diabatic transition probability versus ω_0/ω_B . The blue solid lines show the numerical data for the ‘noisy’ LZ model. The red dashed lines show numerical data for $\phi(t) = A \sin(\omega_0 t)$, with $A = \sqrt{2}$ (corresponding to $\langle \phi^2 \rangle = 0.5$). The system parameters are, $V_0 = 0.0625$ for (a), $V_0 = 0.09375$ for (b), $V_0 = 0.125$ for (c) and in all cases $F_0 = 0.00762$, $\Gamma = 0.00762$ and $\langle \phi^2 \rangle = 0.5$.

Figure 4.12 compares the numerical data for the ‘noisy’ LZ model with the data for the deterministically oscillating phase. The numerical simulation has been done as outlined in section 4.1, but with $\phi(t) = A \sin(\omega_0 t)$ in the deterministic case. It is apparent that the deterministic phase model captures the features of the ‘noisy’ LZ model with mixed success, and the agreement is the worst for $V_0 = 0.125$. Interestingly enough, the best agreement in all three figures is achieved in the case of very low ω_0 where the harmonic noise does not show sinusoidal behaviour. Yet, this is easily explained. In the low ω_0 regime the noise fluctuates so slowly that the functional form of $\phi(t)$ does not play an important role. In this case, the noise just leads to a rescaled coupling term.

Moreover, in figures 4.12a and 4.12b the deterministic model accurately reproduces the position of the minima and maxima of the ‘noisy’ LZ model. It can therefore be concluded, that the oscillations and the initial decay in the transition probability stem from the oscillatory nature of the harmonic noise. The effect of the damping Γ and the varying amplitude of ϕ in the ‘noisy’ LZ model can then be identified as a broadening and reduction of the peaks in figure 4.12.

But the most interesting feature in the above figures is not the position of the minima and maxima, but the height of the peaks in the deterministic phase model. In figure 4.12b, the diabatic transition probability changes from 0.039 at $\omega_0/\omega_B = 6.58$ to 0.981 at $\omega_0/\omega_B = 7.48$, thus only a slight change in the frequency leads from practically no

transition to a full transition. This behaviour is especially interesting from an experimentalists point of view, because it provides an excellent means to control the transport properties of a BEC in an optical lattice. It is not unlikely that changing the system parameters even leads to stronger ‘jumps’ in the transition probability.

The reason for the strongly damped oscillations in the ‘noisy’ model lies in the fluctuation of the amplitude $\phi(t)$. Even in the case of $\Gamma = 0$, i.e. when $\phi(t)$ describes a sinusoidal curve, the amplitude of $\phi(t)$ is still not the same for different noise realisations, but distributed according to (Eq.(2.46)). Different amplitudes lead to variations in the strength of the oscillations. Averaging over the amplitude according to (Eq.(2.46)) thus leads to a damping of the oscillations (see appendix, figure 7.1a). Another point is of course that for $\Gamma \neq 0$ the power spectrum of $\phi(t)$ contains more than one frequency. Even though the spectrum may be very narrowly peaked around ω_0 it is still expected that this reduces the height of the peaks in figure 4.12 and broadens them (see appendix, figure 7.1b).

In the next chapter, an attempt is made to back up the results and interpretations given here, with analytical calculations.

5 Analytical investigation

Eugene Wigner once said “It is nice to know that the computer understands the problem. But I would like to understand it too” [43]. This chapter is kept in the spirit of Wigner and an analytical solution for the diabatic transition probabilities discussed in the previous chapter, is derived. The first section is spent on deriving a formal solution to the problem at hand, whereas in the second section it is applied to two limiting cases. Namely, the ‘small coupling’ and the ‘small coupling, small damping’ limits specified below.

5.1 Formal solution of the transition probabilities

In this section, a formal solution for the asymptotic transition probabilities for a LZ model with stochastic off-diagonal terms is derived. The derivation closely follows the approach taken by Kayanuma [1, 44], but extends it to complex off-diagonal terms. Without a doubt, there exist other approaches to the problem based on the evolution of the density matrix [45] that may be more elegant than the one introduced here, but, in the authors opinion, they are less instructive.

5.1.1 Time evolution of states

Recall that the system under consideration is governed by the time-dependent Schrödinger equation

$$i\partial_t|\psi(t)\rangle = \frac{1}{2} \begin{pmatrix} -F_0t & V_0(1 + e^{i\phi(t)}) \\ V_0(1 + e^{-i\phi(t)}) & F_0t \end{pmatrix} |\psi(t)\rangle . \quad (5.1)$$

Assuming that the system is initially in the ground state $|1\rangle_d$ at time $t = -\infty$, its time evolution is given by

$$|\psi(t)\rangle = \hat{U}(t, -\infty)|1\rangle_d , \quad (5.2)$$

where $\hat{U}(t, -\infty)$ is the time evolution operator defined as,

$$\exp_+ \left(-i \int_{-\infty}^t \hat{H}_{LZ,N}(\tau) d\tau \right) . \quad (5.3)$$

Here, $\hat{H}_{LZ,N}(\tau)$ is the time dependent Hamiltonian of Eq.(3.3) and the \exp_+ denotes the positively time ordered exponential given by a *Dyson series* [46] of the form

$$\exp_+ \left(-i \int_{-\infty}^t \hat{H}_{LZ,N}(\tau) d\tau \right) = 1 + \sum_{n=1}^{\infty} (-i)^n \int_{-\infty}^t d\tau_1 \int_{-\infty}^{\tau_1} d\tau_2 \dots \int_{-\infty}^{\tau_{n-1}} d\tau_n \hat{H}_{LZ,N}(\tau_1) \hat{H}_{LZ,N}(\tau_2) \dots \hat{H}_{LZ,N}(\tau_n) \quad (5.4)$$

According to standard quantum theory, the diabatic transition probability from state $|1\rangle_d$ to state $|2\rangle_d$ at any time t is given by $P_{tra}(t) = {}_d\langle 2|\psi(t)\rangle\langle\psi(t)|2\rangle_d$, with $|\psi(t)\rangle$ of Eq.(5.2). For simplicity it is assumed that the system starts at $t = -\infty$ in $|1\rangle_d$ and evolves until $t = \infty$. Furthermore the Hamiltonian in Eq.(3.3) contains stochastic off-diagonal terms, so the transition probability has to be averaged over the noise process. This yields a transition probability given by [1],

$$P_{tra}(\infty) = \left\langle {}_d\langle 2| \exp_+ \left(-i \int_{-\infty}^{\infty} \hat{H}_{LZ,N}(\tau) d\tau \right) |1\rangle_d \langle 1| \exp_- \left(i \int_{-\infty}^{\infty} \hat{H}_{LZ,N}(\tau) d\tau \right) |2\rangle_d \right\rangle, \quad (5.5)$$

where $\langle \dots \rangle$ denotes the average over the noise process and \exp_- is the negatively time ordered exponential, defined in accordance to Eq.(5.4).

The above equation can be brought into a more amendable form by applying *Feynman's disentanglement theorem* [1, 47].

5.1.2 Feynman's disentanglement theorem

The Hamiltonian $\hat{H}_{LZ,N}(t)$ can be re-expressed as a sum of the two Hamiltonians $\hat{H}_0(t)$ and $\hat{H}_{int}(t)$ with,

$$\begin{aligned} \hat{H}_0 &= \frac{1}{2} F_0 t [-|1\rangle_d \langle 1| + |2\rangle_d \langle 2|] \\ \hat{H}_{int}(t) &= \frac{1}{2} [V(t) |1\rangle_d \langle 2| + V^*(t) |2\rangle_d \langle 1|], \end{aligned} \quad (5.6)$$

where ‘*’ denotes the complex conjugate and $V(t) = V_0(1 + e^{i\phi(t)})$. Because of the time ordering constraint it is not possible to simply split the Hamiltonian in the exponential of Eq.(5.4) and expand the two terms separately. In the following, the off-diagonal part of the Hamiltonian will be treated as a perturbation and a theorem is presented that allows to drop the time ordering constraint on the diagonal part of the Hamiltonian.

Feynman's disentanglement theorem:

Let $F[M(\tau), N(\tau), \dots]$ be a functional that defines the order of operation of the operators $M(\tau), N(\tau), \dots$ via the order parameter τ , and let further $U(\tau)$ be another operator depending on τ . Then the two functional expressions $F[M(\tau), N(\tau), \dots]$ and $F[M'(\tau), N'(\tau), \dots]$, with $M'(\tau) = U^{-1}(\tau)M(\tau)U(\tau), N'(\tau) = U^{-1}(\tau)N(\tau)U(\tau), \dots$ are related via:

$$\exp\left(\int_{\tau_0}^{\tau_1} P(\tau)d\tau\right)F[M(\tau), N(\tau), \dots] = U(\tau_1)F[M'(\tau), N'(\tau), \dots]U^{-1}(\tau_0) , \quad (5.7)$$

with $\exp(\int_{\tau_0}^{\tau_1} P(\tau)d\tau)$ being ordered with respect to τ and $P(\tau)$ is defined via $U(\tau) = \exp\left(\int_c^\tau P(\tau')d\tau'\right)$, where the lower integration limit c can be set arbitrarily.

It is important to note that in the defining equation of $P(\tau), U(\tau) = \exp\left(\int_c^\tau P(\tau')d\tau'\right)$, the variable τ' has nothing to do with the time ordering constraint and is thus just a *dummy* variable. This means that $U(\tau)$ only acts at the time point τ . Therefore, whereas on the left hand side of the theorem the two expressions are subject to the same time ordering constraint, on the right hand side the operators $U(\tau_1)$ and $U^{-1}(\tau_0)$ act at specific times τ_1 and τ_0 and are thus disentangled from the time ordering constraint on $F[M'(\tau), N'(\tau), \dots]$. The disentanglement of $U(\tau)$ from the time ordering constraint is also the main difference to the more routinely used *interaction picture* [46].

In the case studied in this thesis,

$$\exp_+ \left(-i \int_{-\infty}^{\infty} \hat{H}_{LZ,N}(\tau)d\tau \right) = \exp_+ \left(-i \int_{-\infty}^{\infty} \hat{H}_0(\tau)d\tau \right) \exp_+ \left(-i \int_{-\infty}^{\infty} \hat{H}_{int}(\tau)d\tau \right) \quad (5.8)$$

$F[M(\tau)]$ can be associated with $\exp_+ \left(-i \int_{-\infty}^{\infty} \hat{H}_{int}(\tau)d\tau \right)$ and $P(\tau)$ is given by $-iH_0(\tau)$. Furthermore, the start and end times are given by $\tau_0 = -\infty$ and $\tau_1 = \infty$, respectively. Hence, direct application of the above theorem yields,

$$\exp_+ \left(-i \int_{-\infty}^{\infty} \hat{H}_{LZ,N}(\tau)d\tau \right) = U(\infty) \exp_+ \left(-i \int_{-\infty}^{\infty} \tilde{H}_{int}(\tau)d\tau \right) U^{-1}(-\infty) , \quad (5.9)$$

where

$$U(\tau) = \exp \left(-i \int_c^\tau \hat{H}_0(\tau)d\tau \right) \quad \text{and} \quad \tilde{H}_{int}(\tau) = U^{-1}(\tau)\hat{H}_{int}(\tau)U(\tau) . \quad (5.10)$$

Setting $c = -\infty$ simplifies the above expression as it implies that $U(-\infty) = 1$ and hence $U^{-1}(-\infty) = 1$. As has been pointed out previously, the operators $U(\infty)$ and $U(-\infty)$ now act at *specific* time points and are thus not subject to the time ordering anymore. The new interaction part $\tilde{H}_{int}(\tau)$ can be evaluated as

$$\tilde{H}_{int}(\tau) = \frac{1}{2}V(\tau) \exp(-iF_0 \int_{-\infty}^{\tau} \tau' d\tau')|1\rangle_d \langle 2| + \frac{1}{2}V^*(\tau) \exp(+iF_0 \int_{-\infty}^{\tau} \tau' d\tau')|2\rangle_d \langle 1| \quad (5.11)$$

by invoking the definitions of Eq.(5.6) and recalling that

$$\exp\left(\begin{pmatrix} a & 0 \\ 0 & b \end{pmatrix}\right) = \begin{pmatrix} \exp(a) & 0 \\ 0 & \exp(b) \end{pmatrix}. \quad (5.12)$$

Finally, the disentangled expression for the positively time ordered exponential is given by,

$$\exp_+ \left(-i \int_{-\infty}^{\infty} \hat{H}_{LZ,N}(\tau) d\tau \right) = \exp \left(-i \int_{-\infty}^{\infty} H_0(\tau) d\tau \right) \exp_+ \left(-i \int_{-\infty}^{\infty} \tilde{H}_{int}(\tau) d\tau \right) \quad (5.13)$$

with $\tilde{H}_{int}(\tau)$ defined in Eq.(5.11). In principal, the same procedure can be applied to the negatively time ordered exponential. However, it is more convenient to calculate the matrix element containing the positively time ordered exponential first. The negatively time ordered matrix element is then obtained by invoking that it is the *hermitian conjugate* of the positively time ordered one, but with negative time ordering.

5.1.3 A perturbation series solution

The positive time ordered exponential in Eq.(5.13) can be expanded using the Dyson series defined in Eq.(5.4). By taking the two-one matrix element ($\langle 2 | \dots | 1 \rangle$) of the series and multiplying it by its hermitian conjugate, the transition probability is obtained as a perturbation series in terms of the off-diagonal coupling strength V_0 [1, 44]. For the sake of clarity, the details of this derivation are omitted here and only the final result is given (the interested reader is referred to the appendix, section 7.3),

$$P_{tra}(\infty) = \left\langle \sum_{n=1}^{\infty} (-1)^{2n} \left(\frac{V_0^2}{4} \right)^n L^{(n)} \right\rangle, \quad (5.14)$$

with

$$\begin{aligned} L^{(n)} = & \sum_{m=1}^n \int_{-\infty}^{\infty} d\tau_1 \int_{\tau_1}^{\infty} d\tau_2 \dots \int_{\tau_{2m-2}}^{\infty} d\tau_{2m-1} \int_{-\infty}^{\tau_{2m-1}} d\tau_{2m} \int_{-\infty}^{\tau_{2m}} d\tau_{2m+1} \dots \int_{-\infty}^{\tau_{2n-1}} d\tau_{2n} \\ & \times G(\tau_1) G^*(\tau_2) \dots G(\tau_{2m-1}) G^*(\tau_{2m}) G(\tau_{2m+1}) \dots G^*(\tau_{2n}) \\ & \times \exp \left(i \frac{F_0}{2} \sum_{k=1}^{2n} (-1)^k \tau_k^2 \right), \end{aligned} \quad (5.15)$$

where $G(\tau) = (1 + e^{i\phi(\tau)})$. The above perturbation series is analogous to the one derived by Kayanuma [1, 44], but extends it to complex off-diagonal coupling terms. In the case of constant off-diagonal coupling terms, i.e. the standard LZ model, Kayanuma has shown that the series can be summed up to give the LZ formula,

$$P_{sur}(t = \infty) = 1 - e^{-\frac{\pi V_0^2}{2F_0}},$$

given in Eq.(2.36). It is evident that the applicability of this perturbation series will be strongly dependent on the ability to evaluate the integrals of $L^{(n)}$. In particular, the

exact form of $G(\tau)$ will play a crucial role and for the system studied in this thesis this already proves tricky for the lowest order terms, as the number of terms that have to be integrated to calculate $L^{(n)}$ grows as 4^n . Nevertheless the formula can be used to obtain a qualitative understanding of the dependence of the transition probability on the noise parameters specifying $\phi(t)$. Kayanuma himself studied the influence of exponentially correlated noise in the off-diagonal on the transition probability. He could show that in the limit of very rapid fluctuations (correlation time $\rightarrow 0$) and large average value of the off-diagonal term ($V_0 \rightarrow \infty$), the transition probability is $P_{tra}(\infty) = \frac{1}{2}$.

A similar behaviour has been demonstrated in section 4.2.2 for large V_0 and high characteristic frequency ω_0 . One could therefore speculate that Kayanuma's statement, "... in the presence of the rapid fluctuations with large amplitude, the system forgets from which branch [which initial state, ${}_d\langle 1|$ or $|2\rangle_d$] it has come and is equally distributed to ${}_d\langle 1|$ and $|2\rangle_d$ after the passage of the crossing region", is a general feature of noise influenced LZ transitions.

5.2 Application of the solution to limiting cases

In this section, the perturbation series in Eq.(5.14) will be used to calculate the transition probability from the diabatic ground state $|1\rangle_d$ to the diabatic first excited state $|2\rangle_d$. Unfortunately, the rather complex structure of the formal solution does not allow us to give a closed form expression for the expansion coefficients $L^{(n)}$. Emphasis will therefore be put on two limiting cases that shed light onto the numerical results obtained in chapter 4. The first limiting case considered is the 'small coupling' limit, i.e. $\frac{V_0^2}{2F_0} \ll 1$ and the second one is the 'small coupling, small damping' limit, i.e. $\frac{V_0^2}{2F_0} \ll 1$ and $\Gamma \ll 1$.

5.2.1 Small coupling limit

It is expected, that in the small coupling limit only the first few terms of the perturbation series will contribute, as higher order terms scale with $(V_0^2)^n$. In the following the first term of Eq.(5.14) is calculated explicitly and an estimate of the second order correction is given. Using that the average of a sum, is the sum of the averages, Eq.(5.14) and Eq.(5.15) define the first order term as,

$$\begin{aligned} P_{tra}^{(1)}(\infty) &= \frac{V_0^2}{4} \left\langle \int_{-\infty}^{\infty} d\tau_1 \int_{-\infty}^{\infty} d\tau_2 (1 + e^{i\phi(\tau_1)})(1 + e^{-i\phi(\tau_2)}) \exp\left(\frac{iF_0}{2}(\tau_2^2 - \tau_1^2)\right) \right\rangle \\ &= \int_{-\infty}^{\infty} d\tau_1 \int_{-\infty}^{\infty} d\tau_2 (1 + \langle e^{i\phi(\tau_1)} \rangle + \langle e^{-i\phi(\tau_2)} \rangle + \langle e^{i(\phi(\tau_1) - \phi(\tau_2))} \rangle) \exp\left(\frac{iF_0}{2}(\tau_2^2 - \tau_1^2)\right) \end{aligned} \quad (5.16)$$

The first three terms of this integral are constant in τ_1 and τ_2 , as Eq.(2.46) can be used to evaluate the average of $e^{i\phi(\tau)}$ as,

$$\langle e^{i\phi(\tau_1)} \rangle = \exp\left(-\frac{\langle \phi^2 \rangle}{2}\right) = \langle e^{-i\phi(\tau_2)} \rangle. \quad (5.17)$$

Furthermore, the term $\langle e^{i(\phi(\tau_1)-\phi(\tau_2))} \rangle$ can be evaluated by invoking that the static probability density distribution of $\phi(\tau)$ is of gaussian form and that for gaussian processes the relation

$$\left\langle \exp \left(i \sum_{o=1}^p q_o X_o \right) \right\rangle = \exp \left(-\frac{1}{2} \sum_{o,r=1}^p q_o q_r \langle X_o X_r \rangle + i \sum_{o=1}^p \langle X_o \rangle q_o \right), \quad (5.18)$$

where X_o is a gaussian process, holds [39]. Hence, application of Eq.(5.18) and Eq.(2.48) yields

$$\begin{aligned} \langle e^{i(\phi(\tau_1)-\phi(\tau_2))} \rangle &= \exp \left(\frac{1}{2} \langle \phi(\tau_1) \phi(\tau_2) \rangle \right) \\ &= \exp \left(\frac{\langle \phi^2 \rangle}{2} e^{-\Gamma(\tau_2-\tau_1)} \left(\cos(\omega_1(\tau_2 - \tau_1)) + \frac{\Gamma}{\omega_1} \sin(\omega_1(\tau_2 - \tau_1)) \right) \right), \end{aligned} \quad (5.19)$$

as $\langle \phi(\tau) \rangle = 0$. In spite of the seemingly complex functional dependence on τ_1 and τ_2 in the above equation, the first order term of the perturbation series can still be calculated explicitly. A change of variable to $\mu = (\tau_1 + \tau_2)/2$ and $\sigma = (\tau_2 - \tau_1)$ [1] recasts Eq.(5.16) in the following form,

$$\begin{aligned} P_{tra}^{(1)}(\infty) &= \frac{V_0^2}{4} \int_{-\infty}^{\infty} d\mu \int_{-\infty}^{\infty} d\sigma \exp(iF_0\mu\sigma) \left[\left((1 + 2 \exp\left(-\frac{\langle \phi^2 \rangle}{2}\right) \right. \right. \\ &\quad \left. \left. + \exp\left(\frac{\langle \phi^2 \rangle}{2}\right) e^{-\Gamma\sigma} \left(\cos(\omega_1\sigma) + \frac{\Gamma}{\omega_1} \sin(\omega_1\sigma) \right) \right) \right]. \end{aligned} \quad (5.20)$$

The integration over μ gives,

$$\begin{aligned} P_{tra}^{(1)}(\infty) &= \frac{V_0^2\pi}{2} \int_{-\infty}^{\infty} d\sigma \delta(F_0\sigma) \left[\left((1 + 2 \exp\left(-\frac{\langle \phi^2 \rangle}{2}\right) \right. \right. \\ &\quad \left. \left. + \exp\left(\frac{\langle \phi^2 \rangle}{2}\right) e^{-\Gamma\sigma} \left(\cos(\omega_1\sigma) + \frac{\Gamma}{\omega_1} \sin(\omega_1\sigma) \right) \right) \right], \end{aligned} \quad (5.21)$$

as $\delta(x) = \frac{1}{2\pi} \int_{-\infty}^{\infty} dk e^{ikx}$, where $\delta(x)$ is the Dirac Delta function. And finally the integration over σ yields a closed form expression for $P_{tra}^{(1)}(\infty)$,

$$P_{tra}^{(1)}(\infty) = \frac{V_0^2\pi}{2F_0} \left(1 + 2 \exp\left(-\frac{\langle \phi^2 \rangle}{2}\right) + \exp\left(\frac{\langle \phi^2 \rangle}{2}\right) \right). \quad (5.22)$$

The first term of $P_{tra}^{(1)}$ gives the contribution stemming from the constant coupling term in Eq.(5.1), modelling the first optical lattice. This is evident from the fact that a Taylor expansion to first order of the LZ formula (Eq.(2.36)) gives exactly this first term. Term two and three then provide a correction due to the second stochastic coupling terms in Eq.(5.1), modelling the second stochastic optical lattice. It is immediately obvious that $P_{tra}^{(1)}$ can only give a reasonable approximation to $P_{tra}(\infty)$ for $\frac{V_0^2}{F} \ll 1$. Furthermore, the expression for $P_{tra}^{(1)}$ is unbounded with respect to $\langle \phi^2 \rangle$ and hence the condition $\langle \phi^2 \rangle < 1$

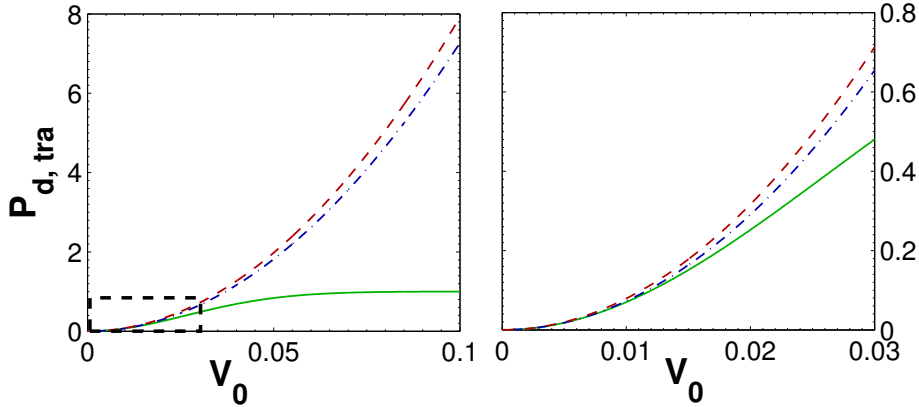


Figure 5.1: Both figures show the diabatic transition probability versus the coupling strength. The figure on the right shows the part highlighted by the rectangle in the left figure. The red dashed line is given by $P_{d,tra}^{(1)}$ (Eq.(5.22)). The green solid line shows the transition probability given by the standard LZ formula $P_{d,tra}(\infty) = 1 - \exp\left(\frac{-\Delta E_{eff}^2 \pi}{2F_0}\right)$, with an effective potential band gap $\Delta E_{eff} = 1.878V_0$ as introduced in Eq.(3.6). The blue dashed-dotted line shows the transition probability as obtained from a first order Taylor expansion of the LZ formula defining the green solid line, i.e. $P_{d,tra}(\infty) = \frac{\Delta E_{eff} \pi}{2F_0}$.

has to be fulfilled as well.

Figure 5.1 shows the diabatic transition probability versus the coupling strength V_0 . As expected the analytical solution $P_{tra}^{(1)}$ diverges quickly with increasing V_0 . On the other hand, in the regime of very small V_0 , shown in the right figure, the analytical solution and the LZ prediction for an effective band gap are in good agreement. Hence, it is anticipated that in the regime of very small V_0 , the analytical solution should give a good estimate of the ‘real’ diabatic transition probability.

Figure 5.2 shows the diabatic transition probability versus the rescaled noise frequency ω_0/ω_B . As expected from figure 5.1, the analytical solution provides a good estimate of the ‘average’¹ value of the transition probability in the regime of very small V_0 (figure on the left). However, the discrepancies between the analytical solution and the numerical solution become larger if V_0 is increased (figure on the right). Moreover, the analytical formula in Eq.(5.22) cannot account for *any* frequency dependence of the transition probability. As a result, the practical use of the analytical solution derived in this section is very limited, as all of the interesting physics lies in the ω_0 dependence of the transition probability.

¹Here, ‘average’ is understood as the mean value of the transition probability around which the numerical solution fluctuates for varying ω_0 .

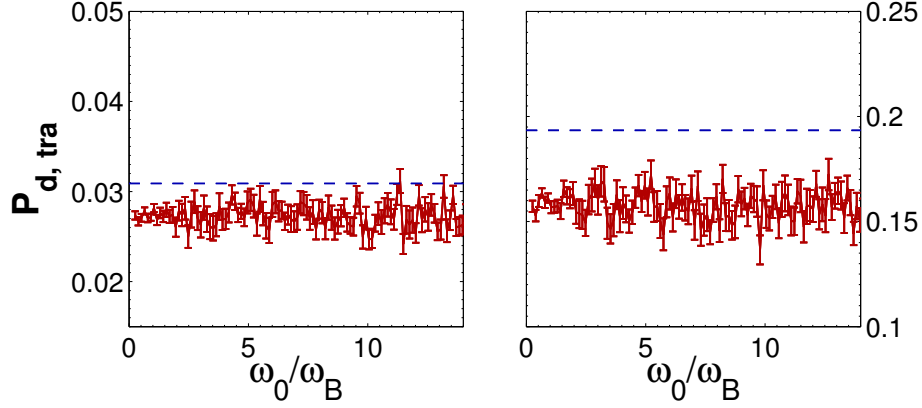


Figure 5.2: Both figures show the diabatic transition probability versus ω_0/ω_B . The red solid line shows the transition probability as obtained from numerical simulations of the ‘noisy’ LZ model (Eq. (3.3)). The blue dashed line shows the transition probability as calculated from Eq.(5.22). The parameters are $F_0 = 0.00762, \Gamma = 0.00762, \langle \phi^2 \rangle = 0.5$ and $V_0 = 0.00625$ (left figure) and $V_0 = 0.015625$ (right figure).

As an aside, preliminary calculations have shown that the 2nd order term $P_{tra}^{(2)}$ leads to a negative correction of the order of $\frac{V_0^4 \pi}{8F_0^2}$, which will slow down the rapid divergence of the solution in Eq.(5.22); it is also anticipated that the second order perturbation term will carry a dependence on ω_0 .

5.2.2 Small coupling and small damping limit

It has been pointed out in section 2.4 that in the limit of small damping, i.e. $\Gamma \rightarrow 0$, the harmonic noise amplitude ϕ exhibits sinusoidal motion. In section 4.2.3 an effective model has been presented that approximates the harmonic noise variable $\phi(t)$ by a deterministically oscillating phase [6, 42] such that,

$$\phi(t) = A \sin(\omega_0 t) , \text{ with } A \approx 2\sqrt{\langle \phi^2 \rangle} . \quad (5.23)$$

This form of ϕ modifies the function $G(\tau)$ in Eq.(5.15) according to, $G(\tau) = (1 + e^{iA \sin(\omega_0 \tau)})$. Thus, the first term in the perturbation series of the transition probability of Eq.(5.14) is given by,

$$\begin{aligned} P_{tra,ZD}^{(1)}(\infty) &= \frac{V_0^2}{4} \int_{-\infty}^{\infty} d\tau_1 \int_{-\infty}^{\infty} d\tau_2 (1 + e^{iA \sin(\omega_0 \tau_1)})(1 + e^{-iA \sin(\omega_0 \tau_2)}) \exp\left(\frac{iF_0}{2}(\tau_2^2 - \tau_1^2)\right) \\ &= \int_{-\infty}^{\infty} d\tau_1 \int_{-\infty}^{\infty} d\tau_2 (1 + e^{iA \sin(\omega_0 \tau_1)} + e^{-iA \sin(\omega_0 \tau_2)} + e^{i(A \sin(\omega_0 \tau_1) - A \sin(\omega_0 \tau_2))}) \\ &\quad \times \exp\left(\frac{iF_0}{2}(\tau_2^2 - \tau_1^2)\right) . \end{aligned} \quad (5.24)$$

Note that it is not necessary to take the average of the above expression as $\phi(t)$ is a deterministic function of t, ω_0 . The first term in the integral can be evaluated in the

same way as has been done in section 5.2.1 and is obtained as,

$$\frac{V_0^2}{4} \int_{-\infty}^{\infty} d\tau_1 \int_{-\infty}^{\infty} d\tau_2 \exp\left(\frac{iF_0}{2}(\tau_2^2 - \tau_1^2)\right) = \frac{V_0^2\pi}{2F_0}. \quad (5.25)$$

The second term can be calculated by using the Jacobi-Anger expansion,

$$\exp(iA \sin(\alpha)) = \sum_{n=-\infty}^{\infty} J_n(A) \exp(in\alpha), \quad (5.26)$$

where J_n denotes the n-th order Bessel function of the first kind. With this expansion in place, the second term can be written as

$$\begin{aligned} & \frac{V_0^2}{4} \int_{-\infty}^{\infty} d\tau_1 \int_{-\infty}^{\infty} d\tau_2 \exp\left(\frac{iF_0}{2}(\tau_2^2 - \tau_1^2)\right) e^{iA \sin(\omega_0\tau_1)} \\ &= \frac{V_0^2}{4} \int_{-\infty}^{\infty} d\tau_1 \int_{-\infty}^{\infty} d\tau_2 \exp\left(\frac{iF_0}{2}(\tau_2^2 - \tau_1^2)\right) \sum_{n=-\infty}^{\infty} J_n(A) \exp(in\omega_0\tau_1). \end{aligned} \quad (5.27)$$

A change of variable to $\mu = (\tau_1 + \tau_2)/2$ and $\sigma = (\tau_2 - \tau_1)$ yields,

$$\begin{aligned} & \frac{V_0^2}{4} \int_{-\infty}^{\infty} d\tau_1 \int_{-\infty}^{\infty} d\tau_2 \exp\left(\frac{iF_0}{2}(\tau_2^2 - \tau_1^2)\right) \sum_{n=-\infty}^{\infty} J_n(A) \exp(in\omega_0\tau_1) \\ &= \frac{V_0^2}{4} \sum_{n=-\infty}^{\infty} J_n(A) \int_{-\infty}^{\infty} d\mu \int_{-\infty}^{\infty} d\sigma \exp(iF_0\mu\sigma + in\omega_0(2\mu - \sigma)) \\ &= \frac{V_0^2}{4} \sum_{n=-\infty}^{\infty} J_n(A) \int_{-\infty}^{\infty} d\mu \int_{-\infty}^{\infty} d\sigma \exp(i\mu(F_0\sigma + 2n\omega_0)) \exp(-in\omega_0\sigma) \\ &= \frac{V_0^2\pi}{2} \sum_{n=-\infty}^{\infty} J_n(A) \int_{-\infty}^{\infty} d\sigma \delta(F_0\sigma + 2n\omega_0) \exp(-in\omega_0\sigma) \\ &= \frac{V_0^2\pi}{2F_0} \sum_{n=-\infty}^{\infty} J_n(A) \exp\left(\frac{i2n^2\omega_0^2}{F_0}\right) \end{aligned} \quad (5.28)$$

The calculations for term three and four can be done in the same way, but are omitted here for the sake of brevity. In the end, the first term in the perturbation series $P_{tra,ZD}^{(1)}(\infty)$ in the zero damping limit reads,

$$\begin{aligned} P_{tra,ZD}^{(1)}(\infty) &= \frac{V_0^2\pi}{2F_0} \left(1 + \sum_{n=-\infty}^{\infty} J_n(A) \exp\left(\frac{i2n^2\omega_0^2}{F_0}\right) + \sum_{m=-\infty}^{\infty} J_m(-A) \exp\left(\frac{-im^2\omega_0^2}{2F_0}\right) \right. \\ &\quad \left. + \sum_{k,l=-\infty}^{\infty} J_k(A) J_l(-A) \exp\left(\frac{i\omega_0^2}{2F_0}(4k^2 - l^2)\right) \right). \end{aligned} \quad (5.29)$$

Evidently, this formula only gives reasonable results for $\frac{V_0^2\pi}{2F_0} < 1$, as it has already been the case in the ‘small coupling’ limit (Eq.(5.22)). Yet, there is a crucial difference between the ‘small coupling’ limit and the ‘small coupling, zero damping’ limit, represented by

Eq.(5.22) and Eq.(5.29), respectively. Namely, that the formula for $P_{tra,ZD}^{(1)}(\infty)$ carries an *explicit* dependence on ω_0 .

Unfortunately, the formula for $P_{tra,ZD}^{(1)}(\infty)$ comes with two caveats, one more severe than the other. Firstly, the infinite sums in the expression cannot be evaluated to a closed form expression and one therefore can only calculate the $P_{tra,ZD}^{(1)}(\infty)$ by truncating the sums. This is not much of a problem, as higher order Bessel functions quickly decay for $A \approx 1$. Truncating the sums at $n, m, k, l = 20$ stabilised the resulting numerical value for $P_{tra,ZD}^{(1)}$ up to order 10^{-3} , for given V_0 , F_0 and ω_0 . Secondly, the ω_0 dependence of $P_{tra,ZD}^{(1)}$ leads to a small imaginary part in the transition probability, which by definition it should not have. It is not clear to the author if this imaginary term is due to the fact that only the first order term of the perturbation series is considered and if higher order terms will cancel it or not. Nevertheless, it is so small (see figure 5.3), that it will be neglected in the following and only the real part of $P_{tra,ZD}^{(1)}$ is plotted. Still, until this issue is resolved the results to come shall be considered as preliminary.

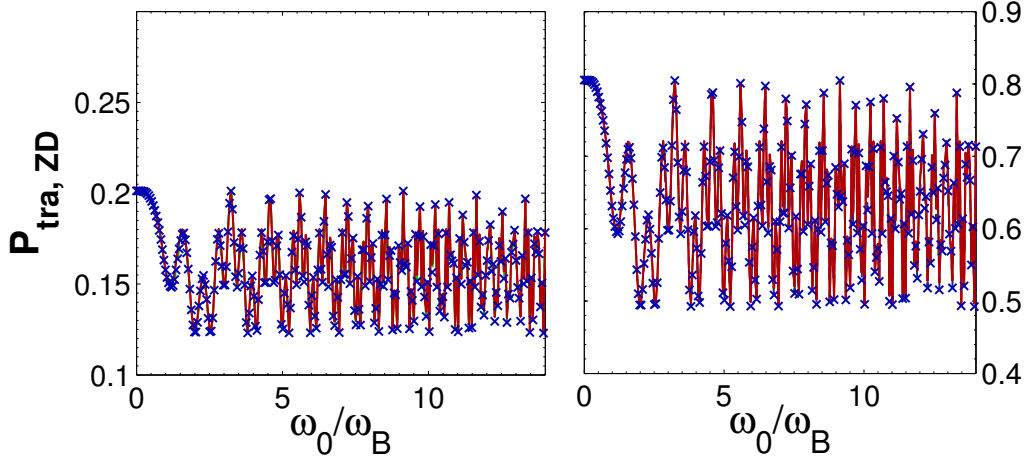


Figure 5.3: Analytical calculation for $P_{tra,ZD}^{(1)}$ vs ω_0 . The red solid lines show the magnitude of $P_{tra,ZD}^{(1)}$, the blue crosses show only the real part of $P_{tra,ZD}^{(1)}$. The parameters are $F_0 = 0.00762$, $A = 1.0$ and $V_0 = 0.015625$ (left figure) and $V_0 = 0.03125$ (right figure). The graphs have been obtained by evaluating the sums (with Mathematica) in Eq.(5.29) up to $n, m, k, l = 20$. No appreciable difference between the real part and the magnitude of $P_{tra,ZD}^{(1)}$ can be seen, therefore the imaginary part will be neglected in the following.

In the following, the analytical prediction for the transition probability with a deterministically oscillating phase, $\phi(t) = A \sin(\omega_0 t)$, is compared to numerical simulations. Figure 5.4 shows a good qualitative agreement between the analytical prediction (red solid line) and the numerical simulation (blue solid line with crosses). The analytical solution accurately predicts the position of the maxima and minima in the range $\omega_0/\omega_B = 0 \dots 8$, but shows some discrepancies for $\omega_0/\omega_B > 8$. Furthermore, the analytical solution systematically overestimates the transition probability. This is, however, expected as only

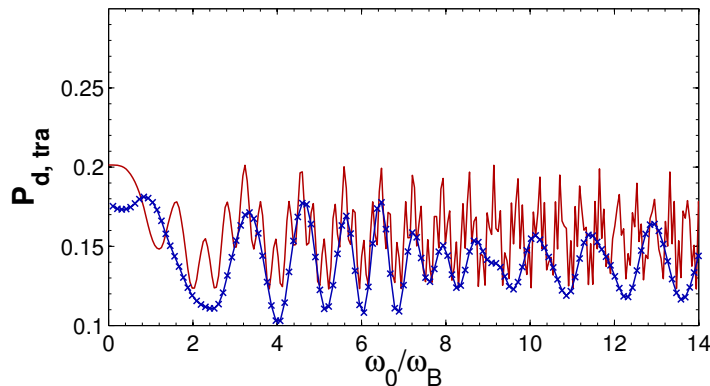


Figure 5.4: The red solid line shows the real part of $P_{tra, ZD}^{(1)}$. The blue solid line with crosses shows the diabatic transition probability as obtained from numerical simulations with a deterministically oscillating phase $\phi(t) = A \sin(\omega_0 t)$ (as described in section 4.2.3). The system parameters are $V_0 = 0.015625$, $F_0 = 0.00762$ and $A = 1.0 \approx 2\langle\phi^2\rangle$ and the truncation points for the sums in Eq.(5.29) are $n, m, k, l = 20$.

the first order term of the perturbation series has been taken into account and the second order term gives a negative correction (see Eq.(5.14)). It is also noticeable, that some of the finer features of the analytical solution cannot be seen in the numerical simulations; it looks as if the numerical results provide an *envelope* for the analytical ones. This may be due to a ‘smoothing’ of the finer features of the analytical solution when higher order terms are considered. Numerical inaccuracies can be ruled out in this case, as the step size in ω_0/ω_B should be small enough to resolve the fine structure of the solution.

A comparison to the numerical simulation with harmonic noise has been omitted, as the noise destroys the oscillatory behaviour of P_{tra} versus ω_0/ω_B in this parameter regime (compare to figure 4.2.2). Figure 5.5 unambiguously demonstrates the breakdown of the analytical solution for large V_0 . Even though the general structure of the analytical solution (red curve) in figure 5.5 is the same as in figure 5.4, the magnitude of it is far larger than unity. Moreover, there is no good qualitative agreement between the numerical data and the analytical solution anymore. Figure 5.5 (right) shows the renormalised analytical solution together with the numerical solution for the ‘noisy’ LZ-model as defined in Eq.(3.3) and the numerical solution for the ‘noisy’ LZ model with a deterministically oscillating phase $\phi(t) = A \sin(\omega_0 t)$, as defined in Eq.(4.8). It can be seen that the period of oscillation and the position of the maxima and minima is approximately the same for the two numerical simulations. However, the oscillations of the diabatic transition probability strongly differ in amplitude (as in section 4.2.3). Nevertheless, the deterministically oscillating phase model still captures the essential features of the noise process in this parameter regime. On the contrary, the analytical solution can neither predict the position of the maxima and minima nor does it show the same period of oscillation. Thus, for higher coupling strengths V_0 the first order perturbation term is not sufficient

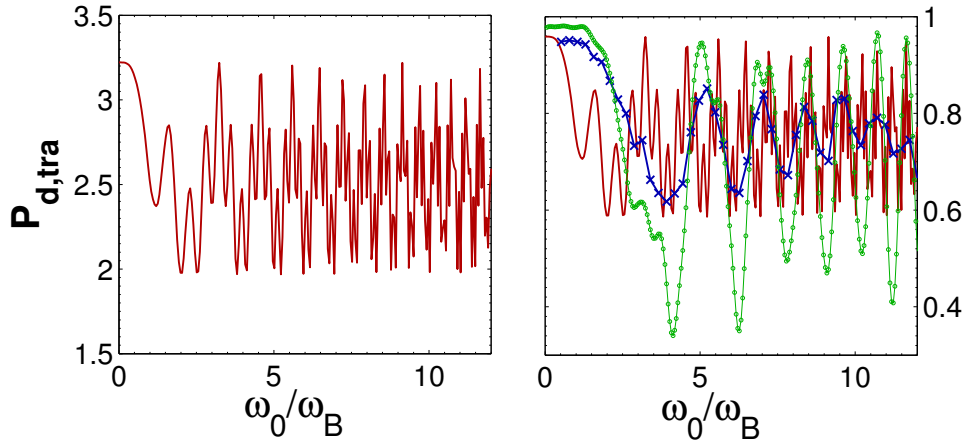


Figure 5.5: The left figure shows the analytical solution as given in Eq.(5.29) ($V_0 = 0.0625, F_0 = 0.00761954$). The figure on the right also shows the analytical solution (red solid line) but *renormalised* such that it approximately coincides with the curves obtained by numerical simulations (blue line with crosses and green line with circles) at $\omega/\omega_B = 0$. The blue line shows the diabatic transition probability for the ‘noisy’ LZ Hamiltonian as defined in Eq.(3.3), with $V_0 = 0.0625, F_0 = 0.00761954, \Gamma = 0.00761954, \langle \phi^2 \rangle = 0.5$. The green line shows the diabatic transition probability for a deterministically oscillation phase $\phi(t) = A \sin(\omega_0 t)$ (as described in section 4.2.3), with $V_0 = 0.015625, F_0 = 0.00762$ and $A = 1.0$.

to capture the important features of the influence of harmonic noise on the transition probability.

The practical use of the analytical results presented in this section is rather limited. Yet, especially the solution with a deterministic phase provides insight into the behaviour of the diabatic transition probability. In Eq.(5.29), the initial decay and the oscillations of the solution are due to the $\exp\left(\frac{i2n^2\omega_0^2}{F_0}\right)$ -like terms. Those terms arise solely due to the sinusoidal nature of $\phi(t)$ (they were introduced via the Jacobi-Anger expansion). Hence, even though the quantitative performance of the analytical solution is not very good, it backs up the idea that the oscillations shown in figures 4.5 to 4.7 are due to a (mis-)matching of energy scales/frequencies of the system and the noise process $\phi(t)$. Moreover, the $\exp\left(\frac{i2n^2\omega_0^2}{F_0}\right)$ -like terms can account for the moving of the position of the first minima with respect to varying F_0 (see figures 4.9 and 4.11), because its position is determined by the argument $\frac{i2n^2\omega_0^2}{F_0}$. Unfortunately, the moving of the position of the first minima with respect to V_0 cannot be explained by the formula in Eq.(5.29). It should also be mentioned that the analytical solutions presented here cannot account for any ‘finite-time’ effects, as an infinitely long time evolution has been assumed in the derivation.

6 Conclusion

In the introduction, three questions were given that this thesis tried to answer. The first question was, “Is it possible to approximate the dynamics of the BEC close to an avoided crossing in the full modified WSS by an effective Landau-Zener model?” Out of the three questions posed this is the only one with a clear answer. In section 3.2 it was shown that it is indeed possible to locally approximate the full modified WSS by a ‘noisy’ two-level LZ model, if and only if the original optical lattice and the stochastic optical lattice have the same spatial periodicity. In such a case the effective LZ Hamiltonian is given by

$$\hat{H}_{LZ,N} = \frac{1}{2} \begin{pmatrix} -F_0 t & V_0(1 + e^{i\phi(t)}) \\ V_0(1 + e^{-i\phi(t)}) & F_0 t \end{pmatrix}, \quad (6.1)$$

where all the terms have the same meaning as previously.

The second question, “Can the effective Landau-Zener model reproduce the functional dependence of the tunnelling probability on the frequency of the stochastic phase (as observed in the full modified Wannier-Stark system)?” was much harder to answer. In section 4.2.2 it was shown that there is a good qualitative agreement between the transition probability as observed in the ‘noisy’ LZ model and the ‘noisy’ WSS (see figure 6.1). It was further pointed out that the LZ model systematically overestimates the diabatic transition probability (i.e. underestimates the tunnelling probability into the first excited band). This behaviour is the worst for small coupling strengths V_0 ($\gamma_{\text{eff}} \gtrsim 1$), but less significant for larger coupling ($\gamma_{\text{eff}} < 1$) (see figures 4.5 to 4.8). This is because the ‘noisy’ LZ model cannot account for transitions far away from an avoided crossing. Those transitions are strongly suppressed in the ‘noiseless’ WSS and for large V_0 in the ‘noisy’ WSS, but can happen for small V_0 ($\gamma_{\text{eff}} \gtrsim 1$) in the ‘noisy’ WSS (see section 4.2.2).

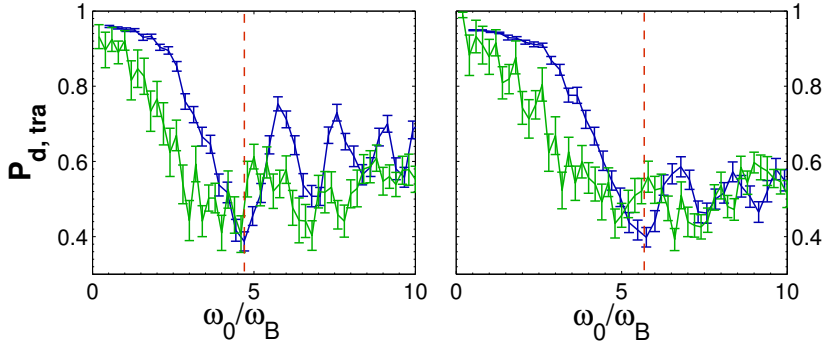


Figure 6.1: Description see figure 4.6.

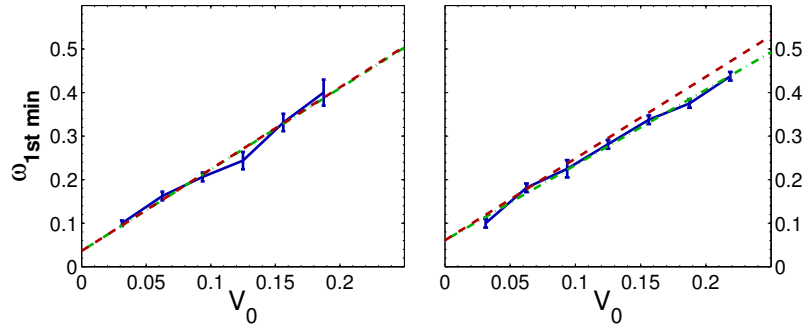


Figure 6.2: For a description see figure 4.11.

Finally, question three, “Is it possible to predict and explain the position of the minimum shown in figure 1.1?”, was answered by numerical simulations and also qualitatively by analytical calculations. It was shown in section 4.2.2 that the position of the minimum is determined by the effective band gap ΔE_{eff} of the ‘noisy’ LZ model, plus a constant positive offset (see figure 6.2). Furthermore, this offset was shown to be sensitive to the driving force F_0 , which was also backed up by analytical calculations for a deterministic oscillating phase (see section 4.2.3). In addition to that, it was demonstrated (see sections 4.2.3 and 5.2.2) that the initial decrease in the diabatic transition probability is due to the sinusoidal nature of the harmonic noise process.

Coming back to question two again, it has to be admitted that it has only been half answered in this thesis. The subsequent rise of the transition probability after the minimum shown in figure 1.1 has not at all been discussed. In section 4.1 it was briefly pointed out that the ‘noisy’ LZ model also, shows an increase in the diabatic transition probability for high ω_0 . It was further mentioned that the point of increase depends on the total integration time.

Analysing this sudden increase is subject to ongoing work, but qualitative explanations can be given here. In the ‘noisy’ WSS this rise has already been explained by Tayebirad and co-workers. They argued that in this regime the stochastic phase $\phi(t)$ fluctuates on a much smaller time scale than the one of the system. In such a case, it is possible to average over the stochastic potential term according to the distribution of $\phi(t)$ (Eq.(2.46)) and one simply obtains a rescaled, but deterministic, potential. This new effective potential describes the asymptotic value of the transition probability for high noise frequencies in the full ‘noisy’ system well [6]. Unfortunately, in the ‘noisy’ LZ model averaging over the harmonic noise variable to obtain an effective band gap ΔE_{eff} (Eq.(3.6)) does not work very well for high noise frequencies (see figure 6.3). Moreover, it can be seen in figure 6.3 that the rise in the diabatic transition probability happens much earlier in the ‘noisy’ LZ model than in the full ‘noisy’ WSS. Yet, there remains a general qualitative agreement between the two models.

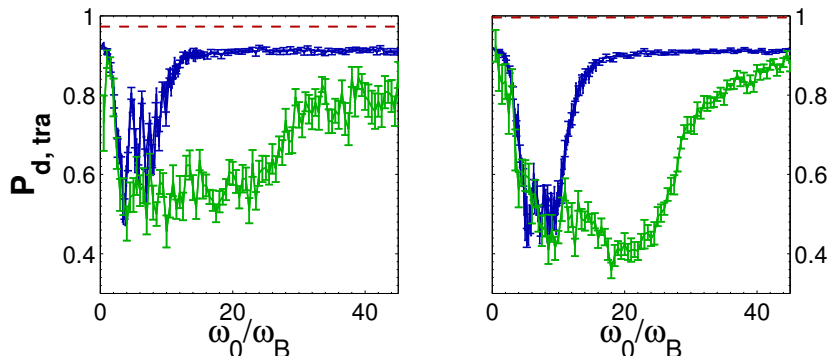


Figure 6.3: Diabatic transition probabilities versus the dimensionless noise frequency ω_0/ω_B . The green solid lines show the numerical simulations for the full ‘noisy’ system. The blue solid lines show the numerical simulations for the ‘noisy’ LZ model. The horizontal dashed lines give the diabatic transition probability as obtained from the LZ formula with an effective band gap ΔE_{eff} . The parameters are $F_0 = 0.00597$, $\Gamma = 0.00762$, $\langle \phi^2 \rangle = 0.5$ and $V_0 = 0.03125$ (left) and $V_0 = 0.0625$ (right).

The sudden rise in the diabatic transition probability (decrease of tunnelling probability) can be intuitively explained within the LZ model. Figure 6.4 shows a schematic representation of the energy levels in the ‘noisy’ LZ model. An atom of the BEC can only tunnel (curly orange lines) from the ground to the first excited band at a specific time t , if it has enough energy to bridge the energy gap between the two bands at time t . If the driving force F_0 is assumed to be small, this energy has to come from the harmonic noise process. However, if the atom’s energy is too large, there is no state that the atom can ‘jump’ to and hence no transition to the upper energy band can take place either (indicated by the crossed out transition in figure 6.4). In the case of an infinitely long time evolution of the system this does not pose a problem, because the energy gap increases linearly for $|t| \gg 1$. So at some point in time even the most energetic atoms can couple to the first excited band.

But if the time evolution is restricted to a finite interval (blue shaded area in figure 6.4), the band gap will never be large enough such that the ‘high’ energy atoms could couple to the upper band. In figure 6.4 this means that the last atoms that can jump into the upper energy band need to bridge an energy of ω' . Consequently, atoms with higher energy than ω' cannot jump into the upper band.

Of course, this argument is rather crude and neglects many important features of a transition process such as the finite jump and relaxation times. Yet, it can explain at least four important features connected to the rise in the diabatic transition probability for high omega. First, it explains the rise itself. If the noise process feeds so much energy into the system that the atoms of the BEC cannot couple to the upper band anymore, tunnelling is suppressed and the diabatic transition probability rises. The frequency ω_0 where this happens should be roughly determined by the maximal effective band gap in the time interval. Secondly, it accounts for the moving of this frequency with respect to

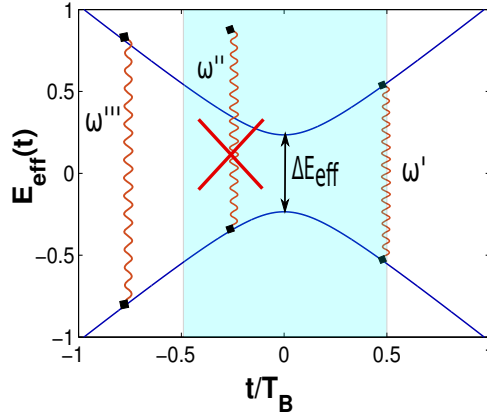


Figure 6.4: Schematic representation of the energy levels in the ‘noisy’ LZ model. The curly orange lines indicate tunnelling (i.e. no diabatic transition) from the ground to the first excited band. The blue shaded area represents the time the system has to evolve, i.e. the total integration time. To compare the ‘noisy’ LZ model to the WSS this time has to be $t/T_B = 1$ (definition of T_B see Eq.(2.18)).

the integration time; a longer integration time leads to a larger maximal effective band gap and hence the critical frequency where the diabatic transition probability starts to rise, increases. Thirdly, this also the reason why this ‘rise’ cannot be seen in the analytical solution, as an infinitely long time evolution was assumed in this case. Lastly, in the ‘noisy’ WSS high energy atoms can also couple to higher bands, thus allowing more tunnelling events than in the ‘noisy’ LZ model and hence a later rise in the diabatic transition probability.

As mentioned previously, this is ongoing work and it goes without saying that a more thorough and quantitative analysis is needed here.

To summarise, the ‘noisy’ LZ model still captures many of the important features of the ‘noisy’ WSS around an avoided crossing, but the agreement is worse than in the ‘noiseless’ case. One of the main shortcomings of the ‘noisy’ LZ model is the systematic overestimation of the diabatic transition probability, which is due to transitions taking place over the full Brillouin zone in the ‘noisy’ system. Moreover, in the ‘noisy’ WSS the influence of higher bands cannot always be neglected (especially for high noise frequencies), which poses a conceptual problem to a description by a LZ model.

‘ We conclude by giving an outlook on possible future work:

- The obvious continuation of the analysis of the BEC’s tunnelling dynamics for high noise frequencies.
- The deterministic phase model given in section 4.2.3 represents an interesting possibility to control the tunnelling dynamics of the BEC by tuning the phase frequency. Hence, a more thorough analysis of the BEC’s behaviour in the full ‘noisy’ WSS

with deterministic phase appears worthwhile.

- In reality, one is usually interested in the tunnelling probabilities of the BEC after many avoided crossings. A natural extension of the work given here is thus to model the ‘noisy’ WSS by subsequent LZ transitions; thereby keeping track of interference effects between the part of the BEC that tunneled into the upper band and the part that remained in the ground band [34] (see section 2.3). Again, studying the influence of the noise on the interference effects might be interesting.
- Extend the ‘noisy’ LZ model to a three or four state model to capture the influence of the next higher bands.
- Concerning a direct analysis of the full ‘noisy’ WSS, it may be a good idea to analyse the energy spectrum of the Hamiltonian given in Eq.(3.1).

7 Appendix

7.1 Numerical algorithm to generate harmonic noise

The algorithm to generate harmonic noise as defined in Eq.(2.44) is presented in this section. The (numerical) integration of stochastic differential equations is not an easy task and to do it rigorously, results from stochastic calculus are needed. Unfortunately, this goes beyond the scope of this thesis and we will not give strict mathematical definitions of the integrals used in the following derivation. Moreover, the algorithm presented in the following has been provided by my co-workers/predecessors Stephan Burkhardt/Ghazal Tayebirad, who themselves received it from Riccardo Mannella in Pisa. So neither the algorithm, nor the way it is derived and presented here are my original works and analogous derivations can also be found in [8, 42].

There are two key steps in the derivation of the algorithm. The first one is to write down a formal solution to the two coupled stochastic differential equations defining harmonic noise,

$$\partial_t \phi = \mu \quad (7.1)$$

$$\partial_t \mu = -2\Gamma\mu - \omega_0^2 \phi + \sqrt{4T\Gamma}\xi(t) . \quad (7.2)$$

This will give $\phi(t)$ and $\mu(t)$ in terms of an integral over the stochastic variable $\xi(t)$, which itself will be a stochastic variable ($\boldsymbol{\alpha}(t)$) again. In the second step, the known properties of $\phi(t)$ and $\mu(t)$, such as first and second moments and (cross-)correlation functions will be used to determine the statistical properties of the new stochastic variable $\boldsymbol{\alpha}(t)$. Once the statistical properties of $\boldsymbol{\alpha}(t)$ are known, it can be easily generated in terms of gaussian random numbers.

The two coupled stochastic differential equations above can be written in matrix form such that,

$$\partial_t \mathbf{x} = \mathbf{A} \mathbf{x} + \sqrt{4T\Gamma} \begin{pmatrix} 0 \\ \xi(t) \end{pmatrix}, \quad (7.3)$$

with

$$\mathbf{x} = \begin{pmatrix} \phi \\ \mu \end{pmatrix} \quad \text{and} \quad \mathbf{A} = \begin{pmatrix} 0 & 1 \\ -\omega_0^2 & -2\Gamma \end{pmatrix} . \quad (7.4)$$

Formally, this equation can be integrated by means of an integrating factor and one obtains,

$$\mathbf{x}(t) = e^{\mathbf{A}t} \mathbf{x}(\mathbf{0}) + \int_0^t \sqrt{4T\Gamma} e^{\mathbf{A}(t-t')} \begin{pmatrix} 0 \\ \xi(t') \end{pmatrix} dt' . \quad (7.5)$$

The stochastic nature of $\xi(t)$ does not allow to interpret the integral as a standard Riemann integral. However, due to the gaussian nature of $\xi(t)$ and because the function $\sqrt{4T\Gamma}e^{A(t-t')}$ does not depend on $\xi(t)$, the integral can be thought of as a sum over gaussian variables [48]. Furthermore, this implies that the above integral will simply be another gaussian variable with mean zero, as the sum over gaussian variables also is a gaussian variable and $\langle \xi(t) \rangle = 0$, as defined in Eq.(2.45). This new gaussian variable will be called $\alpha(t)$ from now on. Moreover, the term $\exp(\mathbf{A})$ can be evaluated explicitly by using the identity

$$\exp(\mathbf{A}) = \mathbf{U}^{-1} \exp(\mathbf{U}\mathbf{A}\mathbf{U}^{-1})\mathbf{U} , \quad (7.6)$$

where \mathbf{U} is the matrix composed of the eigenvectors of \mathbf{A} . This yields $\mathbf{M}(t) = \exp(\mathbf{A})$ with,

$$M(t)_{1,1} = \frac{1}{\lambda_- - \lambda_+} \left(-\lambda_- e^{t\lambda_+} + \lambda_+ e^{t\lambda_-} \right), \quad (7.7)$$

$$M(t)_{2,2} = \frac{1}{\lambda_- - \lambda_+} \left(\lambda_+ e^{t\lambda_+} - \lambda_- e^{t\lambda_-} \right), \quad (7.8)$$

$$M(t)_{1,2} = \frac{1}{\lambda_- - \lambda_+} \left(e^{t\lambda_+} - e^{t\lambda_-} \right), \quad (7.9)$$

$$M(t)_{2,1} = \frac{\lambda_- \lambda_+}{\lambda_- - \lambda_+} \left(-e^{t\lambda_+} + e^{t\lambda_-} \right) \quad (7.10)$$

and $\lambda_{\pm} = -\Gamma \pm \sqrt{\Gamma^2 - \omega_0^2}$. Here and in the following subscripts indicate matrix/vector elements. Finally, Eq.(7.5) can be re-expressed as

$$\mathbf{x}(t) = \mathbf{M}(t)\mathbf{x}(0) + \alpha(t) . \quad (7.11)$$

So far, nothing apart from a formal integration of Eq.(2.44) and algebraic manipulations has happened. But the fact that the statistical properties of the variables $\phi(t)$ and $\mu(t)$ are known (see Eq.(2.47)), will be used to determine those of the gaussian variable $\alpha(t)$. This can be done by matching the first/second moment and the correlation function $\langle \phi(t)\mu(t) \rangle$ of the left hand side of Eq.(7.5) with those on the right hand side. I.e.

$$\left\langle \begin{pmatrix} \phi \\ \mu \end{pmatrix} \right\rangle = \langle \mathbf{M}(t)\mathbf{x}(0) + \alpha(t) \rangle , \quad (7.12)$$

which gives,

$$\begin{aligned}
\langle \phi(t)^2 \rangle &= \frac{T}{\omega_0^2} = \left\langle \left[\left(\mathbf{M} \begin{pmatrix} \phi(0) \\ \mu(0) \end{pmatrix} \right)_1 + \alpha_1 \right]^2 \right\rangle \\
&= \langle \phi(0)^2 \rangle M_{1,1}^2 + \langle \mu(0)^2 \rangle M_{1,2}^2 + \langle \alpha_1^2 \rangle \\
&\Rightarrow \langle \alpha_1^2 \rangle = \frac{T}{\omega_0^2} (1 - M_{1,1}^2 - \omega_0^2 M_{1,2}^2),
\end{aligned} \tag{7.13}$$

$$\begin{aligned}
\langle \mu(t)^2 \rangle &= T = \left\langle \left[\left(\mathbf{M} \begin{pmatrix} \phi(0) \\ \mu(0) \end{pmatrix} \right)_2 + \alpha_2 \right]^2 \right\rangle \\
&\Rightarrow \langle \alpha_2^2 \rangle = T \left(1 - M_{2,2}^2 - \frac{M_{2,1}^2}{\omega_0^2} \right),
\end{aligned} \tag{7.14}$$

$$\begin{aligned}
\langle \phi(t)\mu(t) \rangle &= 0 = \left\langle \left[\left(\mathbf{M} \begin{pmatrix} \phi(0) \\ \mu(0) \end{pmatrix} \right)_1 + \alpha_1 \right] \left[\left(\mathbf{M} \begin{pmatrix} \phi(0) \\ \mu(0) \end{pmatrix} \right)_2 + \alpha_2 \right] \right\rangle \\
&\Rightarrow \langle \alpha_2 \alpha_1 \rangle = -T \left(M_{1,2} M_{2,2} + \frac{M_{2,1} M_{1,1}}{\omega_0^2} \right),
\end{aligned} \tag{7.15}$$

where the definitions of Eq.(2.47) and Eq.(2.48), $\langle \phi(t)^2 \rangle = \frac{T}{\omega_0^2}$, $\langle \mu(t)^2 \rangle = T$ and $\langle \phi(t)\mu(t) \rangle = 0$ have been used. Note that $\langle \alpha_1 \rangle$ and $\langle \alpha_2 \rangle$ are both zero, as $\langle \phi \rangle = 0$ and $\langle \mu \rangle = 0$. The statistical properties of $\alpha(t)$ have now been determined; however, to actually produce a harmonic noise process it is necessary to generate $\alpha(t)$ such that it fulfils the properties defined in Eq.(7.15). This can be done by first generating a vector \mathbf{z} composed of two gaussian random variables with zero mean and unit variance and then multiplying it by a suitably chosen matrix [8], such that

$$\alpha = \mathbf{Bz} = \begin{pmatrix} B_{11} & 0 \\ B_{21} & B_{22} \end{pmatrix} \mathbf{z}, \tag{7.16}$$

where \mathbf{B} is determined by the statistical properties of α . I.e.,

$$\begin{aligned}
\langle \alpha_1^2 \rangle &= \langle (B_{11} z_1)^2 \rangle \\
&= B_{11}^2 \langle z_1^2 \rangle \\
&= B_{11}^2
\end{aligned} \tag{7.17}$$

$$\langle \alpha_2^2 \rangle = B_{21}^2 + B_{22}^2 \tag{7.18}$$

$$\langle \alpha_1 \alpha_2 \rangle = B_{21} B_{11}. \tag{7.19}$$

solving this set of equations gives the components of \mathbf{B} as,

$$B_{11}^2 = \langle \alpha_1^2 \rangle \quad B_{21} = \frac{\langle \alpha_1 \alpha_2 \rangle}{B_{11}} \quad B_{22}^2 = \langle \alpha_2^2 \rangle - B_{21}^2, \tag{7.20}$$

which finally leads to an explicit form of α ,

$$\alpha = \begin{pmatrix} \sqrt{\langle \alpha_1^2 \rangle} & 0 \\ \frac{\langle \alpha_1 \alpha_2 \rangle}{\sqrt{\langle \alpha_1^2 \rangle}} & \sqrt{\langle \alpha_2^2 \rangle - \frac{\langle \alpha_1 \alpha_2 \rangle^2}{\langle \alpha_1^2 \rangle}} \end{pmatrix} \mathbf{z}. \tag{7.21}$$

Lastly, it is possible to write down an iteration formula for the harmonic noise process by inserting the specific form $\boldsymbol{\alpha}$ into Eq.(7.11),

$$\begin{pmatrix} \phi(t + \Delta t) \\ \mu(t + \Delta t) \end{pmatrix} = \mathbf{M}(\Delta t) \begin{pmatrix} \phi(t) \\ \mu(t) \end{pmatrix} + \mathbf{B}(\Delta t)\mathbf{z} . \quad (7.22)$$

Note that the two matrices \mathbf{M} and \mathbf{B} both depend on the system parameters T, Γ and ω_0 via Eqs.(7.7)-(7.10) and Eqs.(7.13)-(7.15), and on the step size Δt . Moreover, both are completely deterministic, the stochasticity of Eq.(7.22) only enters via the vector \mathbf{z} .

The algorithm in Eq.(7.22) can be used to generate the harmonic noise process described in section 2.4. This is done in the following way. For each noise realisation an initial vector $\begin{pmatrix} \phi(t_0) \\ \mu(t_0) \end{pmatrix}$ is chosen according to the probability density distribution in Eq.(2.46). To calculate the new state $\begin{pmatrix} \phi(t_0 + \Delta t) \\ \mu(t_0 + \Delta t) \end{pmatrix}$ two gaussian random numbers with zero mean and unit variance are generated (to give \mathbf{z}). Then the two matrices $\mathbf{M}(\Delta t)$ and $\mathbf{B}(\Delta t)$ are calculated according to Eqs.(7.7)-(7.10) and Eqs.(7.13)-(7.15). Once this is done Eq.(7.22) is used to obtain the new state. In the next step $\begin{pmatrix} \phi(t_0 + \Delta t) \\ \mu(t_0 + \Delta t) \end{pmatrix}$ is used as the new initial state and the procedure above is repeated to obtain $\begin{pmatrix} \phi(t_0 + 2\Delta t) \\ \mu(t_0 + 2\Delta t) \end{pmatrix}$.

There are two important features of this algorithm that should be mentioned. First, the algorithm is accurate for *any* step size Δt . This somewhat surprising feature stems from the fact that in the derivation of the specific form of $\boldsymbol{\alpha}$ no approximations have been made. Secondly, for each time step two gaussian random numbers have to be generated, which leads to a considerable increase in computation time compared to algorithms that only need one random number per step. To conclude, the algorithm presented is highly accurate but rather slow for small step sizes.

7.2 Some more numerical results

In this section, more numerical results are presented to back up qualitative explanations given in the main text (there will be references to the figures presented here). The figures given here have been omitted from the main text to keep it concise and stay focussed on the main results.

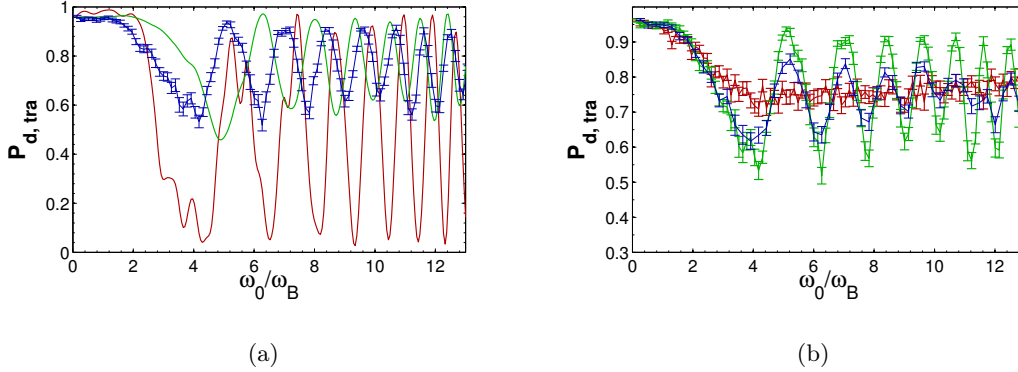


Figure 7.1: Both figures show the diabatic transition probability versus the rescaled noise frequency in the ‘noisy’ LZ model (numerical simulations have been done as described in section 4.1). In figure 7.1a the parameters are $V_0 = 0.0625$, $F_0 = 0.00762$, $\Gamma = 0.0$ and $\langle \phi^2 \rangle = 0.5$ (blue solid line with errorbars); the lines without errorbars have been obtained with a deterministically oscillating phase (see section 4.2.3) with $A = 1.5$ (red solid line) and $A = 0.5$ (green solid line). In figure 7.1b Γ has been varied. V_0 , F_0 and $\langle \phi^2 \rangle$ are the same as in 7.1a, but $\Gamma = 0.0762$ (red solid line), $\Gamma = 0.0152$ (blue solid line) and $\Gamma = 0$ (green solid line).

In figure 7.1a it can be seen that different amplitudes of the deterministically oscillating phase lead to a change in the structure of the peaks. For example, the green line shows much smaller peaks than the red one. Also the position of the peaks varies slightly. Averaging over the amplitude A of the deterministic phase according to the equilibrium distribution of the harmonic noise (Eq.(2.46)), leads to a broadening of the peaks and a reduction of their height (blue solid line).

Figure 7.1b shows the diabatic transition probability in the ‘noisy’ LZ model for different values of the damping Γ . It can be seen that there is hardly any difference between $\Gamma = 0$ (green solid line) and $\Gamma = 0.00762$ (blue solid line), however for $\Gamma = 0.0762$ the peak structure vanishes. For an interpretation of this effect see section 4.2.3.

The following figure (7.2) has not been referenced in the main body of the text and is only given for completeness. This time, the variance of the noise process has been varied. Evidently, increasing the variance of the noise process leads to a stronger influence of the noise on the system and a quicker decay of the transition probability. This can be easily understood in terms of the deterministically oscillating phase model, by recalling

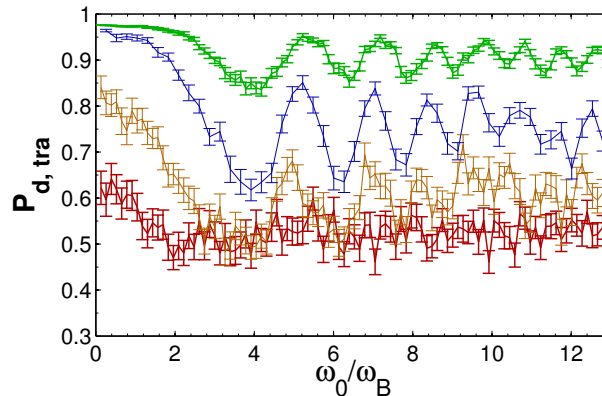


Figure 7.2: The diabatic transition probability versus the rescaled noise frequency in the ‘noisy’ LZ model is shown again. This time the variance of the noise process has been varied. The parameters are $V_0 = 0.0625$, $F_0 = 0.00762$, $\Gamma = 0.00762$ and $\langle \phi^2 \rangle = 10$ (red solid line), $\langle \phi^2 \rangle = 2$ (brown solid line), $\langle \phi^2 \rangle = 0.5$ (blue solid line) and $\langle \phi^2 \rangle = 10$ (green solid line).

that the amplitude $A \propto \sqrt{\langle \phi^2 \rangle}$. Thus if the variance is very small, the harmonic noise amplitude $\phi(t)$ exhibits small oscillations around its mean value and only provides a small perturbation to the noiseless system. However, if the variance is very large, $\phi(t)$ has a large amplitude which leads to ‘wild’ oscillations of the second stochastic optical lattice (see 3.1). Eventually, this destroys the band structure of the system and leads to an incoherent superposition of the diabatic energy states (i.e. the transition probability tends to 1/2 as can be seen in figure 7.2).

7.3 Derivation of the perturbation series for the transition probabilities

In section 5.1.3 a perturbation series in terms of the off-diagonal coupling V_0 has been given for the diabatic transition probability in the ‘noisy’ LZ model. In this section the perturbation series will be derived. It is expected that this treatment is analogous to Kayanuma’s [1, 44], even though he does not give it explicitly in his papers.

Recall that the transition probability is given by,

$$P_{tra}(\infty) = \left\langle {}_d\langle 2 | \exp_+ \left(-i \int_{-\infty}^{\infty} \hat{H}_{LZ,N}(\tau) d\tau \right) | 1 \rangle_d \langle 1 | \exp_- \left(i \int_{-\infty}^{\infty} \hat{H}_{LZ,N}(\tau) d\tau \right) | 2 \rangle_d \right\rangle. \quad (7.23)$$

We proceed by calculating the two matrix elements one at a time and only take the average over the noise process afterwards. Using Eq.(5.13) the first matrix element can be written as,

$${}_d\langle 2 | \exp_+ \left(-i \int_{-\infty}^{\infty} \hat{H}_{LZ,N}(\tau) d\tau \right) | 1 \rangle_d = \quad (7.24)$$

$${}_d\langle 2 | \exp \left(-i \int_{-\infty}^{\infty} H_0(\tau) d\tau \right) \exp_+ \left(-i \int_{-\infty}^{\infty} \tilde{H}_{int}(\tau) d\tau \right) | 1 \rangle_d \quad (7.25)$$

Identity(5.12) can then be used to write

$$\exp \left(-i \int_{-\infty}^{\infty} H_0(\tau) d\tau \right) = \exp\left(\frac{i}{2} \int_{-\infty}^{\infty} F_0 \tau d\tau\right) | 1 \rangle_d \langle 1 | + \exp\left(-\frac{i}{2} \int_{-\infty}^{\infty} F_0 \tau d\tau\right) | 2 \rangle_d \langle 2 | \quad (7.26)$$

$$\equiv A^* | 1 \rangle_d \langle 1 | + A | 2 \rangle_d \langle 2 | , \quad (7.27)$$

where $\exp(-\frac{i}{2} \int_{-\infty}^{\infty} F_0 \tau d\tau)$ has been abbreviated with A . Therefore, the matrix element becomes,

$${}_d\langle 2 | \exp_+ \left(-i \int_{-\infty}^{\infty} \hat{H}_{LZ,N}(\tau) d\tau \right) | 1 \rangle_d = A {}_d\langle 2 | \exp_+ \left(-i \int_{-\infty}^{\infty} \tilde{H}_{int}(\tau) d\tau \right) | 1 \rangle_d . \quad (7.28)$$

Let us proceed by expanding the term $\exp_+ \left(-i \int_{-\infty}^{\infty} \tilde{H}_{int}(\tau) d\tau \right)$ in terms of the Dyson series of Eq.(5.4).

$$\begin{aligned} & \exp_+ \left(-i \int_{-\infty}^{\infty} \tilde{H}_{int}(\tau) d\tau \right) = \\ & 1 + \sum_{n=1}^{\infty} (-i)^n \int_{-\infty}^t d\tau_1 \int_{-\infty}^{\tau_1} d\tau_2 \dots \int_{-\infty}^{\tau_{n-1}} d\tau_n \tilde{H}_{int}(\tau_1) \tilde{H}_{int}(\tau_2) \dots \tilde{H}_{int}(\tau_n) \end{aligned} \quad (7.29)$$

In the following the first few terms of this series are written out explicitly by using the definition of $\tilde{H}_{int}(\tau)$ in Eq.(5.11) and abbreviating $\exp(-iF_0 \int_{-\infty}^{\tau} \tau' d\tau')$ with $e^{-i\alpha(\tau)}$. Inserting it into the matrix element gives:

1st Term:

$$A {}_d\langle 2 | 1 | 1 \rangle_d = 0 \quad (7.30)$$

Furthermore, it can be seen that all terms with *even* n are going to be zero, because an anti-diagonal matrix ($\tilde{H}_{int}(\tau)$) raised to an even power gives a diagonal matrix, i.e. the ${}_d\langle 2 | \dots | 1 \rangle_d$ matrix element is zero.

n=1 term:

$$(-i) A {}_d\langle 2 | \left(\frac{1}{2} \int_{-\infty}^{\infty} V(\tau_1) e^{-i\alpha(\tau_1)} d\tau_1 | 1 \rangle_d \langle 2 | + \frac{1}{2} \int_{-\infty}^{\infty} V^*(\tau_1) e^{i\alpha(\tau_1)} d\tau_1 | 2 \rangle_d \langle 1 | \right) | 1 \rangle_d$$

$$= (-i)A \frac{1}{2} \int_{-\infty}^{\infty} V^*(\tau_1) e^{i\alpha(\tau_1)} d\tau_1 \quad (7.31)$$

n=3 Term:

$$\begin{aligned} & (-i)^2 A_d \langle 2 | \left(\frac{1}{2} \int_{-\infty}^{\infty} \int_{-\infty}^{\tau_1} \int_{-\infty}^{\tau_2} V(\tau_1) V^*(\tau_2) V(\tau_3) e^{-i\alpha(\tau_1)} e^{+i\alpha(\tau_2)} e^{-i\alpha(\tau_3)} d\tau_1 d\tau_2 d\tau_3 | 1 \rangle_d \langle 2 | \right. \\ & \quad \left. + \frac{1}{2} \int_{-\infty}^{\infty} \int_{-\infty}^{\tau_1} \int_{-\infty}^{\tau_2} V^*(\tau_1) V(\tau_2) V^*(\tau_3) e^{+i\alpha(\tau_1)} e^{-i\alpha(\tau_2)} e^{+i\alpha(\tau_3)} d\tau_1 d\tau_2 d\tau_3 | 2 \rangle_d \langle 1 | \right) | 1 \rangle_d \\ & = \frac{1}{2} (-i)^3 A \int_{-\infty}^{\infty} \int_{-\infty}^{\tau_1} \int_{-\infty}^{\tau_2} V^*(\tau_1) V(\tau_2) V^*(\tau_3) e^{+i\alpha(\tau_1)} e^{-i\alpha(\tau_2)} e^{+i\alpha(\tau_3)} d\tau_1 d\tau_2 d\tau_3 \quad (7.32) \end{aligned}$$

⋮

and so on. The positively time ordered matrix element is thus given by:

$$\begin{aligned} & d \langle 2 | \exp_+ \left(-i \int_{-\infty}^{\infty} \hat{H}_{LZ,N}(\tau) d\tau \right) | 1 \rangle_d \\ & = \frac{1}{2} (-i) A \int_{-\infty}^{\infty} V^*(\tau_1) e^{+i\alpha(\tau_1)} d\tau_1 \\ & \quad + \frac{1}{8} (-i)^3 A \int_{-\infty}^{\infty} \int_{-\infty}^{\tau_1} \int_{-\infty}^{\tau_2} V^*(\tau_1) V(\tau_2) V^*(\tau_3) e^{+i(\alpha(\tau_1) - \alpha(\tau_2) + \alpha(\tau_3))} d\tau_1 d\tau_2 d\tau_3 \\ & \quad + \frac{1}{32} (-i)^5 A \int_{-\infty}^{\infty} \int_{-\infty}^{\tau_1} \dots \int_{-\infty}^{\tau_4} d\tau_1 d\tau_2 \dots d\tau_5 V^*(\tau_1) V(\tau_2) \dots V^*(\tau_5) \\ & \quad \quad \quad \times e^{+i(\alpha(\tau_1) - \alpha(\tau_2) + \alpha(\tau_3) - \alpha(\tau_5) + \alpha(\tau_5))} \\ & \quad + \dots \quad (7.33) \end{aligned}$$

Likewise, the negatively time-ordered matrix element can be calculated as,

$$\begin{aligned} & d \langle 1 | \exp_- \left(i \int_{-\infty}^{\infty} \hat{H}_{LZ,N}(\tau') d\tau' \right) | 2 \rangle_d \\ & = \frac{1}{2} i A^* \int_{-\infty}^{\infty} V(\tau'_1) e^{-i\alpha(\tau'_1)} d\tau'_1 \\ & \quad + \frac{1}{8} i^3 A^* \int_{-\infty}^{\infty} \int_{\tau'_1}^{\infty} \int_{\tau'_2}^{\infty} V(\tau'_1) V^*(\tau'_2) V(\tau'_3) e^{-i(\alpha(\tau'_1) - \alpha(\tau'_2) + \alpha(\tau'_3))} d\tau'_1 d\tau'_2 d\tau'_3 \\ & \quad + \frac{1}{32} i^5 A^* \int_{-\infty}^{\infty} \int_{\tau'_1}^{\infty} \dots \int_{\tau'_4}^{\infty} d\tau'_1 d\tau'_2 \dots d\tau'_5 V(\tau'_1) V^*(\tau'_2) \dots V(\tau'_5) \\ & \quad \quad \quad \times e^{-i(\alpha(\tau'_1) - \alpha(\tau'_2) + \alpha(\tau'_3) - \alpha(\tau'_5) + \alpha(\tau'_5))} \\ & \quad + \dots \quad (7.34) \end{aligned}$$

Multiplying both terms together then gives,

Term 1:

$$\frac{1}{4}A^*A \int_{-\infty}^{\infty} \int_{-\infty}^{\infty} V(\tau'_1)V^*(\tau_1)e^{i(\alpha(\tau_1)-\alpha(\tau'_1))}d\tau_1d\tau'_1 \quad (7.35)$$

Term 2:

$$\begin{aligned} & -\frac{1}{4}A^*A \int_{-\infty}^{\infty} \int_{-\infty}^{\infty} \int_{\tau'_1}^{\infty} \int_{\tau'_2}^{\infty} d\tau_1d\tau'_1d\tau'_2d\tau'_3V^*(\tau_1)V(\tau'_1)V^*(\tau'_2)V(\tau'_3) \\ & \quad \times e^{+i(\alpha(\tau_1)-\alpha(\tau'_1)+\alpha(\tau'_2)-\alpha(\tau'_3))} \\ & -\frac{1}{4}A^*A \int_{-\infty}^{\infty} \int_{-\infty}^{\infty} \int_{-\infty}^{\tau_1} \int_{-\infty}^{\tau_2} d\tau'_1d\tau_1d\tau_2d\tau_3V(\tau'_1)V^*(\tau_1)V(\tau_2)V^*(\tau_3) \\ & \quad \times e^{-i(\alpha(\tau'_1)-\alpha(\tau_1)+\alpha(\tau_2)-\alpha(\tau_3))} \end{aligned} \quad (7.36)$$

and so on. There are two more simplifications that can be made here, first $A^*A = 1$, as A is just a phase (see Eq.(7.27)) and secondly the exponents in the integral can be evaluated explicitly. In Eq.(7.35) we have in the exponent,

$$\begin{aligned} i(\alpha(\tau_1) - \alpha(\tau'_1)) &= iF_0 \left(\int_{-\infty}^{\tau_1} \tau' d\tau' - \int_{-\infty}^{\tau'_1} \tau' d\tau' \right) \\ &= iF_0 \int_{\tau'_1}^{\tau_1} \tau' d\tau' = i\frac{F_0}{2}(\tau_1^2 - \tau_1'^2). \end{aligned} \quad (7.37)$$

The exponents in higher order terms can be evaluated in the same way. Putting together all the information gathered here and relabelling the variables $\tau'_1 \dots \tau'_n$ and $\tau_1 \dots \tau_n$ as $\tau_1 \dots \tau_{2n}$ we arrive at a formula similar to the one given by Kayanuma [1, 44].

$$\begin{aligned} & {}_d\langle 2 | \exp_+ \left(-i \int_{-\infty}^{\infty} \hat{H}_{LZ,N}(\tau) d\tau \right) | 1 \rangle_d \langle 1 | \exp_- \left(i \int_{-\infty}^{\infty} \hat{H}_{LZ,N}(\tau) d\tau \right) | 2 \rangle_d \\ &= \sum_{n=1}^{\infty} (-1)^{2n} \left(\frac{V_0^2}{4} \right)^n L^{(n)} \end{aligned} \quad (7.38)$$

with

$$\begin{aligned} L^{(n)} &= \sum_{m=1}^n \int_{-\infty}^{\infty} d\tau_1 \int_{\tau_1}^{\infty} d\tau_2 \dots \int_{\tau_{2m-2}}^{\infty} d\tau_{2m-1} \int_{-\infty}^{\infty} d\tau_{2m} \int_{-\infty}^{\tau_{2m}} d\tau_{2m+1} \dots \int_{-\infty}^{\tau_{2n-1}} d\tau_{2n} \\ & \quad \times G(\tau_1)G^*(\tau_2) \dots G(\tau_{2m-1})G^*(\tau_{2m})G(\tau_{2m+1}) \dots G^*(\tau_{2n}) \\ & \quad \times \exp \left(i\frac{F_0}{2} \sum_{k=1}^{2n} (-1)^k \tau_k^2 \right), \end{aligned} \quad (7.39)$$

where $G(\tau) = (1 + e^{i\phi(\tau)})$. Hence, the transition probability is given by:

$$P_{tra}(\infty) = \left\langle \sum_{n=1}^{\infty} (-1)^{2n} \left(\frac{V_0^2}{4} \right)^n L^{(n)} \right\rangle. \quad (7.40)$$

Acknowledgements

First of all, I want to thank my supervisor Sandro Wimberger who offered me this project in the first place. Further thanks go to the other members of our group, Julia Link, Carlos Parra-Murillo, Felix Ziegler, Georgios Kordas and Anton Ivanov and our office mate Gerald Langhanke. They all made my work in the group an enjoyable experience. Yet, most of all I have to thank Stephan Burkhardt who worked with me on this project. He took the main burden of explaining me the system studied here and tremendously helped me to gain a better understanding of the physics involved. Moreover, he was patient enough to answer all my C++, Linux and ‘bash’ related questions.

I would also like to thank Felix Lucas (University of Duisburg-Essen) for helpful discussions during the spring conference of the *Deutsche Physikalische Gesellschaft* in Stuttgart and Riccardo Mannella (University of Pisa) and Andreas Buchleitner (University of Freiburg) for valuable discussions during a workshop on “Noisy Many-body systems” in Heidelberg.

Further thanks go to all the people at Imperial and Heidelberg who made it possible for me to spend my third year abroad, in particular Yvonne Unruh, Stephanie Smallwood and Adrian Hawksworth.

Finally, I want to thank my family for their lifelong support. Without them, I would have never had the chance to study physics at Imperial.

Bibliography

- [1] Y. Kayanuma. Nonadiabatic Transitions in Level Crossings with Energy Fluctuation. *Journ. of the Phys. Soc. of Japan*, 53:108–122, 1983.
- [2] M. Greiner and S. Fölling. Optical lattices. *Nature*, 453:736–738, 2008.
- [3] R. Feynman. Simulating physics with computers. *Intern. Journ. of Theor. Phys.*, 21:467–488, 1982.
- [4] S. Wilkinson, C. Bharucha, K. Madison, Qian Niu, and M. Raizen. Observation of Atomic Wannier-Stark Ladders in an Accelerating Optical Potential. *Phys. Rev. Lett.*, 76:4512–4515, 1996.
- [5] A. Zenesini, H. Lignier, G. Tayebirad, J. Radogostowicz, D. Ciampini, R. Mannella, S. Wimberger, O. Morsch, and E. Arimondo. Time-Resolved Measurement of Landau-Zener Tunneling in Periodic Potentials. *Phys. Rev. Lett.*, 103:090403, 2009.
- [6] G. Tayebirad, R. Mannella, and S. Wimberger. Engineering interband transport by time-dependent disorder. *Phys. Rev. A*, 84:031605, 2011.
- [7] C. Pethick and H. Smith. *Bose-Einstein Condensation in Dilute Gases*. Cambridge University Press, Cambridge, 2nd edition, 2008.
- [8] Stephan Burkhardt. Noise assisted Interband Transitions in the Wannier-Stark Problem. Master’s thesis, Faculty of Physics and Astronomy, University of Heidelberg, Heidelberg, 2012.
- [9] L. Pitaevskii and S. Stringari. *Bose-Einstein condensation*. Oxford University Press, Oxford, 1st edition, 2003.
- [10] S. Bose. Plancks Gesetz und Lichtquantenhypothese. *Zeit.t für Phys. A Hadrons and Nuclei*, 26:178–181, 1924.
- [11] A. Einstein. Quantentheorie des einatomigen idealen Gases. *Sitzungsberichte der Preussischen Akademie der Wissenschaften. Phys.-math. Klasse*, pages 261–267 and 3–14, 1924 and 1925.
- [12] F. Schwabl. *Statistical Mechanics*. Springer-Verlag, Berlin, 2nd edition, 2006.
- [13] M. Anderson, J. Ensher, M. Matthews, C. Wieman, and E. Cornell. Observation of Bose-Einstein Condensation in a Dilute Atomic Vapor. *Science*, 269:198–201, 1995.

- [14] K. Davis, M. Mewes, M. Andrews, N. van Druten, D. Durfee, D. Kurn, and W. Ketterle. Bose-Einstein Condensation in a Gas of Sodium Atoms. *Phys. Rev. Lett.*, 75:3969–3973, 1995.
- [15] C. Bradley, C. Sackett, J. Tollett, and R. Hulet. Evidence of Bose-Einstein Condensation in an Atomic Gas with Attractive Interactions. *Phys. Rev. Lett.*, 75:1687–1690, 1995.
- [16] C. Foot. *Atomic Physics*. Oxford University Press, Oxford, 1st edition, 2005.
- [17] G. Tayebirad, A. Zenesini, D. Ciampini, R. Mannella, O. Morsch, E. Arimondo, N. Lörch, and S. Wimberger. Time-resolved measurement of Landau-Zener tunneling in different bases. *Phys. Rev. A*, 82:013633, 2010.
- [18] L. Esaki and R. Tsu. Superlattice and Negative Differential Conductivity in Semiconductors. *IBM Journ. of Research and Development*, 14:61–65, 1970.
- [19] G Wannier. Wave Functions and Effective Hamiltonian for Bloch Electrons in an Electric Field. *Phys. Rev.*, 117:432–439, 1960.
- [20] L. Avron, J. Zak, A. Grossmann, and L. Gunther. Instability of the continuous spectrum: The N-band Stark ladder. *Journ. of Math. Phys.*, 18:432–439, 1977.
- [21] A. Bouchard and M. Luban. Semiconductor superlattices as terahertz generators. *Phys. Rev. B*, 47:6815–6818, 1993.
- [22] M. Glück, A. Kolovsky, and H. Korsch. Wannier–stark resonances in optical and semiconductor superlattices. *Physics Reports*, 366:103–182, 2002.
- [23] F. Bloch. Über die Quantenmechanik der Elektronen in Kristallgittern. *Zeit. für Phys. A Hadrons and Nuclei*, 52:555–600, 1929.
- [24] H. Ilbach and H. Lüth. *Festkörperphysik*. Springer-Verlag Heidelberg, 7th edition, 2009.
- [25] M. Abramowitz and I. Stegun. *Handbook of Mathematical Functions with Formulas, Graphs, and Mathematical Tables*. Dover Publications, New York, 1st edition, 1964.
- [26] K. Drese and M. Holthaus. Ultracold atoms in modulated standing light waves. *Chemical Physics*, 217:201–219, 1997.
- [27] M. Holthaus. Bloch oscillations and Zener breakdown in an optical lattice. *Journ. of Opt. B: Quan. and Semicl. Opt.*, 2:589–604, 2000.
- [28] C. Zener. Non-Adiabatic Crossing of Energy Levels. *Proc. of the Roy. Soc. London A*, 137:696–702, 1932.
- [29] L. Landau. Zur Theorie der Energieübertragung. II. *Physics of the Soviet Union*, 2:46–51, 1932.

- [30] E. Stückelberg. Theorie der unelastischen Stöße zwischen Atomen. *Helvet. Phys. Acta*, 5:369–422, 1932.
- [31] E. Majorana. Atomi orientati in campo magnetico variabile. *Nuovo Cimento*, 2:43–50, 1932.
- [32] N. Vitanov and B. Garraway. Landau-Zener model: Effects of finite coupling duration. *Phys. Rev. A*, 53:4288–4304, 1996.
- [33] N. Vitanov. Transition times in the Landau-Zener model. *Phys. Rev. A*, 59:988–994, 1999.
- [34] N. Lörch, F. Pepe, H. Lignier, D. Ciampini, R. Mannella, O. Morsch, E. Arimondo, P. Facchi, G. Florio, S. Pascazio, and S. Wimberger. Wave-function-renormalization effects in resonantly enhanced tunneling. *Phys. Rev. A*, 85:053602, 2012.
- [35] A. Einstein. Über die von der molekularkinetischen Theorie der Wärme geforderte Bewegung von in ruhenden Flüssigkeiten suspendierten Teilchen. *Ann. der Phys.*, 322:549–560, 1905.
- [36] S. Soskin, V. Sheka, T. Linnik, and R. Mannella. Short Time Scales in the Kramers Problem: A Stepwise Growth of the Escape Flux. *Phys. Rev. Lett.*, 86:166In this section, 5–1669, 2001.
- [37] M. Foreman. *Informational limits in optical polarimetry and vectorial imaging*. PhD thesis, Imperial College London, London, 2010.
- [38] L. Schimansky-Geier and C. Zülicke. Harmonic noise: Effect on bistable systems. *Zeit. für Phys. B Condensed Matter*, 79:451–460, 1990.
- [39] P. Kloeden and E. Platen. *Numerical Solutions of Stochastic Differential Equations*. Springer Verlag, 1st edition, 1992.
- [40] W. Press, S. Teukolsky, W. Vetterling, and B. Flannery. *Numerical Recipes in C The Art of Scientific Computing*. Cambridge University Press, Cambridge, 2nd edition, 1992.
- [41] K. Riley, M. Hobson, and S. Bence. *Mathematical Methods for Physics and Engineering*. Cambridge University Press, Cambridge, 3rd edition, 2006.
- [42] Ghazal Tayebirad. *Engineering the Landau-Zener Tunneling of Ultracold Atoms in Tilted Potentials*. PhD thesis, Faculty of Physics and Astronomy, University of Heidelberg, Heidelberg, 2011.
- [43] V. Zelevinsky. Viewpoint: Theory in the computer age. <http://cerncourier.com/cws/article/cern/30156>, June 2007.
- [44] Y. Kayanuma. Stochastic Theory for Nonadiabatic Level Crossing with Fluctuating Off-Diagonal Coupling. *Journ. of the Phys. Soc. of Japan*, 54:2037–2046, 1984.

- [45] V. Pokrovsky and N. Sinitsyn. Fast noise in the Landau-Zener theory. *Phys. Rev. B*, 67:1–11, 2003.
- [46] J. Sakurai and S. Tuan. *Modern Quantum Mechanics, Revised Edition*. Addison Wesley, 1st edition, 1994.
- [47] R. Feynman. An Operator Calculus Having Applications in Quantum Electrodynamics. *Phys. Rev. Lett.*, 84:108–117, 1951.
- [48] C. Gardiner. *Handbook of Stochastic Methods*. Springer-Verlag Heidelberg, 3rd edition, 2004.